



National Library
of Canada

Bibliothèque nationale
du Canada

Canadian Theses Service

Service des thèses canadiennes

Ottawa, Canada
K1A 0N4

NOTICE

The quality of this microform is heavily dependent upon the quality of the original thesis submitted for microfilming. Every effort has been made to ensure the highest quality of reproduction possible.

If pages are missing, contact the university which granted the degree.

Some pages may have indistinct print especially if the original pages were typed with a poor typewriter ribbon or if the university sent us an inferior photocopy.

Reproduction in full or in part of this microform is governed by the Canadian Copyright Act, R.S.C. 1970, c. C-30, and subsequent amendments.

AVIS

La qualité de cette microforme dépend grandement de la qualité de la thèse soumise au microfilmage. Nous avons tout fait pour assurer une qualité supérieure de reproduction.

S'il manque des pages, veuillez communiquer avec l'université qui a conféré le grade.

La qualité d'impression de certaines pages peut laisser à désirer, surtout si les pages originales ont été dactylographiées à l'aide d'un ruban usé ou si l'université nous a fait parvenir une photocopie de qualité inférieure.

La reproduction, même partielle, de cette microforme est soumise à la Loi canadienne sur le droit d'auteur, SRC 1970, c. C-30, et ses amendements subséquents.

UNIVERSITY OF ALBERTA

**THE EFFECTS OF ENHANCED IGNITION SYSTEMS
AND TURBULENCE ON FLAME DEVELOPMENT**

BY



RUSSELL MILES MODIEN

A THESIS

SUBMITTED TO THE FACULTY OF GRADUATE STUDIES AND RESEARCH IN
PARTIAL FULFILLMENT OF THE REQUIREMENTS FOR THE DEGREE OF
MASTER OF SCIENCE.

DEPARTMENT OF MECHANICAL ENGINEERING

EDMONTON, ALBERTA

SPRING, 1991



National Library
of Canada

Bibliothèque nationale
du Canada

Canadian Theses Service Service des thèses canadiennes

Ottawa, Canada
K1A 0N4

The author has granted an irrevocable non-exclusive licence allowing the National Library of Canada to reproduce, loan, distribute or sell copies of his/her thesis by any means and in any form or format, making this thesis available to interested persons.

The author retains ownership of the copyright in his/her thesis. Neither the thesis nor substantial extracts from it may be printed or otherwise reproduced without his/her permission.

L'auteur a accordé une licence irrévocable et non exclusive permettant à la Bibliothèque nationale du Canada de reproduire, prêter, distribuer ou vendre des copies de sa thèse de quelque manière et sous quelque forme que ce soit pour mettre des exemplaires de cette thèse à la disposition des personnes intéressées.

L'auteur conserve la propriété du droit d'auteur qui protège sa thèse. Ni la thèse ni des extraits substantiels de celle-ci ne doivent être imprimés ou autrement reproduits sans son autorisation.

ISBN 0-315-65012-9

UNIVERSITY OF ALBERTA

RELEASE FORM

AUTHOR: **Russell Miles Modien**

TITLE: **The Effects of Enhanced Ignition Systems and
Turbulence on Flame Development**

DEGREE: **Master of Science**

YEAR THIS DEGREE GRANTED: **1991**

Permission is hereby granted to the UNIVERSITY OF ALBERTA LIBRARY to reproduce single copies of this thesis and to lend or sell such copies for private, scholarly, or scientific purposes only.

The author reserves other publication rights, and neither the thesis nor extensive extracts from it may be printed or otherwise reproduced without the authors written permission.


Russell Miles Modien

14828 - 75 Street
Edmonton, Alberta
T5C 0Z9

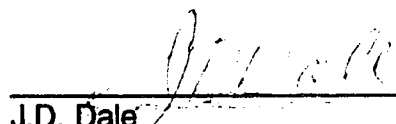
Date: *16 Apr 1991*

UNIVERSITY OF ALBERTA
FACULTY OF GRADUATE STUDIES AND RESEARCH

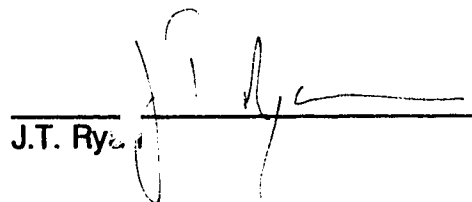
The undersigned certify they have read, and recommend to the Faculty of Graduate Studies and Research for acceptance, a thesis entitled THE EFFECTS OF ENHANCED IGNITION SYSTEMS AND TURBULENCE ON FLAME DEVELOPMENT submitted by Russell Miles Modien in partial fulfillment of the requirements for the degree of Master of Science.



M.D. Checkel (Supervisor)



J.D. Dale



J.T. Ryan

Date: 16 April, 1991

ABSTRACT

In this investigation, various methods were used to measure the effects of three spark ignition circuits. One standard and two "enhanced" ignition circuits were tested using lean methane - air mixtures. Ignition system effects on flame development were quantified using both quiescent and turbulent combustion cells. Primary ignition system effects were only seen during the very early flame development period. Secondary effects were seen in what is thought to be electromagnetic movement of the spark kernel, resulting in a favourable flame geometry. These secondary effects caused calculations based on the pressure trace to be biased. Thus, accurate comparisons of the effects of different ignition systems could not be made from pressure traces. Schlieren photographic flame size measurements and combustion time measurements were used to reduce flame geometry biases. It was shown that enhanced ignition circuits accelerated early flame kernel growth. The effects of ignition systems were only seen during the early stages of combustion.

The effects of turbulence on flame growth were also investigated. Precise turbulence characteristics could be generated with the apparatus used in this investigation. By allowing only one parameter to vary, tests were done to determine the effects of turbulence intensity and scale on burning velocity. Burning velocity was shown to be strongly dependent on intensity and only slightly dependent on length scale. From photographic measurements, it was shown that the flame development period was ignition-dominated and independent of mixture turbulence.

The benefits of both enhancements could be realised by combining a high energy ignition system with mixture turbulence. High energy ignition systems accelerate the early flame development while mixture turbulence increases the speed of a developed flame. Enhanced ignition system benefits were shown to be independent of the mixture turbulence, so higher relative gains in burning time were seen for highly turbulent mixtures than for quiescent mixtures.

TABLE OF CONTENTS

	Page
1 INTRODUCTION TO THIS INVESTIGATION	
1.1 Background to this Investigation	1
1.2 Objectives of this Investigation	4
1.3 Overview of this Investigation	5
2 EXPERIMENTAL EQUIPMENT AND PROCEDURES	
2.1 Fuel-Air Mixer	7
2.2 Quiescent Combustion Cell	10
2.3 Turbulent Combustion Cell	11
2.4 Turbulence Measurements	15
2.5 Schlieren Photography System	20
2.6 Cell Instrumentation	23
2.7 Ignition Systems and Spark Discharge Modes	29
3 COLLECTION AND ANALYSIS OF DATA	
3.1 Data Acquisition System	31
3.2 Numerical Smoothing	34
3.2.1 Effects of Numerical Smoothing	35
3.3 Flame Growth Diagnostics	41
3.3.1 Flame Growth From Schlieren Photography Measurements	41
3.3.2 Flame Growth From Ionisation Probe Measurements	43
3.3.3 Flame Growth From Models Based on Pressure Trace	43
3.3.3.1 Lewis and von Elbe and Dabora Models	44
3.3.3.2 The Multi-zone Thermodynamic Equilibrium Model	46
3.3.4 Comparison of Flame Growth Diagnostics	51
4 EFFECTS OF ENHANCED IGNITION SYSTEMS IN QUIESCENT MIXTURES	
4.1 Overview of Enhanced Ignition Systems	60
4.1.1 Benefits of Enhanced Ignition Systems	60
4.1.2 Overview of Enhanced Ignition System Testing in Quiescent Mixtures	62
4.2 Experimental Details of Enhanced Ignition System Testing	63
4.2.1 Ignition System - Spark Plug Combinations	63
4.2.2 Description and Characteristics of the Ignition Systems	64
4.2.3 Description of the Spark Plugs Used in the Quiescent Cell	68
4.3 Experimental Measurements in the Quiescent Combustion Cell	70
4.4 Experimental Results in the Quiescent Combustion Cell	72
4.4.1 Burning Velocities in the Quiescent Combustion Cell	74
4.4.2 Pressure - Time Based Results in the Quiescent Combustion Cell	76
4.4.3 Effect of Stored Voltage in the Breakdown Ignition System	82
4.4.4 Central and Side Ignition Differences in the Quiescent Combustion Cell	86
4.4.5 Ignition System Testing in the Turbulent Combustion Cell	88

4.5	Summary of Enhanced Ignition System Testing	90
5	EFFECTS OF MIXTURE TURBULENCE	
5.1	Overview of Turbulent Combustion Studies	94
5.1.1	Benefits of Mixture Turbulence	94
5.1.2	Turbulent Mechanisms	95
5.1.3	Overview of the Turbulent Combustion Program	96
5.2	Experimental Details of Mixture Turbulence Testing	98
5.2.1	Measurement Differences from the Quiescent Combustion Cell	98
5.2.2	Experimental Measurements	100
5.3	Experimental Results	100
5.3.1	Flame Growth and Burning Velocity	102
5.3.1.1	Effects of Turbulence Intensity	105
5.3.1.2	Effects of Turbulence Scale	107
5.3.2	Turbulence Decay and Rapid Distortion Theory	108
5.3.3	Turbulence Regimes	117
5.4	Summary of Turbulent Testing	120
6	COMBINED EFFECTS OF TURBULENCE AND ENHANCED IGNITION	
6.1	Overview of Testing Program	123
6.2	Experimental Results	123
6.3	Flame Kernel Growth Regimes	127
6.4	Summary of Combined Effects	127
7	SUMMARY OF RESULTS AND CONCLUSIONS	
7.1	Overview of this Investigation	128
7.2	Trends of Results and Conclusions	129
7.3	Suggested Improvements and Further Research	130
	REFERENCES	133
	APPENDIX	138

LIST OF TABLES

	Page
Table 2.1 Minimum upstream pressures for critical flow.	10
Table 2.2 RMS intensity decay constants.	18
Table 2.3 Integral scale growth constants.	19
Table 2.4 Spark discharge modes.	30
Table 3.1 Comparison between the equilibrium model and STANJAN.	50
Table 4.1 Ignition circuit - spark plug combinations.	63

LIST OF FIGURES

Figure 1.1	Air-standard Otto cycle variation of thermal efficiency with equivalence ratio for different compression ratios.	2
Figure 2.1	Fuel-air mixer shown as installed with associated plumbing and combustion cell.	8
Figure 2.2	The cylindrical quiescent combustion cell.	12
Figure 2.3	The cubical turbulent combustion cell.	14
Figure 2.4	The perforated plate movement mechanism.	16
Figure 2.5	The perforated plates.	17
Figure 2.6	The schlieren photography principle.	21
Figure 2.7	The schlieren photography set-up.	22
Figure 2.8	A digitally enhanced, high-contrast image of a typical schlieren photograph and corresponding microdensitometer chart.	24
Figure 2.9	A typical ionisation probe.	27
Figure 2.10	The photomultiplier apparatus.	28
Figure 3.1	Data acquisition system.	32
Figure 3.2	An unsmoothed and a smoothed pressure trace.	36
Figure 3.3	Turbulent/laminar flame speed ratio based on an unsmoothed pressure trace.	38
Figure 3.4	Turbulent/laminar flame speed ratio based on a smoothed (numerically filtered) pressure trace.	39
Figure 3.5	A smoothed turbulent/laminar flame speed ratio based on an unsmoothed pressure trace.	40
Figure 3.6	A digitally enhanced, high-contrast image of a typical schlieren photograph.	42
Figure 3.7	Operation of the multi-zone thermodynamic equilibrium model	48

Figure 3.8	Comparison of the equilibrium model, the Lewis and von Elbe model, and the Dabora model with the photographic data standard.	53
Figure 3.9	Mass fraction burned comparison between the equilibrium model and the Lewis and von Elbe model.	55
Figure 3.10	A comparison of various methods used for burning velocity calculations with the equilibrium model standard ($S_u = 0.216$ m/s).	57
Figure 3.11	Illustration of differences between spherical and hemispherical flame shapes.	58
Figure 4.1	Schematics of the ignition circuits used.	65
Figure 4.2	Spark discharge characteristics for the ignition circuits used.	67
Figure 4.3	Average power and spark duration comparison of the ignition circuits used in this study and those used by Anderson [11].	69
Figure 4.4	Comparison of spark plugs.	71
Figure 4.5	Typical analog signals recorded by the FM tape recorder during the testing of ignition system effects.	73
Figure 4.6	Calculated burning velocities of lean quiescent mixtures for various ignition systems.	75
Figure 4.7	Flame development period and burn duration shown on a typical pressure trace. 2.5 kPa pressure error is shown in terms of time for 5%, 95%, and maximum pressure rise.	78
Figure 4.8	Flame development period of lean quiescent mixtures for various ignition systems.	80
Figure 4.9	Burn duration of lean quiescent mixtures for various ignition systems.	81
Figure 4.10	Flame development period of lean quiescent mixtures for the breakdown ignition system with various stored voltage levels.	84
Figure 4.11	Burn duration of lean quiescent mixtures for the breakdown ignition system with various stored voltage levels.	85

Figure 4.12	Comparison of photographically measured volume burned with that calculated by the equilibrium model for a lean ($\phi = 0.95$) quiescent mixture.	89
Figure 4.13	Flame growth of lean ($\phi = 0.85$) quiescent mixtures based on photographic data and equilibrium model calculations for standard and breakdown ignition systems.	91
Figure 5.1	Graphical representation of turbulent combustion experimental program.	97
Figure 5.2	Typical analog signals recorded by the FM tape recorder during the testing of turbulence effects.	101
Figure 5.3	Digitally enhanced, high-contrast images of schlieren photographs of lean ($\phi = 0.85$) mixtures with various levels of turbulence.	103
Figure 5.4	Flame growth measured photographically and calculated using the equilibrium model for lean ($\phi = 0.85$) turbulent mixtures.	104
Figure 5.5	Calculated burning velocities for various turbulence RMS intensity with $\Lambda = 3.8$ mm and $\Lambda = 7.6$ mm at the time of ignition for lean ($\phi = 0.85$) turbulent mixtures.	106
Figure 5.6	Calculated burning velocities for various integral length scales with $u' = 0.5$ m/s and $u' = 1.0$ m/s at the time of ignition for lean ($\phi = 0.85$) turbulent mixtures.	109
Figure 5.7	Decay of turbulence RMS intensity with downstream distance.	111
Figure 5.8	Rapid distortion theory turbulence intensity enhancement multiplier in terms of (a) relative radius and (b) pressure for all experiments.	114
Figure 5.9	Turbulence RMS intensity with (a) normal temporal decay and (b) normal temporal decay with rapid distortion enhancements accounted for.	115
Figure 5.10	Calculated burning velocities for various turbulence RMS intensity with rapid distortion enhancements. Average burning velocities and turbulence intensities are averages at pressures of 200 kPa and 250 kPa (about a 40 mm flame radius).	116
Figure 5.11	Various turbulence regimes as reviewed by Zur Loye and Bracco [49].	119

Figure 5.12	Comparisons of turbulence regimes from this study using lean ($\phi = 0.85$) mixtures and those reported.	121
Figure 6.1	Flame growth of lean ($\phi = 0.85$) turbulent mixtures based on equilibrium model calculations for standard and breakdown ignition systems.	124
Figure 6.2	Average flame growth of lean ($\phi = 0.85$) quiescent and turbulent mixtures using standard and breakdown ignition systems.	126

NOMENCLATURE

A	= decay/growth constant
\mathbf{B}	= magnetic induction vector
c	= normal strain due to geometrical straining
C	= constant
C_p	= constant pressure specific heat
CR	= compression ratio
d	= diffusion coefficient
D	= diameter
i	= counting index
\mathbf{J}	= current density vector
k'	= thermal conductivity
Le	= Lewis number
mf	= mass fraction
n	= decay/growth exponent
P	= pressure
r	= radius
R	= Reynolds number
S	= burning velocity
t	= time
T	= temperature
u'	= turbulence RMS intensity = $\sqrt{u^2}$
v	= velocity
V	= volume
w	= filtering width
x	= downstream distance
γ	= specific heat ratio = C_{p0}/C_{v0}
Δ	= incremental change
η	= Kolmogorov length scale
η_{th}	= thermal efficiency
λ	= Taylor length scale
Λ	= integral length scale
μ	= turbulence energy
ν	= kinematic viscosity
ρ	= density
ϕ	= lean equivalence ratio
ζ	= compression factor

Subscripts

b	= burned	s	= spherical
e	= end	T	= turbulent
h	= hemispherical	u	= unburned
i	= initial	o	= ambient
l	= laminar	$*$	= critical

1 INTRODUCTION TO THIS INVESTIGATION

1.1 Background to this Investigation

In an effort to increase fuel economy and reduce exhaust emission levels, engine researchers are exploring the use of leaner combustible mixtures. A lean fuel - air mixture is one that has more air available than is required, or excess air according to chemical stoichiometry, to burn all of the available fuel. The standard thermodynamic operating cycle for spark ignition engines is the Otto cycle. For an ideal air-standard Otto cycle, the thermal efficiency, η_{th} , can be expressed in terms of the specific heat ratio, γ , and the compression ratio, CR , [1]*:

$$\eta_{th} = 1 - \frac{1}{CR^{\gamma-1}} \quad (1.1)$$

Lean mixtures permit the use of higher compression ratios by inhibiting engine knock [58, 59]. Lean mixtures also have slightly larger specific heat ratios than rich mixtures which result in slightly higher thermal efficiency as seen in Figure 1.1. The equivalence ratio, ϕ , is the stoichiometric air/fuel ratio divided by the actual air/fuel ratio on a mass basis. Higher compression ratios result in dramatically higher thermal efficiencies. Figure 1.1 also shows the effect of compression ratio on thermal efficiency. Raising the compression ratio from 6:1 to 12:1 results in about a 25% gain in thermal efficiency. A CR of 6:1 represents those found in low performance stationary engines designed for use with poor quality fuel, while a CR

* Numbers in brackets, [], indicate references.

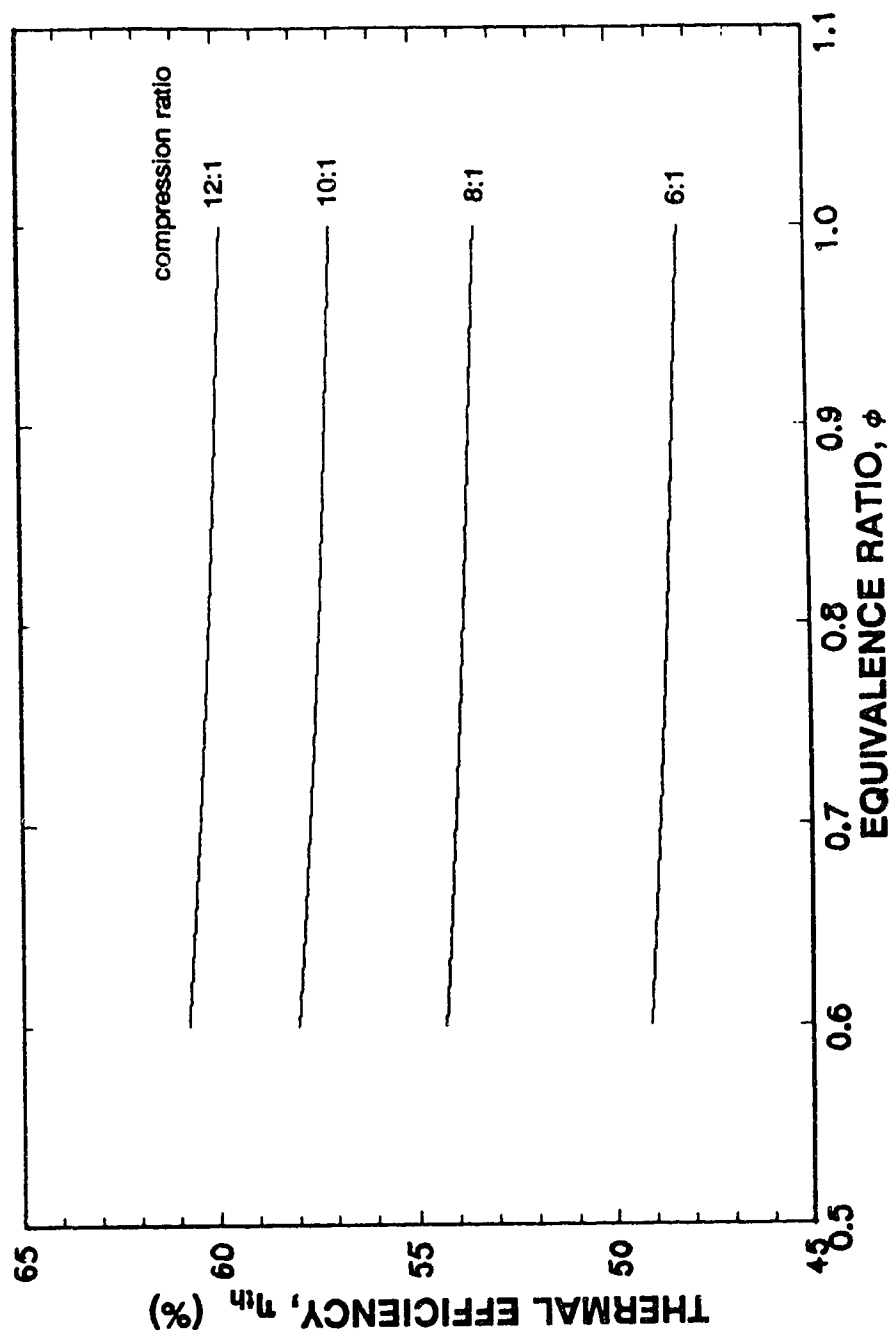


Figure 1.1 Air-standard Otto cycle variation of thermal efficiency with equivalence ratio for different compression ratios.

of 12:1 represents the practical maximum used in past automotive engines. The thermal efficiencies shown are for ideal conditions. Lower efficiencies are to be expected under actual conditions. However, trends similar to those shown in Figure 1.1 would be realised by burning leaner mixtures and using higher compression ratios.

One of the major drawbacks when using lean fuel - air mixtures is that they burn significantly slower than mixtures that are closer to being stoichiometrically balanced [2, 3]. Slow burning mixtures can lead to a decrease in power since combustion will be incomplete as the expansion stroke begins in an engine. Combustion of faster burning mixtures is normally well developed when the piston is at top-dead-centre. Other problems related to slow burning mixtures include misfire and increased cyclic variability. Ignition systems have been seen to affect both ignition and burning of lean mixtures and can extend the lean operating limit of an engine [4-8]. High energy or enhanced ignition systems have recently been shown to accelerate the early flame kernel development in a mixture [7-14]. Some studies have also shown that enhanced ignition systems increase the overall burning velocity of a mixture after ignition [9, 11], when spark effects are normally dominated by other factors. With some of the previous work, the explanations of mechanisms causing the results were often inconsistent, possibly due to the analysis methods used. In this work, the flame growth and burning velocities of lean fuel - air mixtures ignited by two, high-energy, ignition circuits are examined

using several methods of analysis. The objectives are to study the effects of the ignition sparks and to study the analysis methods.

Another means of increasing the burning velocity of a mixture is by increasing mixture turbulence [15-20]. Turbulence is usually characterised in terms of fluctuating velocity, or intensity, and time or length scales. It is through the controlled quantitative analysis of the effects of various turbulence characteristics that advances are made in understanding the role of turbulence on combustion. In the past, much of the research did not isolate the effects of intensity and length scale. Some studies examined only one of the characteristics while not isolating the other, giving somewhat inconclusive results. Many of the controlled studies were done under steady state conditions in combustion cells. These steady state conditions are useful for quantifying the effects of turbulence on combustion. However, they do not represent the unsteady turbulence field found in an operating internal combustion engine during the combustion period. Both turbulence intensity and turbulence integral length scale, representing the speed and size of the average energy-containing eddies, are examined in this study. A carefully controlled, decaying turbulent mixture was used to determine their isolated effects.

1.2 Objectives of this Investigation

To gain a better understanding of the effects of ignition systems and turbulence characteristics on burning velocity, research using a fully instrumented

combustion cell is essential. In this study, two high-energy ignition circuits were investigated over a range of lean equivalence ratios ($\phi = 0.65$ to 0.95) to determine their effects on lean quiescent mixtures in comparison with a standard ignition system.

The effects of turbulence RMS intensity and turbulence integral length scale on a combustible mixture were studied. A turbulent combustion cell was used to determine how burning velocity is affected by the scale and intensity of the mixture turbulence. The highest turbulence intensity levels studied here (~ 2 m/s) were higher than those studied in most previous research in combustion cells [e.g. 20-22].

Once the individual effects of ignition systems and turbulence had been measured, the combined effects were studied. Growth of flames ignited by an enhanced ignition system were compared with those ignited by a standard ignition system in a lean turbulent mixture.

1.3 Overview of this Investigation

In this study, two combustion test cells were used to measure ignition system and turbulence effects on burning velocity for lean methane - air mixtures. Four ignition system - spark plug combinations were compared in lean quiescent mixtures. Two ignition systems were compared in lean mixtures with turbulence of various intensity and scale. The specialized experimental equipment, the data acquisition system, and the flame growth diagnostics that were used in this study

are also described.

2 EXPERIMENTAL EQUIPMENT AND PROCEDURES

This study required specialized equipment and procedures. The equipment and related procedures are covered in this chapter and include the following:

fuel - air mixer,
quiescent and turbulent combustion cells,
combustion cell instrumentation,
turbulence measurements, and
schlieren photography system.

Ignition system requirements and spark discharge modes will also be discussed here. The details of the base-line and enhanced ignition systems will be described in Section 4.2 where it will be more relevant.

2.1 Fuel - Air Mixer

The fuel - air mixing apparatus had two functions. It had to regulate the volumetric flow rate of each of the gases and mix them ensuring a homogeneous mixture. The fuel could be methane, propane, or a combination of both. Only methane was used in this study. Extra dry air and fuel (93.1% pure methane) were supplied from cylinders. A schematic of the fuel - air mixer installation is shown in Figure 2.1.

Flow regulation was accomplished using critical flow nozzles. The critical flow nozzles consisted of brass orifice plates with diameters of 0.1 mm for the fuels

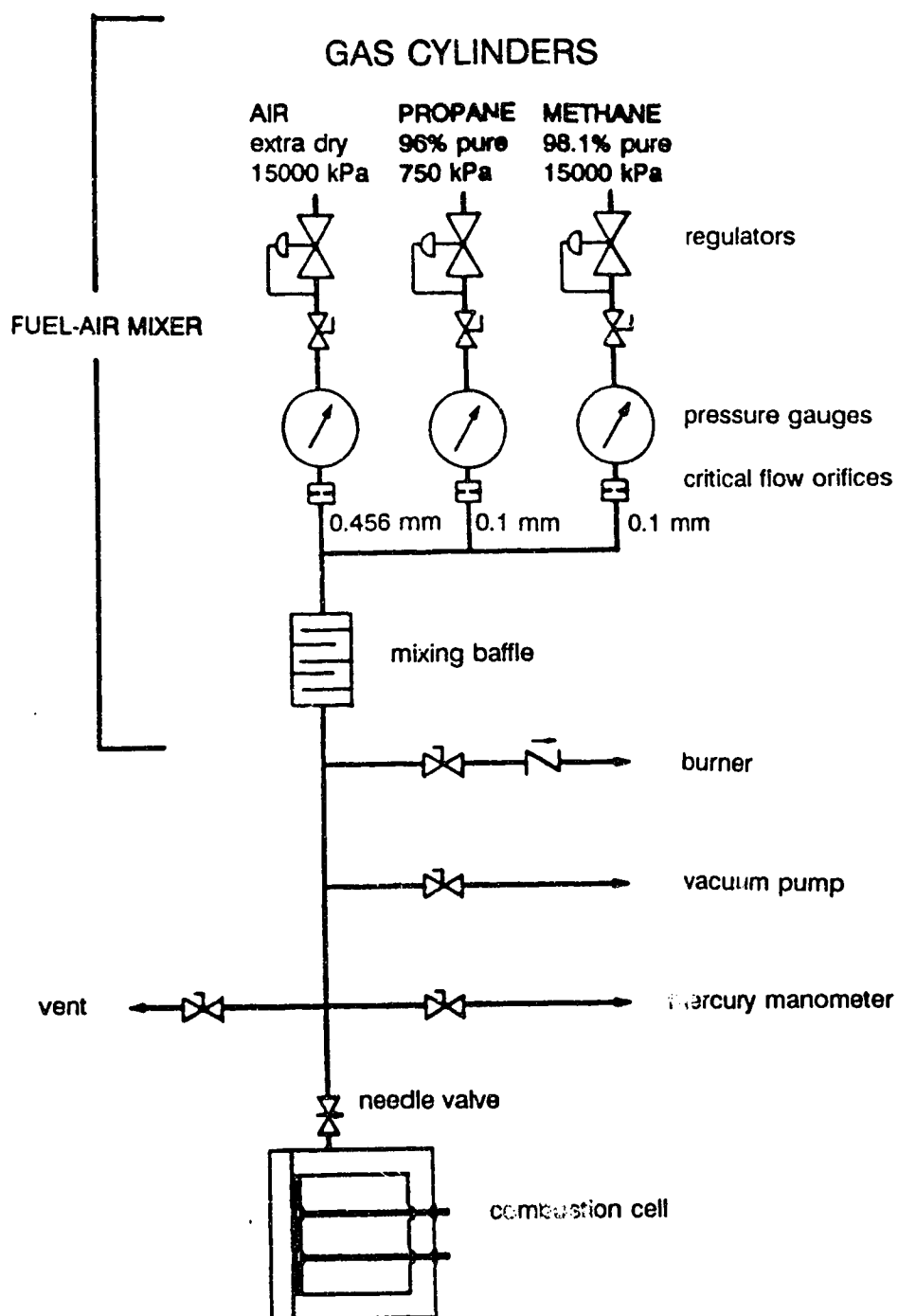


Figure 2.1 Fuel-air mixer shown as installed with associated plumbing and combustion cell.

and 0.456 mm for the air. Flow rate was a function of only upstream gas pressure and temperature when critical flow was obtained. The essentially constant, atmospheric temperatures in this study resulted in flow rate being directly proportional to upstream gas pressure. The upstream pressure had to satisfy the critical flow condition of Equation 2.1 [1]:

$$\frac{P_*}{P_o} \geq \left(\frac{2}{\gamma + 1} \right)^{\frac{\gamma}{\gamma - 1}} \quad (2.1)$$

where: γ = specific heat ratio
 P_o = downstream (ambient) pressure
 P_* = upstream (gas) pressure

The upstream gas pressures had to be greater than those listed in Table 2.1 to ensure critical flow. Table 2.1 shows minimum upstream pressures for downstream pressures of 92.5 kPa, average atmospheric pressure in Edmonton, and 101.325 kPa, standard atmospheric pressure. For convenience, methane gas pressure was held constant at 220 kPa gauge while air pressure was varied to form the required mixture stoichiometry.

Table 2.1 Minimum upstream pressures for critical flow.

Gas	$P_{*92.5}$	$P_{*161.325}$
Air	175.1 kPa abs	191.8 kPa abs
Methane, CH ₄	169.4 kPa abs	185.6 kPa abs
Propane, C ₃ H ₈	159.7 kPa abs	174.9 kPa abs

Flow rates from the gas mixer were calibrated using a bubble flowmeter made from a modified burette tube. A soap bubble was introduced into the gas stream to give a visual indication of the gas flow. The duration for a fixed volume of gas to flow was timed using a stopwatch. This procedure was repeated five times for each measured flow rate. A linear least squares fit of upstream pressure against flow rate was done to produce a calibration equation. All tests were corrected to local, standard, atmospheric conditions (700 mm Hg, 25°C). Required gas flow rates were achieved by regulating the upstream pressure according to the calibration equation. Reconfirmation of the fuel and air flow rates was done periodically to maintain an accurate, homogeneous mixture. The gas mixer provided a lean air/fuel equivalence ratio uncertainty of $\pm 0.65\%$, based on measurement uncertainty.

2.2 Quiescent Combustion Cell

The quiescent combustion cell has a cylindrical stainless steel body with circular glass ends. The internal dimensions of the cell are 80 mm in diameter and

102 mm in length. There are eight equally spaced threaded holes (18 mm and 3/8" NPT) around the circumference of the cell at the centre of its length for gas valves, spark plug(s), pressure transducer(s), thermocouple(s), and ionisation sensor(s). The windows are 24.4 mm thick, annealed BK7 glass held in place by threaded, removable, aluminum end-caps and are sealed with O-rings and paper gaskets. The glass is optically correct to facilitate schlieren photography. The cell is shown in Figure 2.2. Further cell design and testing details have been outlined by Wilson et al [23].

Cell operation included purging, filling, and igniting the gases in it. Using a vacuum pump, previously burned gases were purged from the cell and the cell was flushed with atmospheric air. The absolute pressure after evacuation to between 1 mm Hg and 4 mm Hg was recorded. A fuel - air mixture from the gas mixer was introduced and allowed to come to equilibrium at standard atmospheric temperature and pressure (25°C, 101.325 kPa). The combustion cell was then sealed by closing the valve from the gas mixer. Finally, the mixture was ignited while pressure, photographic, and flame arrival data were acquired.

2.3 Turbulent Combustion Cell

The mechanisms required to generate known levels of turbulence makes the operation of the turbulent combustion cell much more complex than that of the quiescent combustion cell. Construction, operation, and electronics of the turbulent combustion cell will be discussed here.

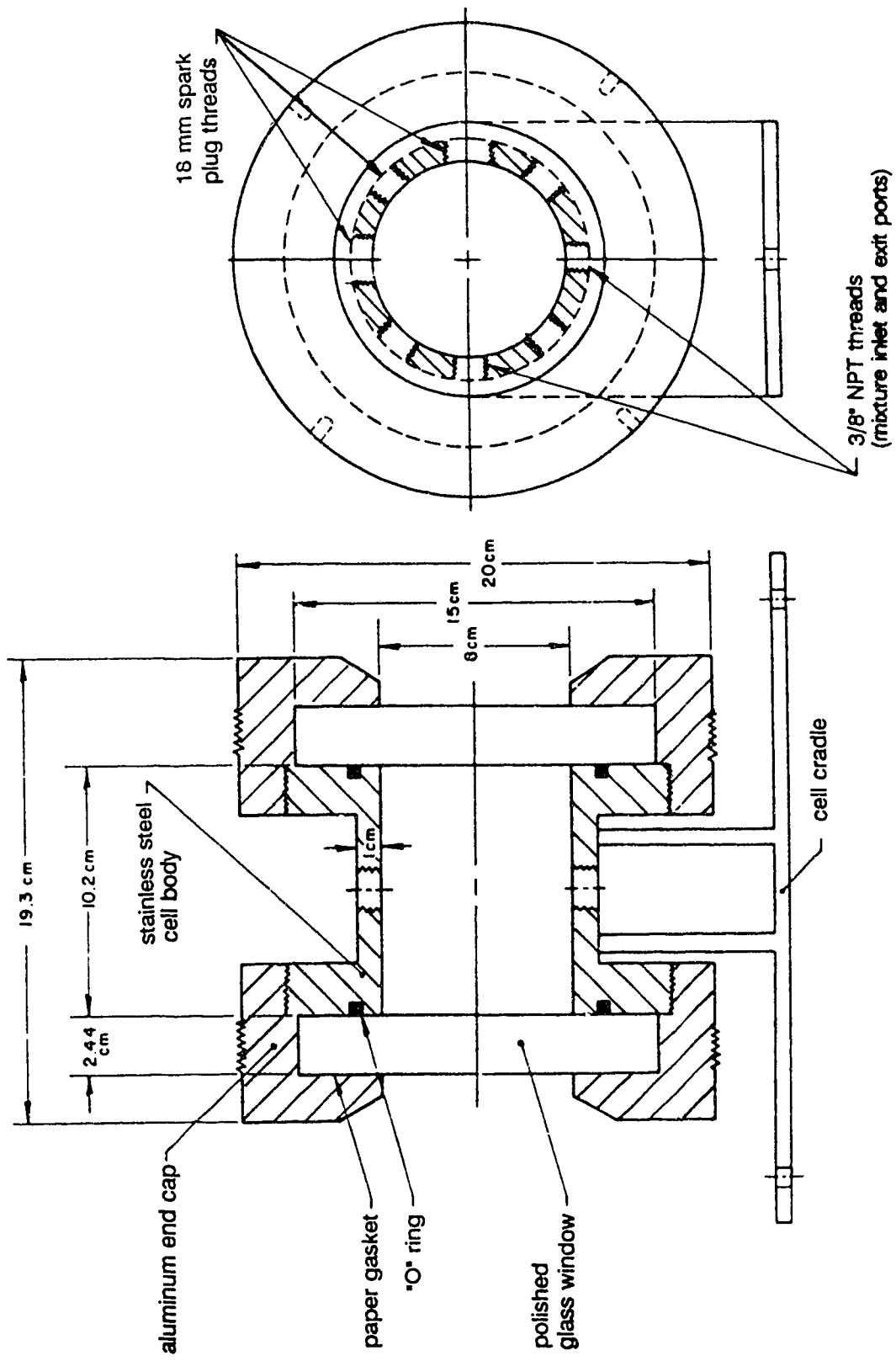


Figure 2.2 The cylindrical quiescent combustion cell.

This cell was based on an earlier cell [24, 25] and has been described in detail by McDonell [22]. The aluminum cell has an internal cubical dimension of 125 mm. A cubical shape approximates an ideal spherical shape, yet allows turbulence to be generated by quickly drawing a flat perforated plate across the cell. Two opposing sides contained 25.4 mm thick, annealed, BK7 glass windows which allowed for direct and schlieren photography, and allowed for light emission measurements to be made. The cell used central, platinum tipped, spark electrodes mounted on a micrometer head for spark gap adjustment. The gap between the pointed electrode tips was held constant at 1.0 mm for all experiments in this study. Threaded holes for a pressure transducer, gas valves, ionisation sensors, alternative spark plugs, and thermocouples were also present. The cell is illustrated in Figure 2.3.

The operation of the turbulent combustion cell during evacuation, purging, and introduction of the combustible mixture was identical to that of the quiescent combustion cell. Turbulence in the cell was generated by quickly moving a perforated plate across the cell. The plate starting and finishing positions are shown in Figure 2.3.

The plate was pulled via four rods that extended through sealed openings in the cell wall and attached to a stirrup. To move the stirrup and plate, a heavy flywheel with a small tooth extending from it was spun at a pre-determined speed. The tooth passed freely through a slot in the stirrup until a pin was electromagnetically fired across the slot, thereby engaging the tooth and flywheel. The

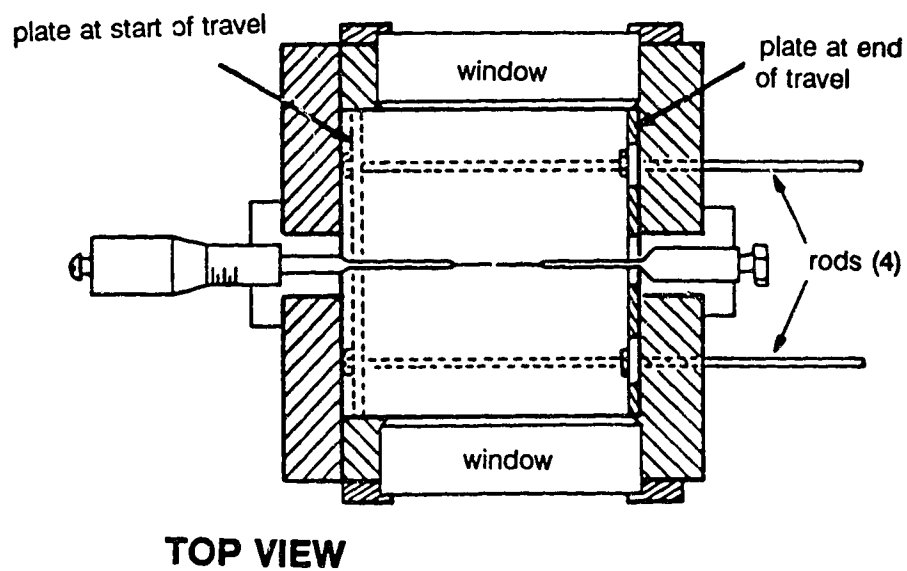
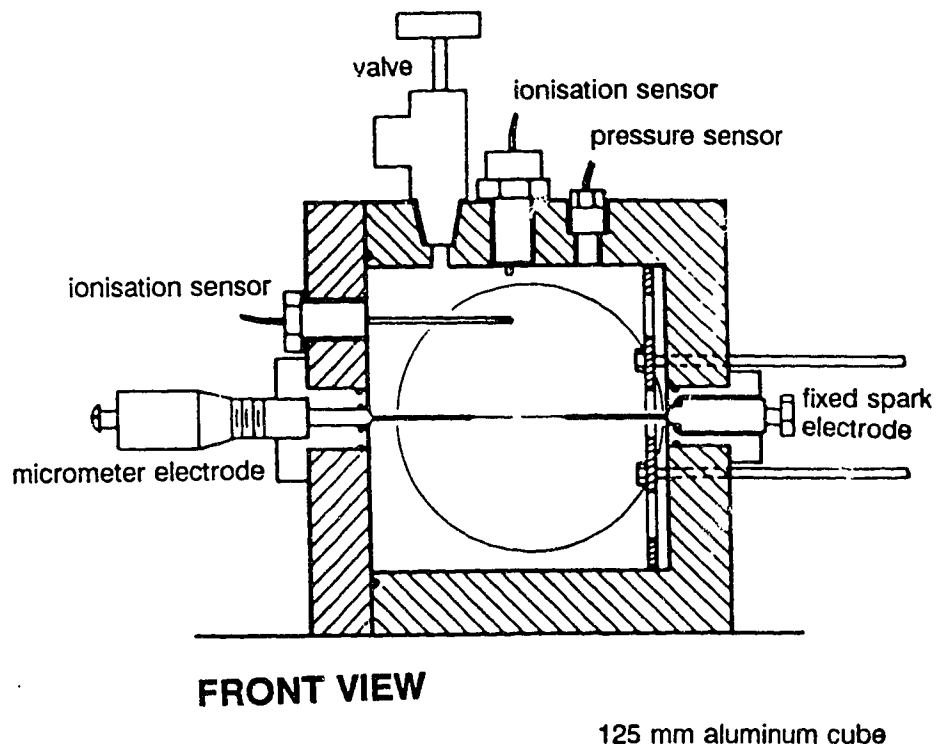


Figure 2.3 The cubical turbulent combustion cell.

stirrup slid in a track until the plate reached its finishing point at the other side of the cell. At the end of plate travel, the stirrup encountered a hydraulic damper which reduced the impact. It was held in place by electromagnets to prevent the plate from rebounding back across the cell. Figure 2.4 shows the entire plate movement mechanism.

To allow for proper plate movement, several photodiode sensors combined with black and white striped scales were used to monitor flywheel rotational speed, plate speed, and flywheel tooth passage. Ignition timing was triggered using a similar sensor. Placement of these sensors is shown in Figure 2.4.

The perforated plates used to produce turbulence in the cell had hole diameters, D , ranging from 2.5 mm to 20 mm. The dimension D is also used as a measure for the hole spacing to ensure geometrical similarity between the perforated plates. With this configuration of hole spacing, each plate had 60% solid area. The perforated plates are shown in Figure 2.5.

2.4 Turbulence Measurements

The turbulence characteristics produced by these perforated plates have been previously documented by Checkel [26] and McDonnell [22]. Detailed turbulence characterisation was performed downstream of similar, stationary, perforated plates in a small wind tunnel. Limited hot wire anemometer measurements in the combustion cell were performed and reported on by Checkel [26], confirming analogous measurements to those in the wind tunnel. The

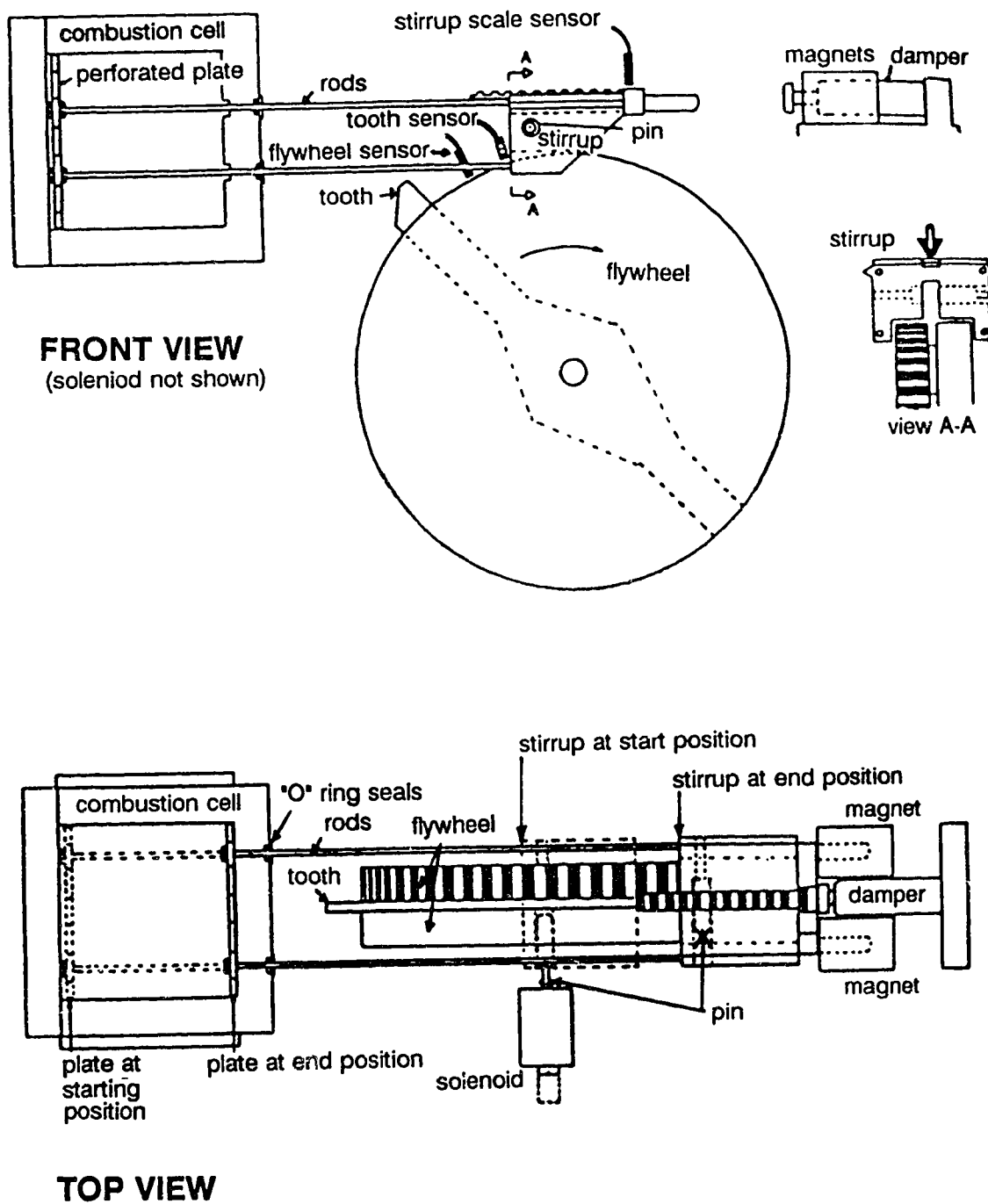
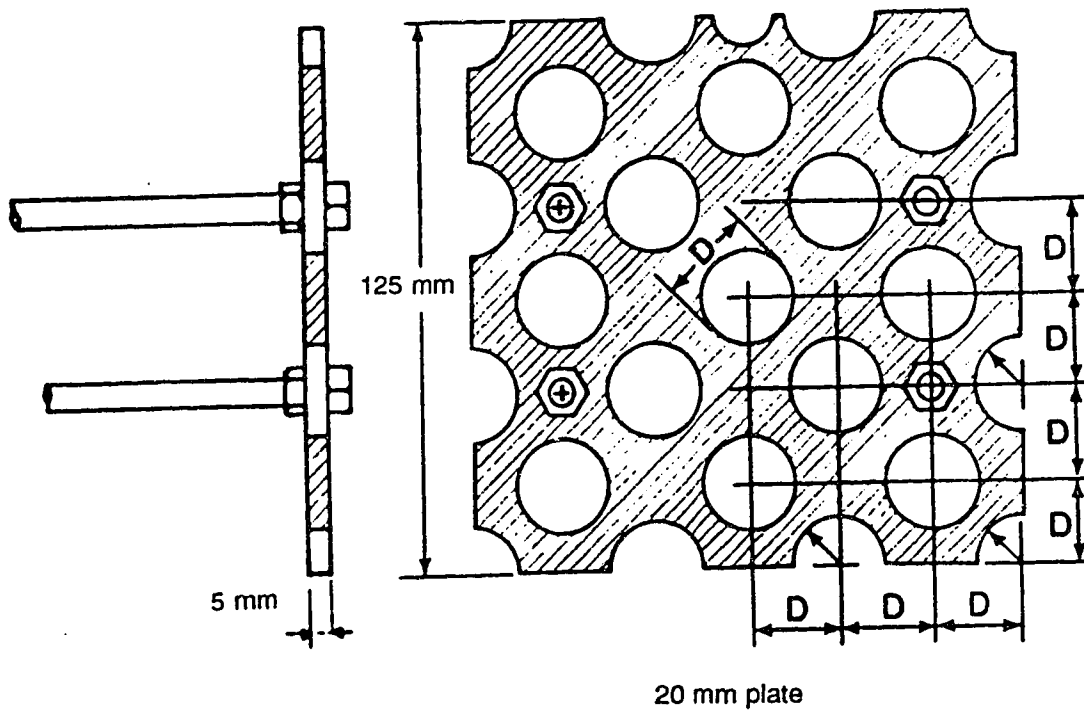
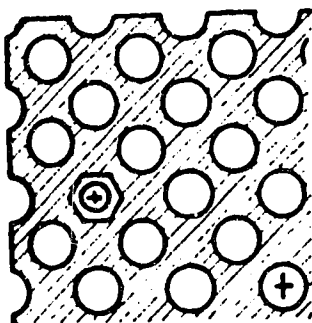


Figure 2.4 The perforated plate movement mechanism.

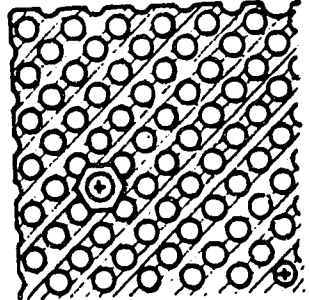


all plates are 5 mm thick aluminum

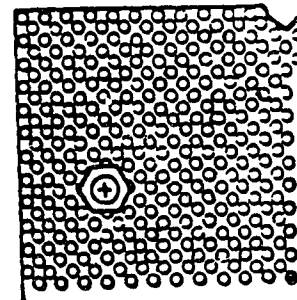
60% solid



10 mm plate



5 mm plate



2.5 mm plate

Figure 2.5 The perforated plates.

turbulence within the cell was homogeneous after a time, $t = x/v$, following the plate passage such that $x/D > 10$. Bulk motion of the mixture was assumed to be negligible compared to the turbulent motion. The wind tunnel measurements resulted in calibration equations of the form shown below:

$$\frac{u'}{v} = A_1 \left(\frac{x}{D} \right)^{n_1} \quad (2.2)$$

where: $u' = \text{RMS intensity } (= \sqrt{u'^2})$
 $v = \text{fluid velocity}$
 $x = \text{downstream distance}$
 $D = \text{perforated plate hole diameter}$

$$\frac{\Lambda}{D} = A_2 \left(\frac{x}{D} \right)^{n_2} \quad (2.3)$$

where: $\Lambda = \text{turbulence integral length scale}$

Table 2.2 RMS intensity decay constants.

Condition	A_1	n_1
$x/D < 10$	10.96	-1.812
$10 < x/D < 20$	2.627	-1.191
$20 < x/D < 40$	0.773	-0.783

Table 2.3 Integral scale growth constants.

Condition	A_2	n_2
$x/D < 14.3$	0.38	0
$x/D > 14.3$	0.1	0.5

Decay/growth constants A_1 , A_2 , n_1 , and n_2 for Equations 2.2 and 2.3 are listed in Tables 2.2 and 2.3. Only x/D values greater than 10 were used. Otherwise the jetting action of the airflow through the holes may result in inhomogeneous turbulence. The perforated plate speed is related to the wind tunnel velocity, and spark delay time to the dimensionless downstream distance, x/D . Using these calibration equations, variable combinations of turbulence RMS intensity (u') and turbulence length scale (Λ) were obtained at the time of ignition.

The turbulence scale and intensity were set for the time of ignition. After ignition, the turbulence initially continued to decay but some increase in turbulence was seen due to rapid distortion at the flame front. Flame growth and expansion caused the rapid distortion. A model developed by Chew and Britter [27] was used to calculate the level of turbulence RMS intensity enhancement, giving actual turbulence RMS intensity during combustion. The rapid distortion model and its results will be discussed in Section 5.4.2.

2.5 Schlieren Photography System

The basic principle of schlieren photography is that light is refracted by density gradients in the media through which it passes. In the case of parallel rays of light passing through a combustion cell, the light rays remain parallel assuming flat window surfaces. As portions of light pass through a density gradient (i.e. a burning flame front), they refract slightly. After passing through the cell, the parallel light rays are focused to a point. An iris can be used to block the refracted light rays which do not focus at that point because they are no longer parallel. Areas of large density gradients result in dark images on film. Figure 2.6 shows the application of the schlieren principle to form an image of a flame.

In this study, a HYCAM K20S4E, high speed, 16 mm, movie camera was used to film the schlieren image of a combustive mixture. A film rate of 1000 frames per second was used which resulted in one image per millisecond. A faster rate would have reduced the sensitivity of the system, resulting in an unclear image. The film was 16 mm, Eastman 7250, high speed, tungsten, Ektachrome Video News Film. It was pushed by two f-stops when developed to increase the effective sensitivity.

The light source was a halogen gas filled lamp, similar to that used in an automobile high beam headlamp. Filming sensitivity was lowered by light intensity reductions due to pin-hole irises and absorption and reflection from surfaces (mirrors, lenses, and windows). The image was projected directly onto the film in the camera without using a camera lens to avoid focusing problems and further

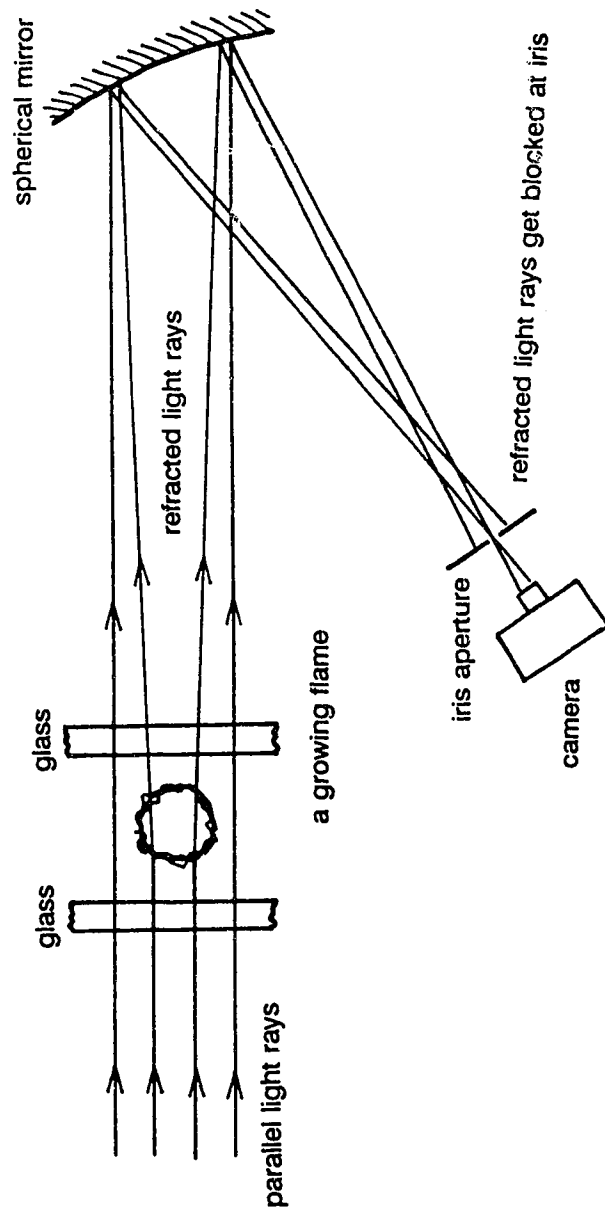


Figure 2.6 The schlieren photography principle.

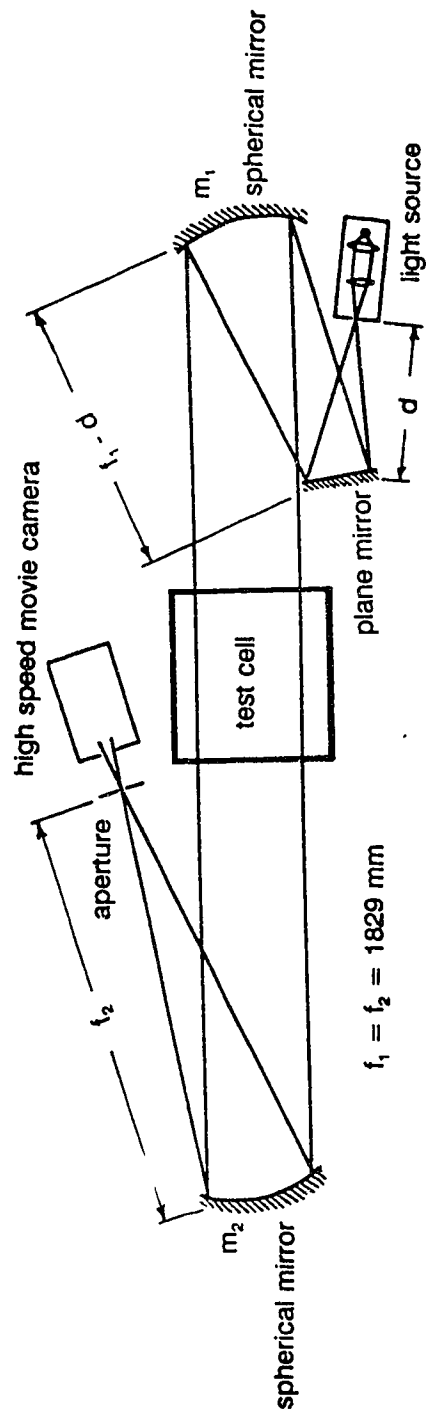


Figure 2.7 The schlieren photography set-up.

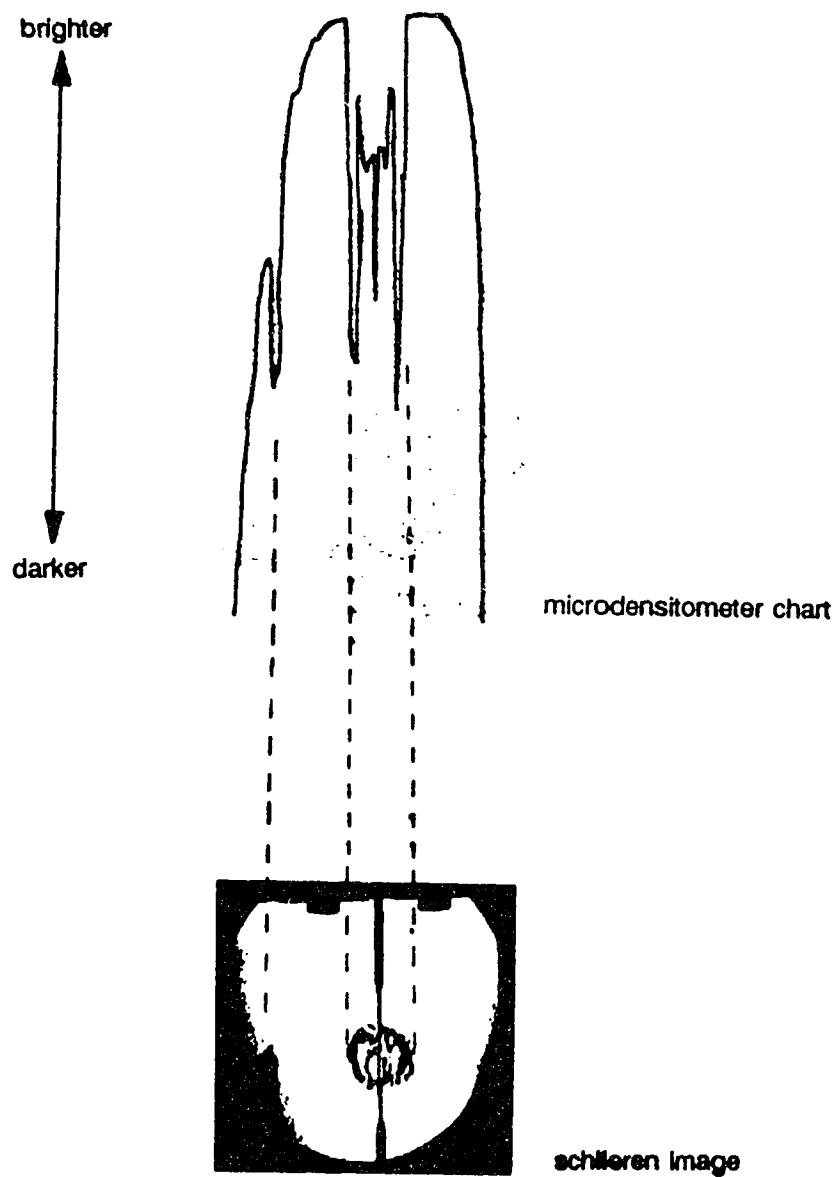
losses in light intensity. Figure 2.7 shows a schematic of the high speed schlieren photography system.

After the film was developed, a Joyce-Loebl, Model III CS microdensitometer was used to produce an enlarged strip chart of the image along the centre-line of the film. The scanning direction was perpendicular to the electrode orientation in the turbulent cell. Using this chart, the size of the flame front was calculated more accurately than by directly measuring from the film. Figure 2.8 shows a typical schlieren image of a flame with its corresponding microdensitometer chart. The occurrence of the spark was read directly from the film which produced a maximum uncertainty of ± 0.5 ms in the spark timing. Flame size measurements taken from the microdensitometer had an error of ± 0.1 mm.

The schlieren photography system was used as a standard for flame size measurements and provided direct confirmation of the flame sizes deduced from measured combustion pressures. Flame size measurements could only be made until the flame grew to the size of the combustion cell windows. Also, schlieren photography allowed for a visual confirmation of the flame structure and geometry which are important for modelling flame growth during combustion.

2.6 Cell Instrumentation

Each of the combustion cells was instrumented with a pressure transducer and one or more flame ionisation probes. The turbulent combustion cell also used a light emission sensor.



$\phi = 0.85$
 turbulent: $u' = 1.0 \text{ m/s}$, $\Lambda = 3.8 \text{ mm}$
 turbulent (cubical) cell
 $t = 3 \text{ ms}$
 $r_b = 24.0 \text{ mm}$

Figure 2.8

A digitally enhanced, high-contrast image of a typical schlieren photograph and corresponding microdensitometer chart.

The pressure sensor was a Norwood model 111 four-active-arm strain gauge pressure transducer with a response frequency of 45 kHz. The strain gauge bridge circuit was custom made by the Department of Mechanical Engineering's electronics shop at the University of Alberta. It had variable offset and an amplification factor of 100. The pressure transducer was regularly calibrated from 0 kPa to 1500 kPa using a dead weight pressure tester. Maximum non-linearity was less than $\pm 1\%$. The calculated pressure transducer calibration equation was utilized by a computer program to provide accurate digital pressure records.

Early in this study, an AVL 12QP 300cvk, piezoelectric, pressure transducer with Kistler 507, dual mode, differential charge amplifier was used due to its high response frequency of 60 kHz. This set-up was far too sensitive to electrical charge and quickly failed. It was unacceptable for use with the high energy enhanced ignition systems in this study because of the electrical noise they produced. Also, shifts in pressure signal due to ignition system electrical noise caused many problems in an earlier study that used this system [22]. It was recommended to use a more stable type of pressure transducer such as the Norwood model 111 used in this study.

Ionisation probes were used to detect the arrival of a flame front. A constant d.c. voltage potential, from 50 V to 150 V, was held across the exposed tips of 22 ga. platinum wire which were separated by 0.1 to 0.5 mm. When the flame front reached the gap between the wire tips, current flowed between the tips

carried by the ions in the flame front. Current amplifiers produced a spike in the ionisation probe output signal. A typical ionisation probe is shown in Figure 2.9.

The ionisation probes in the quiescent cell were located 40 mm and 70 mm perpendicularly from the wall-mounted spark plug (i.e. at the centre of the cell and 10 mm from the wall opposite the spark plug). The probes in the turbulent cell were 40 mm and 60 mm (2.5 mm from the wall) from the spark gap as can be seen in Figure 2.3. When placed at these known locations in the combustion cells, the times of the current pulses through the ionisation probes were measured to determine flame arrival times. This diagnostic was compared with flame and pressure deduced times for equivalent flame sizes.

Light emission measurements were made using a photomultiplier in the turbulent combustion cell. A 431.5 nm optical band pass filter was used to allow only the blue light given off by the CH radical to reach the photomultiplier. This resulted in an output signal from the photomultiplier that changed with the flame size of the burning mixture. The light given off by the flame was first randomized by diffusing it to ensure equal photomultiplier sensitivity to light from all areas of the cell. Then the light was gathered using an optical lens to produce an unfocused image on the photocathode. The system sensitivity was regulated by varying an iris aperture and the cathode voltage in the photomultiplier tube. The photomultiplier tube was set up as shown in Figure 2.10.

Past research has shown that the early light emissions are related to the subsequent burning rate of a hydrocarbon mixture [28]. Using a photomultiplier

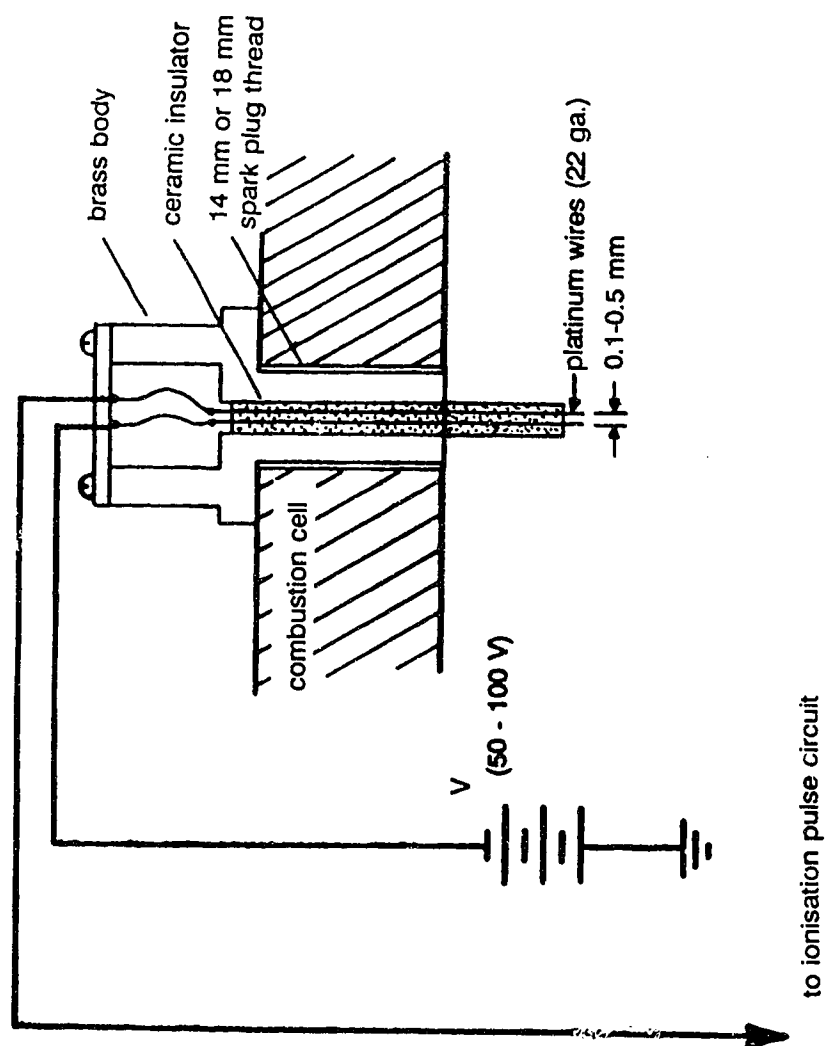


Figure 2.9 A typical ionisation probe.

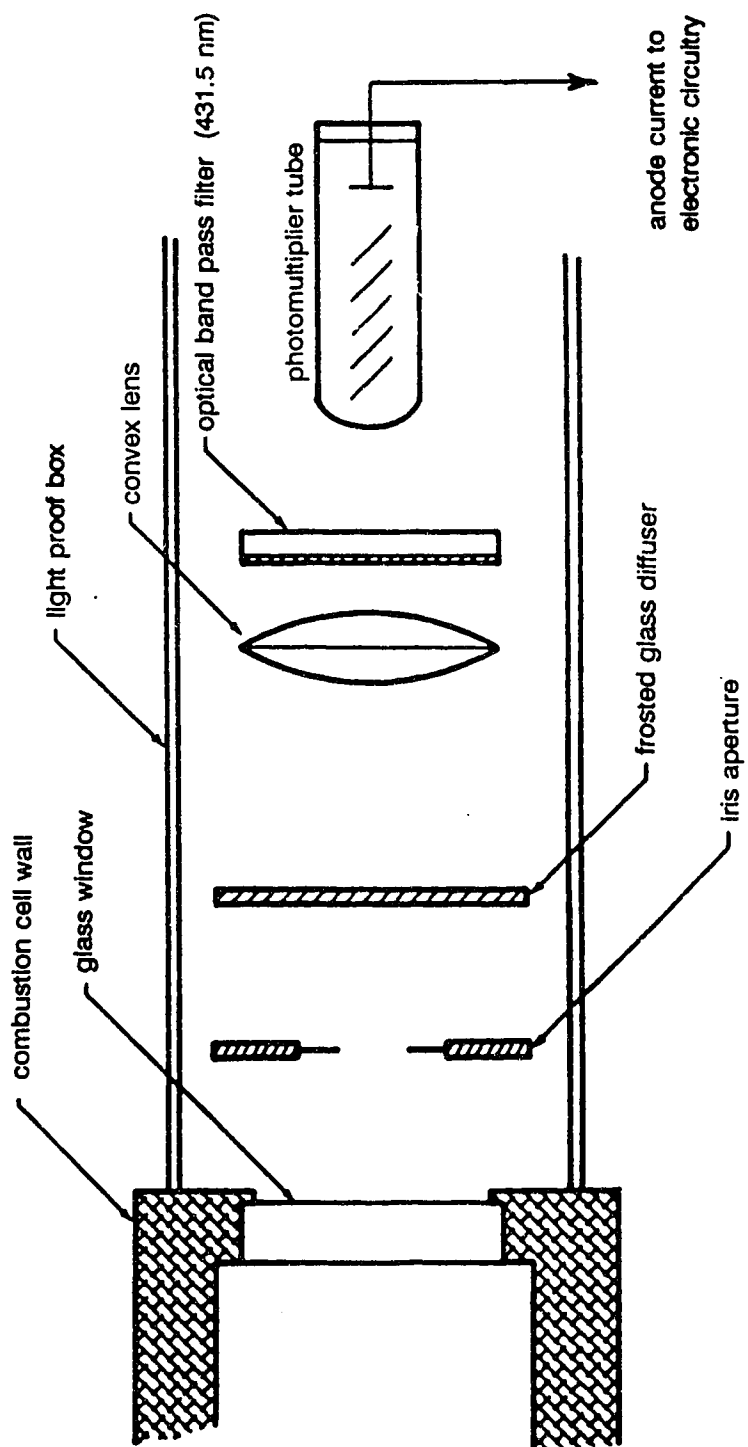


Figure 2.10 The photomultiplier apparatus.

set-up as just described, McDonell [22] has shown that light emissions levels are strongly related to the area of the flame. Throughout these tests, the photomultiplier sensitivity varied dramatically and repeatability was poor. Due to this variability, this technique of studying flame growth was found to be much less accurate than the others used and hence, was not studied further.

2.7 Ignition Systems and Spark Discharge Modes

In addition to a standard transistor-switched coil ignition system, two enhanced ignition systems were used in this study. The general requirements of an ignition system and characteristics of an ignition spark will be discussed here. The details of these ignition systems will be discussed in Section 4.2.

An ignition system must be capable of delivering energy in the form of an electrical spark to the mixture within the combustion chamber of an engine. There is a minimum quantity of energy that will cause the fuel - air mixture to ignite and perpetuate the combustion reaction. This minimum quantity depends on the following factors:

- chemistry of the mixture (fuel type, mixture strength, etc.),
- the flow field within the combustion chamber (turbulence),
- the type of spark plug being used, and
- the rate at which the energy is delivered.

Lewis and von Elbe [29] list minimum ignition energies for quiescent methane - air mixtures ($\phi = 1.0$) to be 0.45 mJ.

Having met the minimum ignition energy requirement, an ignition system can play an important role in the flame development period, and possibly the burn duration and the burning velocity of a mixture. The amount of energy delivered and the duration of the energy delivery have both been shown to influence combustion of a mixture [30]. More recently, the rate of energy delivery has been investigated [11]. Energy delivery rate is closely related to the modes of spark discharge which are shown in Table 2.4 along with their durations and efficiencies [8, 31]. Efficiency is defined as the fraction of the total energy delivered to the spark gap that is imparted to the mixture.

Table 2.4 Spark discharge modes.

Discharge Mode	Typical Duration	Typical Efficiency
breakdown	20 ns	94%
arc	1 μ s	50%
glow	1 ms	30%

Standard coil-based ignition systems typically deliver most of their energy in the inefficient glow discharge phase because of their slow spark delivery [14]. It would be very beneficial to deliver a spark in a short duration so that most of its energy could be discharged in the highly efficient breakdown mode or in the arc mode. The enhanced ignition systems used in this investigation made use of these more efficient spark discharge modes.

3 COLLECTION AND ANALYSIS OF DATA

In the following sections, the data acquisition system and numerical smoothing will be discussed. In addition, flame growth diagnostics which include photographic, ionisation probe, and pressure based measurements will be compared.

3.1 Data Acquisition System

The experiments in this study required a high speed data acquisition system to analyze combustion events which only last tens of milliseconds. Experimental data were first recorded in analog form then converted to digital form. Calculations were performed using the data in a digital form. The data acquisition system is shown schematically in Figure 3.1.

Analog data were recorded and stored on magnetic tape using a four channel, Racal Store 4DS, FM tape recorder. The analog output from pressure transducers, photodetectors, ionisation sensors, and other devices were recorded on the four channels of magnetic tape. The input range on each of the four channels was selected to provide a maximum signal-to-noise ratio and the best measurement resolution for the signal being recorded.

After completion of an experiment or set of experiments, the stored analog data were digitized using a Data Translation DT 2782, eight channel, analog to digital, 12 bit converter. This converter was operated at 25 kHz and was part of

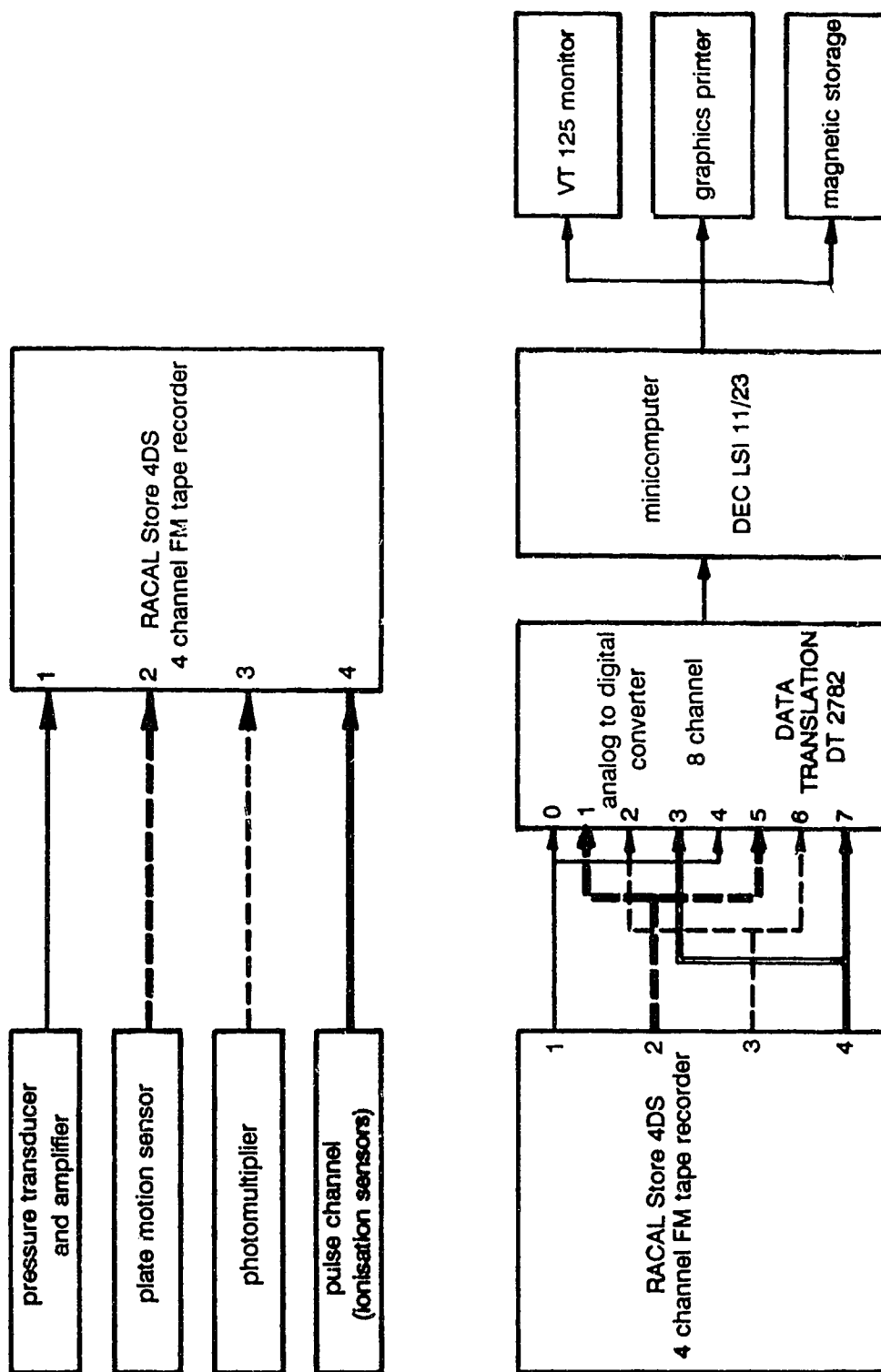


Figure 3.1 Data acquisition system.

a DEC LSI-11/23 minicomputer. The recording speed of 30 inches per second (ips) was reduced to one eighth ($3\frac{3}{4}$ ips) during digitisation. This provided a total effective data acquisition rate of 200 kHz, that is, 50 kHz per tape recorded channel -- a $20\ \mu\text{s}$ time resolution.

The A/D system was calibrated by recording two known d.c. voltage signals onto the magnetic tape after the input ranges were selected. These signals were later used to provide an overall calibration for each channel of the FM tape recorder and each A/D channel of the computer. These linear calibrations provided an offset in integers and a slope in integers/V for each channel. Once the data had been converted to a digital format, they were adjusted to store actual pressures and voltages using pressure (V/kPa) and digital (integers/V) calibrations.

The time scale was compressed by an integer factor so that only 512 integer data points containing the relevant pressure information were stored. A similar compression was performed for the light emission data. Compression to 512 points was done so that experimental runs could be represented by standard data files which were all the same size. The standard data file contained 512 pressure integers (in $\text{kPa} \times 10$), 512 light emission integers (in mV), and 256 integers containing coded information about the experiment. Integer data were used so that they could be stored in a compact binary format for bulk data storage if necessary. The standard data files at this time were ready to be used by specially developed computer software written in BASIC and FORTRAN languages. Many of the integer data files were transferred from the LSI-11/23

minicomputer to an IBM PC-XT compatible computer where subsequent analysis of results took place. This was done to take advantage of the software available on the PC.

There were two reasons for first recording an analog signal on magnetic tape and then playing back rather than directly recording digitally. An eight-fold increase in effective data acquisition rate (50 kHz vs. 6.25 kHz) was obtained by recording data at a high tape speed then reducing the playback speed. This faster data acquisition rate was required to give a time resolution of 20 μ s. The other reason for recording on magnetic tape is for electrical noise isolation. Digital computers tend to be affected adversely or fail due to electrical noise when operating adjacent to the very high voltage and current associated with enhanced ignition systems. By recording the data first, this helped isolate the digital computer from electrical noise.

3.2 Numerical Smoothing

Numerical calculations using unsmoothed digital data may lead to erroneous results. The cause of the error is the electrical noise present in analog signals that have been digitized. Although often small compared to the value of the signal, this noise is a digital discontinuity and may cause errors in calculations such as differentiation. Numerical smoothing using a simple averaging technique was used to reduce signal noise without changing the effective signal. Equation 3.1 is the method used.

$$Smoothed_i = \frac{\sum_{n=i-w}^{n=i+w} Unsmoothed_n}{2w + 1} \quad (3.1)$$

In Equation 3.1, w is the averaging width or number of points on each side of point i to be used in calculating the new average value for point i .

This type of simple smoothing was chosen over a more sophisticated numerical filter because of its rugged characteristics. It works on any frequency signal and will smooth any amount of noise. Although the resulting smoothed signal may be slightly altered, the use of this simple filter is very predictable.

3.2.1 Effects of Numerical Smoothing

An example will be discussed in this section to illustrate the effect of numerical smoothing on a digital signal. Subsequent calculations using that signal will also be examined. The example will use a digital pressure signal to calculate a non-linear function of pressure -- the turbulent to laminar burning velocity ratio (S_T/S_L).

A digitized pressure signal shown in Figure 3.2 usually contains some electrical noise, especially near the time of 0 ms where the spark occurs. A pressure signal free of apparent noise is obtained by smoothing this signal twice using $w = 10$. This smoothed signal is also shown in Figure 3.2. At first glance, there appears not to be too large a difference between the unsmoothed and

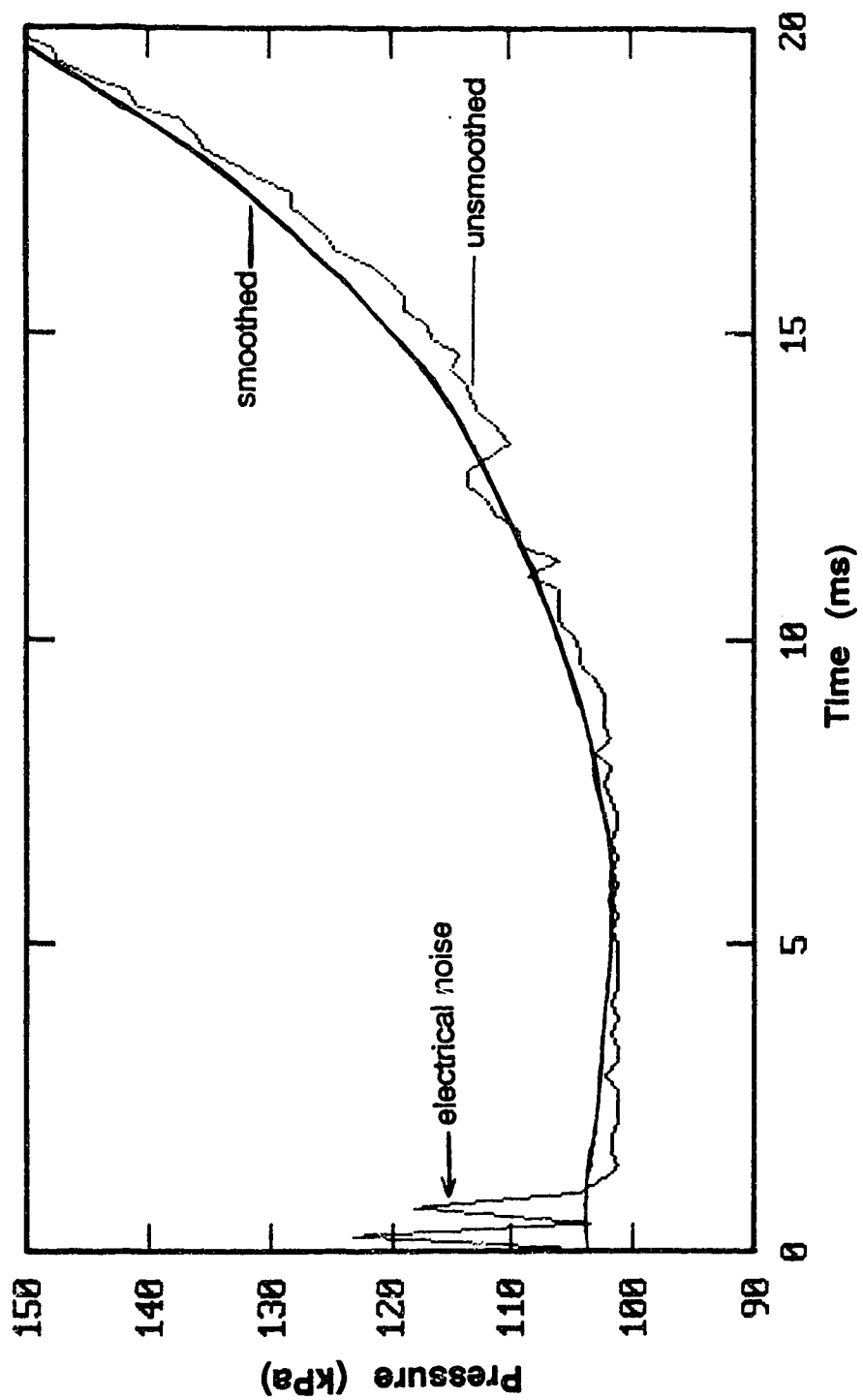


Figure 3.2 An unsmoothed and a smoothed pressure trace.

smoothed pressures. When examined closely, the spark noise present in the unsmoothed signal tended to raise all the early pressure values (0 ms to 5 ms) of the smoothed pressure signal. The pressure decreased over the first 5 ms. This is physically untrue during these combustion reactions since pressure must rise. The apparent decrease is due to smoothing the spark noise.

In calculating a non-linear function of pressure, S_T/S_L , from the unsmoothed pressure signal, the noise can be amplified. S_T/S_L calculations are similar in form to Equations 3.3 and 3.4 in Section 3.3.3.1. Amplification of signal noise is illustrated in Figure 3.3 which was calculated from the unsmoothed pressure signal in Figure 3.2. It is very difficult to extract information from this figure because of the amplification of pressure signal noise.

S_T/S_L calculated from the smoothed pressure signal in Figure 3.2 results in smoother calculated results as shown in Figure 3.4. Accuracy of this curve is suspect since numerical smoothing altered the original pressure signal.

The calculations in this study did not implement signal smoothing until the final calculations had been completed. The S_T/S_L curve from Figure 3.3 has been smoothed using the same method as was used for pressure, and is shown in Figure 3.5. There is a difference resulting from when the smoothing takes place which can be seen by comparing Figures 3.4 and 3.5. In this case, the difference is most apparent near a relative flame radius (r_b/r_{cell}) of 0.5. Since the original digitised pressure signal was retained through all the calculations in Figure 3.5, it had less error than if the smoothed and thus altered pressure signal had been

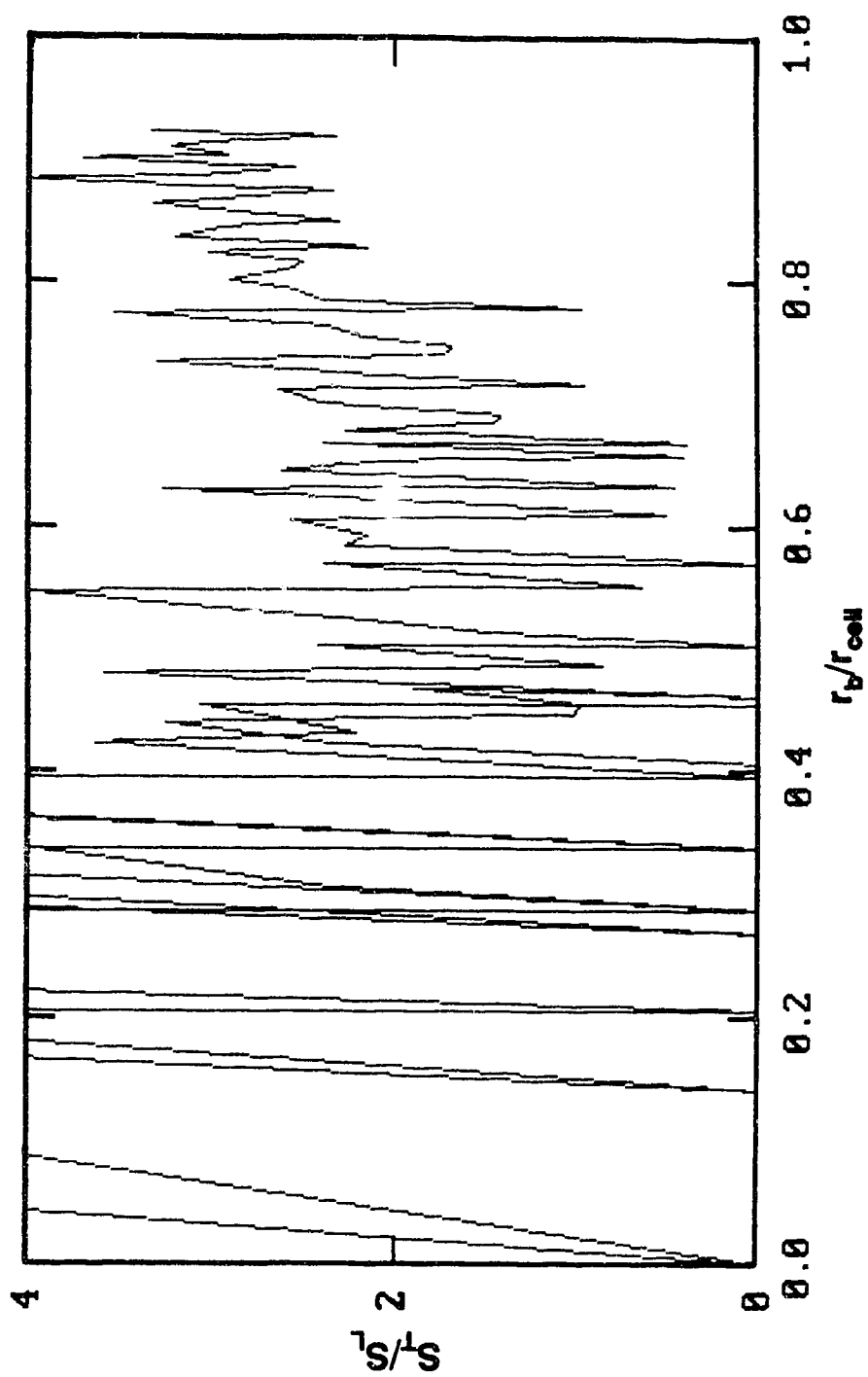


Figure 3.3 Turbulent/laminar flame speed ratio based on an unsmoothed pressure trace.

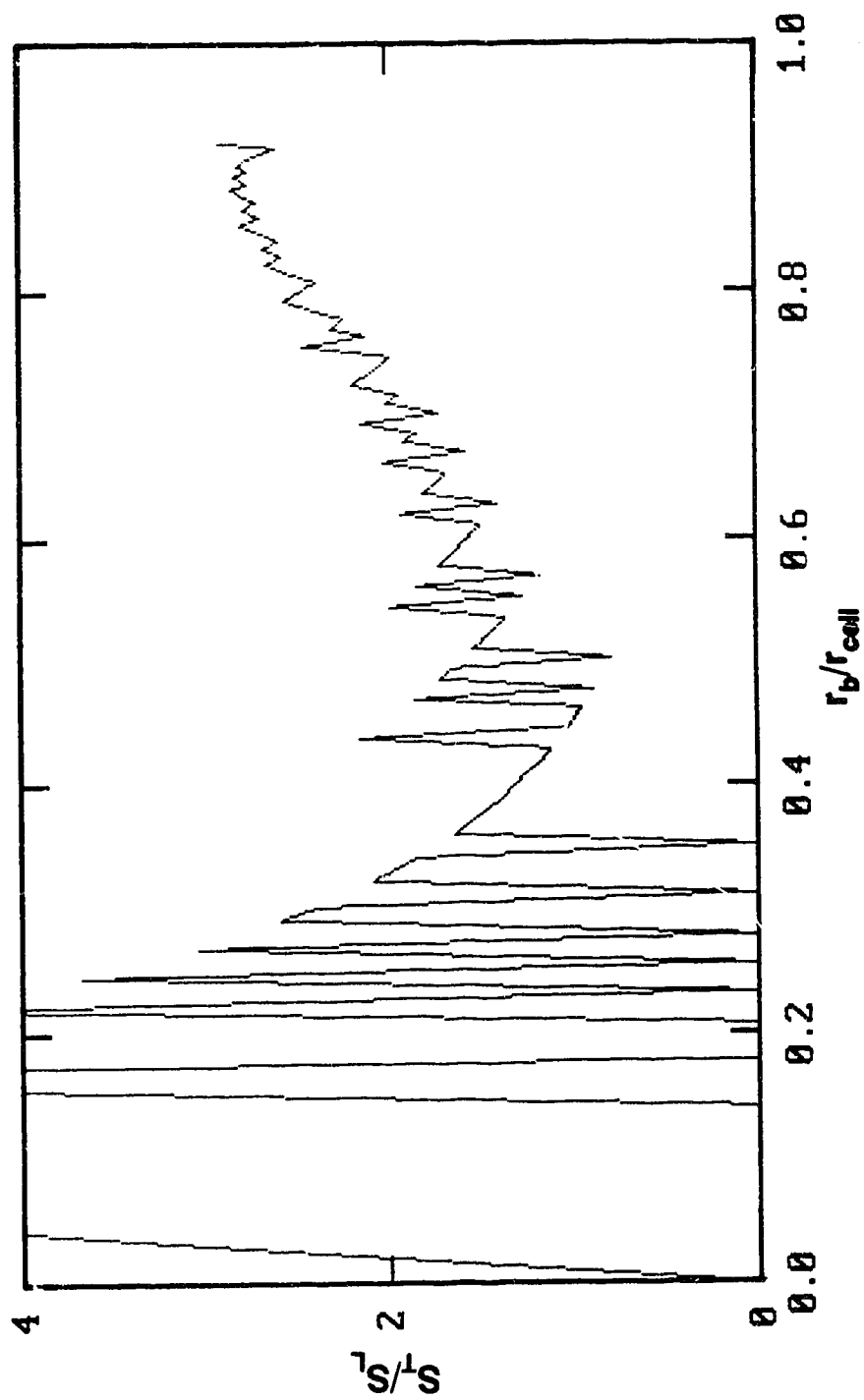


Figure 3.4 Turbulent/laminar flame speed ratio based on a smoothed (numerically filtered) pressure trace.

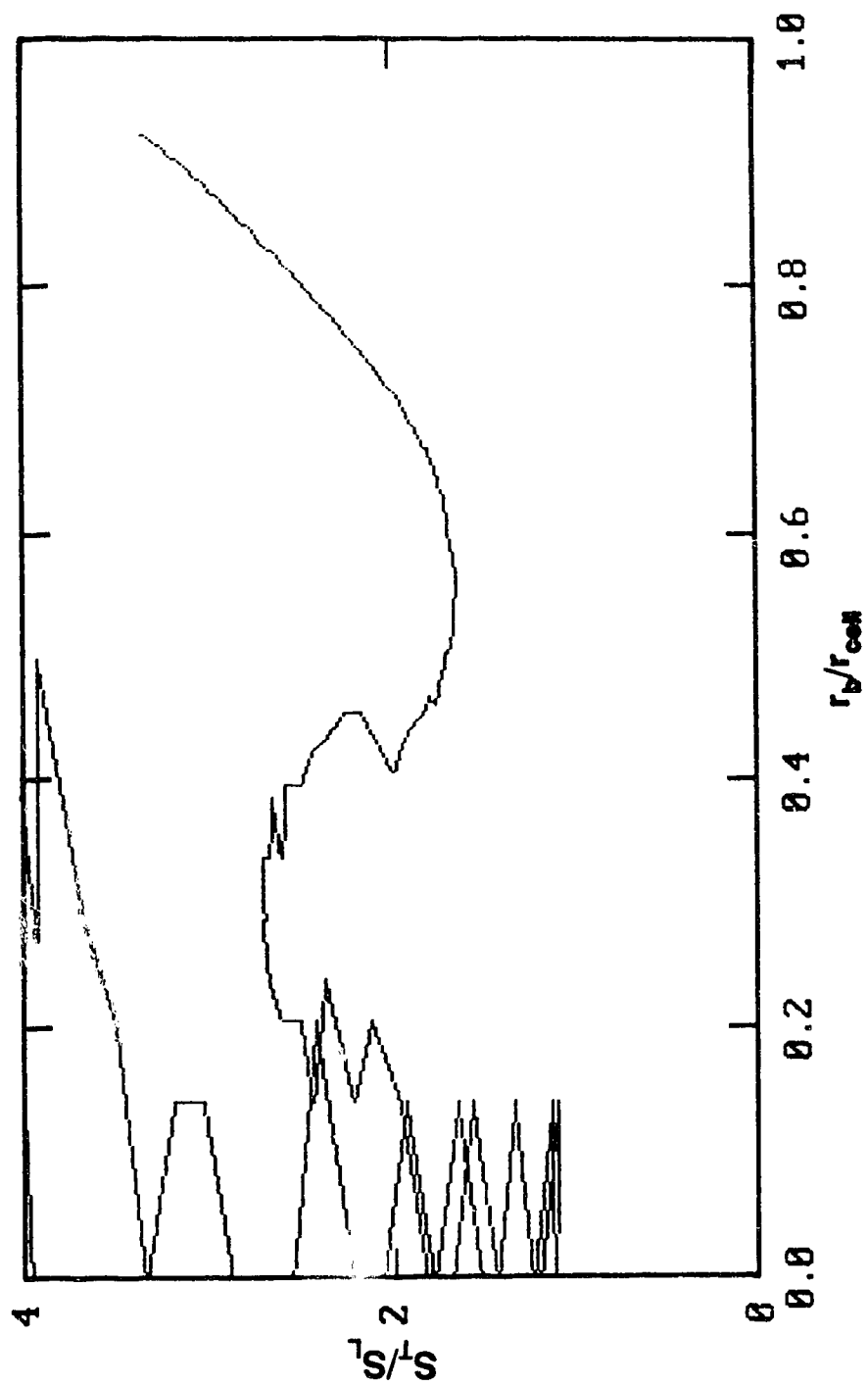


Figure 3.5 A smoothed turbulent/laminar flame speed ratio based on an unsmoothed pressure trace.

used through all calculations.

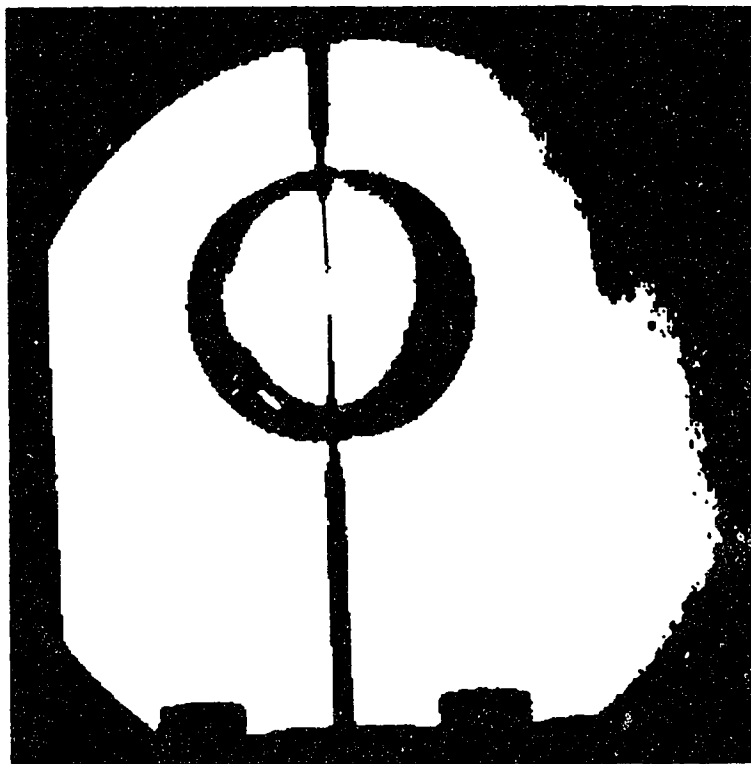
3.3 Flame Growth Diagnostics

Flame growth rates and thus burning velocities were determined by schlieren photography, by ionisation probe flame arrival times, and by pressure traces. These will now be described and compared.

3.3.1 Flame Growth From Schlieren Photography Measurements

High speed schlieren cinematography was used as the standard for measuring flame radius. The principle and set-up of the schlieren photography system were described in Section 2.5. The camera speed was 1000 frames per second, resulting in a 1 ms time resolution. This speed was limited by the system sensitivity based on the light source intensity. Flame radii were measured directly from the film along spark kernel centres using a microdensitometer. Flame volumes could be calculated from the radii. Each flame was assumed to be spherical which is a reasonable assumption except for spark kernels less than 3 mm diameter or when the flame is near the wall. A spherical shape is seen in a digitally enhanced schlieren image of a typical quiescent flame shown in Figure 3.6.

Since the schlieren image is based on a density gradient, the flame image coincides with a point just before the leading edge of the visible flame. These photographic data could also be used to calculate burning velocities using



$\phi = 0.85$
quiescent
turbulent (cubical) cell
 $t = 10 \text{ ms}$
 $r_b = 19.9 \text{ mm}$

Figure 3.6 A digitally enhanced, high-contrast image of a typical schlieren photograph.

calculated volume expansion factors from the thermodynamic equilibrium model which will be described later in this chapter.

3.3.2 Flame Growth From Ionisation Probe Measurements

Times of flame arrival at the ionisation probes, described in Section 2.6, were used to directly measure the arrival of the flame front at certain fixed points within the combustion cell. Ionisation probe locations were also given in section 2.6. These flame arrival times were used to calculate the average flame growth rate over the distance between two fixed points. Since ionisation probes rely on ions in a burning flame for current to flow, ionisation probe measurements were expected to coincide with the leading edge of the flame passing the probe tips.

The flame growth rates calculated from flame arrival times represented an average over a large change in flame radius. This span included periods where the flame may have still been in its developmental stage. It also included periods where the flame was influenced by its arrival at the cell wall. Part of a spherical flame first touches the wall at 80% of the equivalent cell radius. Overall, the ionisation probe measurements only provided a rough confirmation of average flame growth rates.

3.3.3 Flame Growth From Models Based on Pressure Trace

Experimentally measured pressure traces were used to calculate burning velocities using the following three models: Lewis and von Elbe model, Dabora

model, and multi-zone thermodynamic equilibrium model. These models will be described and compared in the following subsections.

3.3.3.1 Lewis and von Elbe and Dabora Models

Lewis and von Elbe [29] proposed a relationship which derived burning velocity from a pressure record. This method assumes:

- a) combustion propagates isotropically forming two concentric spherical zones (burned gases and unburned gases) with an abrupt interface (i.e. an interface with no mass or volume),
- b) properties are uniform within each zone,
- c) pressure and temperature rise according to adiabatic compression and that no heat is transferred to the vessel walls,
- d) a temperature difference is developed between the burned gases and unburned gases, and
- e) pressure throughout the vessel is uniform.

The mass fraction burned, mf_b , is proportional to the fractional pressure rise as in Equation 3.2,

$$mf_b = \frac{P - P_i}{P_o - P_i} \quad (3.2)$$

where: P = instantaneous pressure,
 P_i = initial pressure, and
 P_o = final pressure.

The burning velocity is expressed using the Lewis and von Elbe model as shown in Equations 3.3a and 3.3b. Equation 3.3a is a general description of burning velocity in terms of flame size in a spherical cell while Equation 3.3b substitutes quantities from the Lewis and von Elbe model.

$$S_u = \frac{dr_l}{dt} \left(\frac{r_l}{r_b} \right)^2 \left(\frac{P_l}{P} \right)^{\frac{1}{\gamma_u}} \quad (3.3a)$$

where: S_u = burning velocity,
 r_l = the nominal radius of burned gases in their unburned state,
 r_b = the burned radius,
 γ_u = the specific heat ratio of the unburned gases.

In terms of pressure only,

$$S_u = \frac{r_{cell}}{3(P_\theta - P_l)} \frac{dP}{dt} \left(\frac{P_l}{P} \right)^{\frac{1}{\gamma_u}} \left(1 - \left(\frac{P_\theta - P}{P_\theta - P_l} \right) \left(\frac{P_l}{P} \right)^{\frac{1}{\gamma_u}} \right)^{-\frac{2}{3}} \quad (3.3b)$$

where: r_{cell} = the hydraulic radius or equivalent spherical radius of the combustion cell.

This model has been used with acceptable accuracy since the assumptions are reasonable. Its accuracy will be discussed and compared with other models in Section 3.3.4.

The relationship given by Dabora [32] is based on assumptions similar to those of Lewis and von Elbe. However, it was developed for a flat disk-shaped combustion cell. It assumes that the flame kernel develops as a cylinder with the same axial length as the cell. The combustion cell used in this study had a much

lower diameter/length ratio so the flame was more spherical. It was expected that calculated burning velocities using Dabora's correlation would be high because the flame was only assumed to grow in two dimensions and not in three dimensions as would really occur. With an actual flame increasing geometrically in three dimensions, this model would lead to a greater calculated burning velocity. The Dabora burning velocity relationship is:

$$S_u = \frac{\gamma_u r_{coll} \frac{d}{dt} \left(\frac{r_b}{r_{coll}} \right)}{\gamma_u - 1 + \frac{P_e}{P}} \quad (3.4)$$

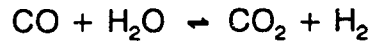
where,

$$\frac{r_b}{r_{coll}} = \sqrt{\frac{\left(\frac{P - P_l}{P_e - P_l} \right) + \left(\frac{P}{P_l} \right)^{\frac{1}{\gamma_u}} - 1}{\left(\frac{P}{P_l} \right)^{\frac{1}{\gamma_u}}}} \quad (3.5)$$

3.3.3.2 The Multi-zone Thermodynamic Equilibrium Model

Flame growth and burning velocity data were also calculated from pressure traces using a multi-zone thermodynamic equilibrium model. The unburned gases

were treated as a mixture of pure fuel (CH_4 in this case) and air (considered to be 21% oxygen and 79% nitrogen). The burned gases were represented by six species (CO , CO_2 , O_2 , N_2 , H_2 , and H_2O). All of the mixture components and combustion products were treated as ideal gases using properties defined by the equations of Benson [33]. The model accounted for dissociation reactions in terms of the following carbon dioxide dissociation and water-gas reactions:



It was found that these dissociation reactions represented the energy and species effects on combustion with reasonable accuracy. For a more detailed representation of minor species, a more refined series of reactions would be required.

The combustible mixture was split into 1500 zones or elements, each containing an equal fraction of the total mass. Each zone reacted sequentially to produce a pressure rise for a given mass fraction burned. As each zone reacted, its equilibrium composition, temperature, and pressure were calculated using an iterative scheme. The flow chart in Figure 3.7 shows the operation of the multi-zone thermodynamic equilibrium model. Starting with a pressure estimate for a given element, the volume and energy properties for all the previously burned elements and all the unburned elements were calculated. Then, properties of the burning element were determined while considering the work required to compress all of the non-reacting zones to the new estimated pressure. The

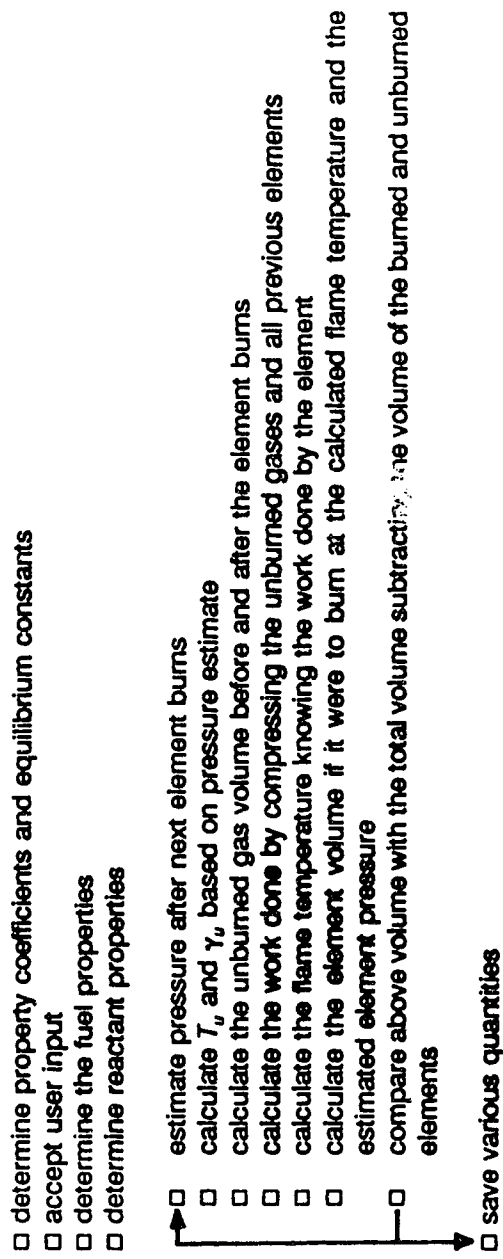


Figure 3.7 Operation of the multi-zone thermodynamic equilibrium model.

pressure iteration was deemed correct if the calculated sum of all the element volumes was equal to the total volume of the cell. Heat transfer between zones and between unburned gases and the wall was neglected.

It was possible with this model to allow equilibrium compositions to change in the burned elements due to temperature rises from isentropic compression. This only resulted in a 0.9% difference in calculated pressure, up to the period of wall contact, from when each zone is held constant and is not allowed to react -- frozen equilibrium. Requiring four to five times more computational time, allowing the equilibrium composition to change resulted in negligible changes in flame size calculations. Therefore, equilibrium was frozen for model calculations in this study.

The model provided flame growth in terms of volume burned or mass burned. These quantities were a function of pressure rise for a given set of initial conditions. Other calculated quantities (mf_b , ΔV_b , ΔV_u , T_b , T_u , γ_u) were stored with pressure and flame growth in a model data base.

To use this model, the pressure - flame growth relationship was interpolated onto an experimental pressure - time record to give burned mass and volume as a function of time. Depending on the assumed flame shape, spherical or hemispherical, the burned volume was used to calculate flame area as a function of time. From this, the burning velocity of the mixture was calculated. The equilibrium model determined flame size and various mixture properties corresponding to measured pressure data. All of the relevant data were stored in a data file for use by any of the subsequent data analysis programs.

As with any model, the calculated results were validated against a standard. The standard used in this study was the STANJAN computer model [34] which uses the method of element potentials and JANNAF data tables to calculate multi-component equilibrium compositions. The equilibrium model was compared with the STANJAN model using 16 product species for initial conditions of 101325 Pa, 293.15 K, and $\phi = 0.85$. Table 3.1 lists comparisons of properties between the multi-zone equilibrium model and the STANJAN model for 1/2000th of the total mass burned. Since the model essentially calculated volume and pressure for a given mass, density was a suitable property for comparison. The equilibrium model density was in error by less than 0.2% when compared with the STANJAN model that uses 16 species. This error is 1.5% if the compression work done on the other elements is ignored.

Table 3.1 Comparison between the equilibrium model and STANJAN.

	Equilibrium model	STANJAN 16 species	$\Delta\%$
P	101741	101741	-
T	2035	2065	1.5
ρ	167.0	164.5	1.5

3.3.4 Comparison of Flame Growth Diagnostics

As previously mentioned, the standard used for flame sizes were photographic measurements with an accuracy of ± 0.1 mm. The ionisation probe measurements provided a ± 1 mm indication of flame position but only average flame growth rates could be calculated.

The methods based on pressure trace described in Section 3.3.3 can be used to calculate flame growth rates and burning velocities. A major disadvantage of all these methods is that they have poor sensitivity during the early period of combustion when the pressure rise is only 1 or 2 kPa. This early combustion period is where most of the effects of ignition systems are expected to occur. The signal level (ΔP) and the noise level are roughly the same magnitude when the pressure rise is small during the early stages of combustion. The error in flame radius was high, ± 5 mm, during these small pressure rises. The signal-to-noise ratio became high enough (20:1 or higher) to produce accurate flame radius calculations (± 0.5 mm) once the pressure had risen above 120 kPa.

One drawback to the Lewis and von Elbe method and the Dabora method is that the adiabatic and two-zone assumptions are only acceptable for small pressure rises, as seen during the early combustion period, until the flame reaches the wall. This is not a problem with the multi-zone equilibrium model where the assumptions remain acceptable during the later stages of combustion. It should be noted that all of the models remained inaccurate for pressures below 120 kPa.

As discussed earlier, the Dabora model assumes two dimensional flame growth while real flame growth is in three dimensions. This results in calculated burning velocities being high for the Dabora model. The real flame area is higher than the assumed flame area. Depending on the burned radius and axial cell length, the real flame area could be double the flame area assumed by the Dabora model. When compared with photographically measured values, the equilibrium model and the Lewis and von Elbe model predict flame growth, and thus burning velocity, with equivalent accuracy. It is expected that the equilibrium model will remain more accurate when pressures become higher. A calculated flame growth comparison between the three models and the photographically measured values is shown in Figure 3.8. The Dabora model is about 20% low in its flame size calculations at low pressures. A smaller calculated flame size results in a smaller flame area and higher burning velocity -- exactly as expected when using the Dabora model. The multi-zone thermodynamic equilibrium model was used to measure flame growth rate and burning velocity in most of this study. As the standard, schlieren photographic results were used periodically to confirm the equilibrium model results, to provide results for the early stages of combustion, and to show flame structure.

To determine error sources for the Lewis and von Elbe model, its calculated mass fraction burned, mf_b , was compared with that of the equilibrium model. The assumption that the mass fraction burned is proportional to the fractional pressure rise as in Equation 3.2 by the Lewis and von Elbe burning

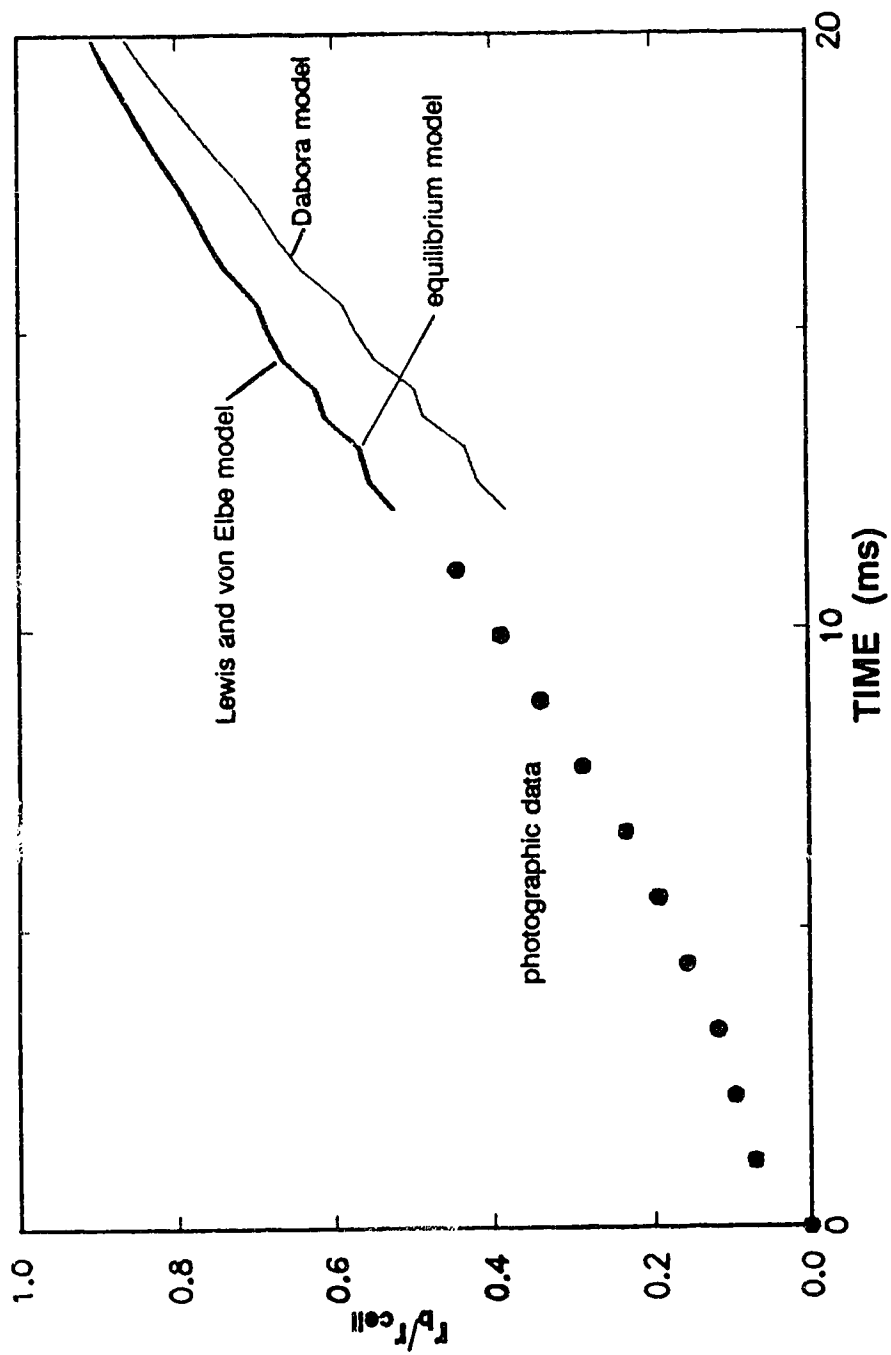


Figure 3.8 Comparison of the equilibrium model, the Lewis and von Elbe model, and the Dabora model with the photographic data standard.

velocity relationship is 5% higher than that calculated by the multi-zone equilibrium model. However, using the measured end pressure instead of the adiabatic end pressure, the mass fraction burned is 25% higher. Not knowing the correct adiabatic end pressure may cause erroneous results with the Lewis and von Elbe model. Figure 3.9 compares the mass fraction burned with pressure for the proportional relationship of Equation 3.2 and that calculated by the multi-zone equilibrium model.

Several of the previously discussed methods used in calculating burning velocity were compared with the accepted equilibrium model results for an equivalence ratio of 0.95 using a standard ignition system in the quiescent combustion cell with a wall-mounted spark plug. The comparison is shown in Figure 3.10. The meaningful range of burning velocities were measured between 50% and 80% of the cell radius. The signal-to-noise ratio was too small with the pressure transducer used to get an accurate indication of burning velocity below 50% of the effective cell radius. Above 80% of the effective cell radius, the flame was too close to the wall. In fact, parts of a spherical flame begin to contact the wall at 80% of r_{cell} .

The equilibrium model results were not used in the initial parts of this study because the model was not fully developed until late in the experimental program. Therefore, the Lewis and von Elbe method was used for the initial ignition system comparisons. As shown in Figure 3.10, its flame growth and burning velocity calculations were more than adequate for relative comparison.

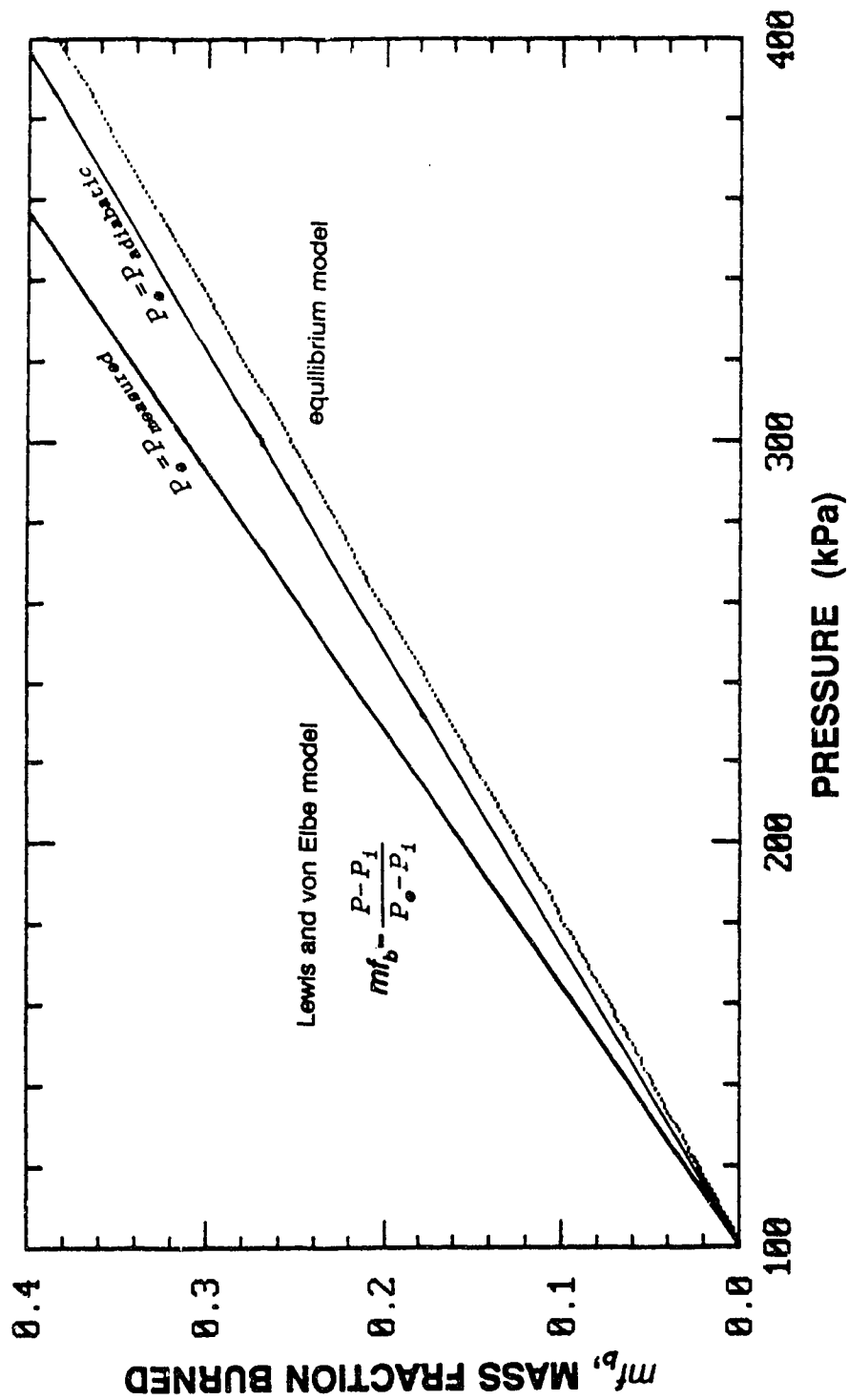


Figure 3.9 Mass fraction burned comparison between the equilibrium model and the Lewis and von Elbe model.

The burning velocity calculated using the Dabora method was about 30% higher than that of Lewis and von Elbe. This was expected due to the assumption of a cylindrical flame shape which under-estimates active flame area with the Dabora model. According to Andrews and Bradley [2], the expected burning velocity of a $\phi = 0.95$ methane-air mixture is 0.325 m/s as measured from a nozzle burner. Using an average of instantaneous burning velocities at 200 kPa and 250 kPa, the equilibrium model calculated the burning velocity to be 0.214 m/s. This equilibrium model value is 34% lower than the reported value [2]. The large discrepancy between the values in Figure 3.10 and the published value can be attributed to the following: 1) burning velocity decreases with increases of pressure, as the equilibrium model shows, 2) heat loss to the wall with side ignition, and 3) the assumed flame shape. All of these models have assumed that heat loss can be neglected which is not a bad assumption for a flame growing in the centre of a combustion cell, but for a flame growing against a wall, it is a poor assumption. As well, these models have assumed that the flame grows spherically; however, the actual growth shape for an ideal flat sidewall ignition source would be hemispherical.

A comparison of several properties of spherically and hemispherically growing flames can be made. As shown in Figure 3.11, a spherically growing flame has a larger active flame area for a given burned volume than a hemispherically growing flame that is quenched against a wall. For a given burned volume or pressure rise, an assumed hemisphere has a radius larger by $\sqrt[3]{2}$ but

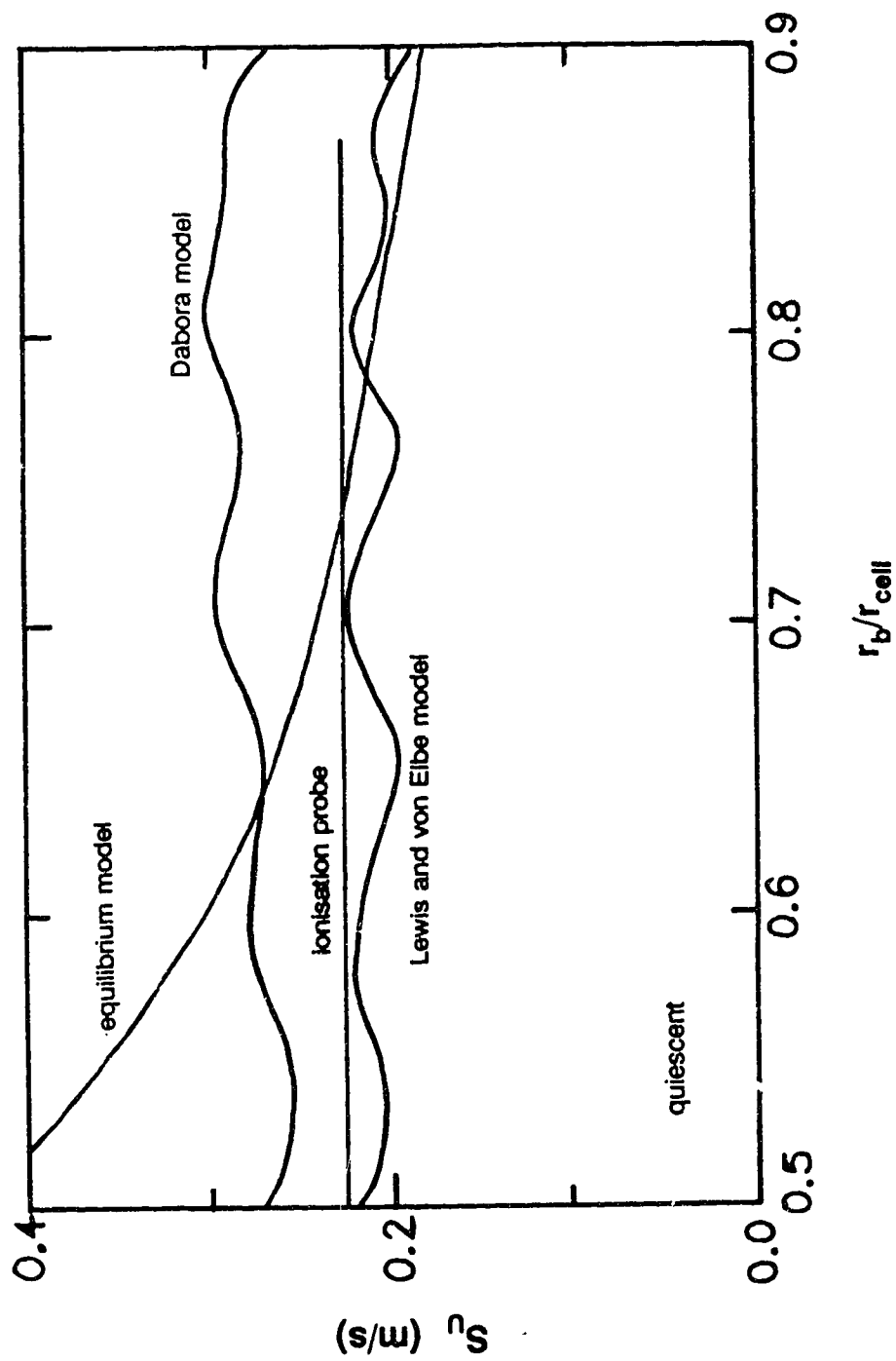
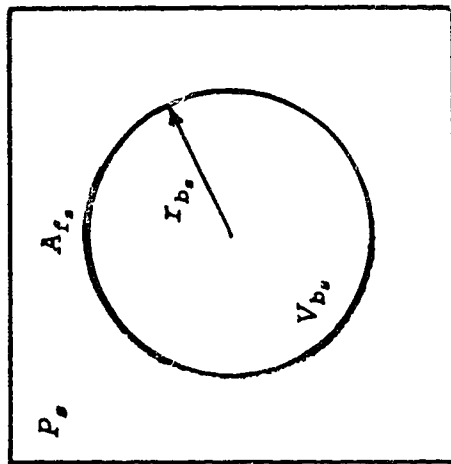


Figure 3.10 A comparison of various methods used for burning velocity calculations with the equilibrium model standard ($S_u = 0.216$ m/s).



Compare volume:

$$\text{For the same pressure } (P_s = P_h), \quad V_{b_s} - V_{b_h} = \frac{4}{3} \pi r_{b_s}^3 - \frac{2}{3} \pi r_{b_h}^3 = \frac{2}{3} \pi (r_{b_s}^3 - r_{b_h}^3)$$

Compare flame area:

$$\frac{A_{f_s}}{A_{f_h}} = \frac{4 \pi r_{b_s}^2}{2 \pi r_{b_h}^2} = \frac{2 r_{b_s}^2}{r_{b_h}^2} = \frac{r_{b_s}^2}{r_{b_h}^2}$$

Compare burning velocity:

$$\frac{S_{u_s}}{S_{u_h}} = \frac{\left(\frac{\Delta V}{\Delta t} \right)_{f_s}}{\left(\frac{\Delta V}{\Delta t} \right)_{f_h}} = \frac{A_{f_s}}{A_{f_h}} \cdot \frac{1}{\sqrt{2}}$$

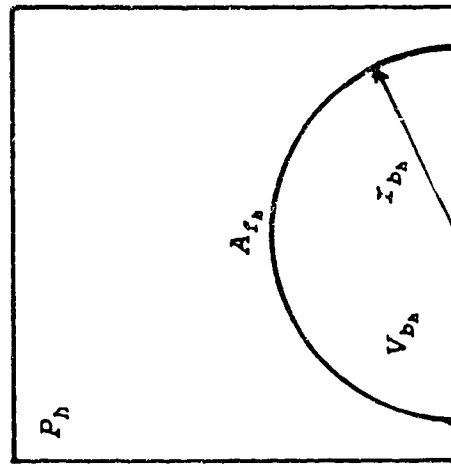


Figure 3.11 Illustration of differences between spherical and hemispherical flame shapes.

an active flame area smaller by $\sqrt[3]{2}$. The result is that inferred burning velocity is smaller by $\sqrt[3]{2}$ for an assumed sphere. Much of the discrepancy between the published and measured burning velocity in Figure 3.10 can be accounted for by the assumed shape error. The flames growing against walls in the cylindrical quiescent combustion cell are not truly hemispherical because the walls are not flat.

4 EFFECTS OF ENHANCED IGNITION SYSTEMS IN QUIESCENT MIXTURES

4.1 Overview of Enhanced Ignition Systems

Much of the experimental work done in this investigation involved the use of high energy, enhanced ignition systems. Enhanced ignition systems deliver more energy or higher power to a combustible mixture. Benefits of such systems and the testing methods used to determine their effects will be described in this chapter.

4.1.1 Benefits of Enhanced Ignition Systems

The classic reason for using more powerful ignition systems on operating spark ignition engines was to reduce the cyclic variations in pressure or burning time which occur as the lean operating limit of the engine is approached. These variations are due to misfire or partial burning¹ and can usually be reduced by increasing the early growth rate of the flame kernel [54-57]. For an operating spark ignition engine, reducing these cyclic variations or increasing the early flame growth rate makes the engine run more smoothly and efficiently with lower exhaust emission levels. Misfire or partial burn is usually caused by attempting to ignite either too lean a fuel - air mixture or an inhomogeneous mixture which is locally lean at the ignition point. This can be the case when high levels of exhaust gas

¹ Misfire is when an initial flame is not developed from the spark discharge. This initial flame is referred to as the flame kernel or ignition kernel. Partial burn is when a flame kernel is developed from the spark discharge but the mixture fails to completely burn.

recirculation, EGR, are used. Many researchers have recognized that misfire or partial burn of lean mixtures could be reduced by obtaining a higher energy spark over a longer duration and/or across a larger spark gap [e.g. 7, 30]. That is, the lean operating limit is extended by using a higher energy ignition system to decrease the early flame kernel development period.

Recently, benefits of using high energy, short duration enhanced ignition systems have become apparent. The very early flame development has been shown to be accelerated through large amounts of energy delivered to the combustible mixture by the ignition system [5, 8, 11, 14]. According to Anderson [11], high-energy, enhanced ignition systems may also increase the overall burning speed of combustible mixtures. Increases in burning velocity and increases in the rate of initial flame development both reduce the overall burning time.

Decreased burning time allows for an optimal combustion period in an engine, particularly if combustion is completed before significant volume expansion takes place. The result is higher cylinder pressures and more power. Compact or nearly constant volume combustion may result in higher temperatures and therefore higher burning speeds.

Lean mixtures have slow burning velocities [2, 3] which result in lower mixture temperatures as the expansion stroke takes place in an engine. Lower temperatures further reduce burning velocity. It is important to increase burning velocity or decrease burning times to their practical limits. Reducing the burning

time subsequently reduces the cyclic variations at some equivalence ratio near the lean limit, or for the same level of cyclic variations, the lean limit can be extended.

4.1.2 Overview of Enhanced Ignition System Testing in Quiescent Mixtures

Preliminary experiments were carried out in a quiescent combustion cell to evaluate the performance of four different ignition system - spark plug combinations. The quiescent combustion cell was used for enhanced ignition system performance evaluation because its side-wall mounted spark plug closely matches an engine spark plug configuration. The quiescent combustion cell, described in Section 2.2, was cylindrical in shape and allowed for quick spark plug and ignition system changes. The relative ease of use of the quiescent combustion cell made it more suitable for preliminary testing than the turbulent combustion cell. Experimental results obtained from these preliminary quiescent combustion cell tests served as a basis to establish a subsequent testing program for the turbulent combustion cell. To test a more practical application of the enhanced ignition systems, the turbulent combustion cell was then used to simulate the turbulent conditions found in an engine cylinder. The effects of turbulence characteristics on burning velocity (Chapter 5) and the effects of ignition system on burning velocities of turbulent mixtures (Chapter 6) were determined using the turbulent combustion cell.

4.2 Experimental Details of Enhanced Ignition System Testing

In this section, the ignition system - spark plug combinations which were tested will be described. The characteristics of the ignition systems and the spark plugs used will also be discussed.

4.2.1 Ignition System - Spark Plug Combinations

Three ignition circuits were tested -- one standard and two enhanced. As well, two spark plug types were tested with one of the enhanced ignition systems, resulting in four different ignition system - spark plug combinations. The four combinations tested are listed in Table 4.1.

Table 4.1 Ignition circuit - spark plug combinations.

System Name		Ignition Circuit	Spark Plug
1	ST/SG	standard inductive coil	surface gap
2	BD/SG	breakdown	surface gap
3	PJ/SG	plasma jet	surface gap
4	PJ/PJ	plasma jet	plasma jet cavity

Of the four systems tested, a standard, transistor-switched coil circuit was used to establish base-line performance criteria which could then be used to evaluate the performance of the two enhanced ignition circuits. The enhanced circuits were the high voltage breakdown and the plasma jet circuits. Both stored energy in

high voltage capacitors to supply more energy than the standard circuit. The breakdown ignition circuit stored 20 000 V in 2.7 nF of capacitance while the plasma jet circuit stored 1000 V in 2 μ F.

The same surface gap spark plug was used for all three circuits to provide equivalent initial conditions for all tests. The plasma jet circuit was also tested using a plasma jet cavity spark plug to evaluate the effect of spark plug configuration on the performance of that circuit. A plasma jet cavity spark plug is one where the spark forms in a recessed cylindrical cavity, thereby heating the gases to a very high temperature. The expansion of the gases causes them to jet out of the cavity into the combustion chamber. These spark plugs will be discussed further in Section 4.2.3.

4.2.2 Description and Characteristics of the Ignition Systems

For a better understanding of the systems used, simplified schematic block diagrams of the three ignition circuits are presented in Figure 4.1. A modular arrangement was used to create the various ignition systems by additions to a base unit. This also allowed for quick changes and comparisons to be made between the three ignition systems. The base unit was a standard inductive coil ignition system, typical of automotive engines of the 1960's and 1970's.

A plasma jet ignition system was formed by adding a high voltage capacitor and charging circuit to the spark gap of the standard ignition circuit. Since the energy was stored below the breakdown voltage of the spark gap, a standard

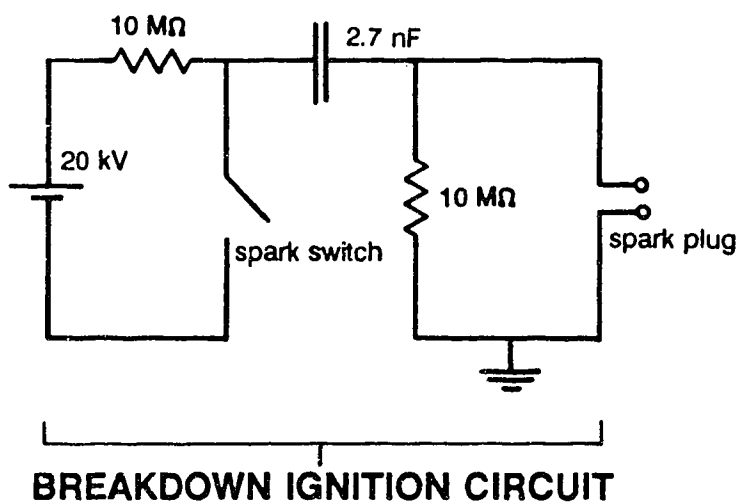
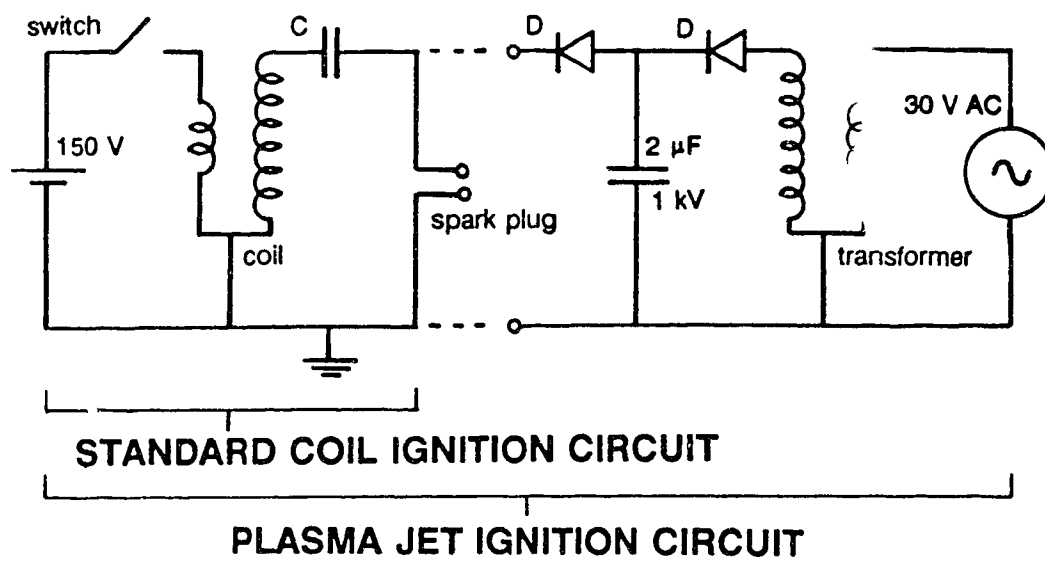
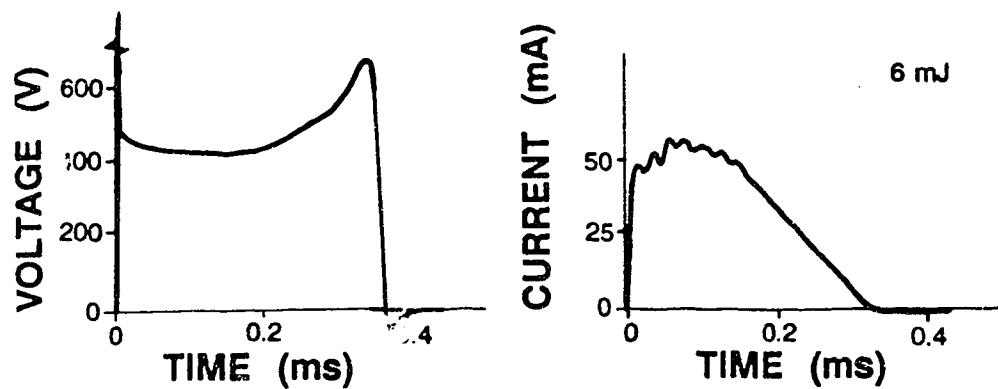


Figure 4.1 Schematics of the ignition circuits used.

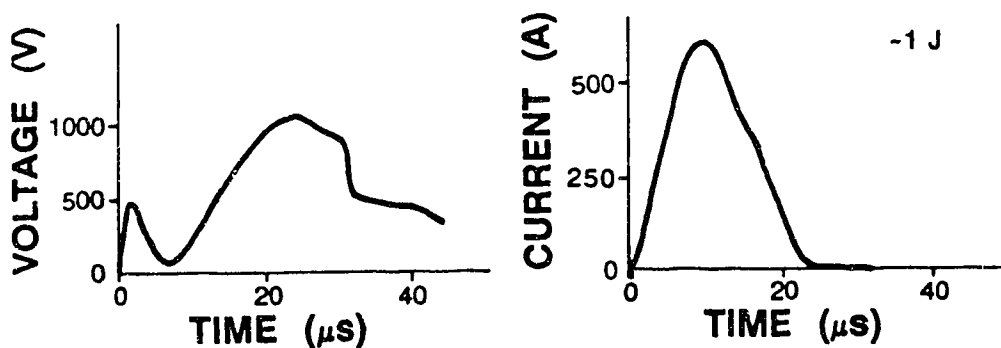
ignition circuit was used to supply a voltage spike to break down the spark gap. With this circuit, additional energy was stored in a capacitor ($2\ \mu\text{F}$) across the spark gap at about 1 kV. The energy delivered to the spark plug was about 1 J.

The breakdown ignition system circuit is different in that all of the energy is stored in a capacitor ($2.7\ \text{nF}$) at breakdown voltage levels which results in a very high voltage, short duration ignition spark. Because of the high voltage potentials used with this breakdown ignition system, a special spark switch was used to trigger the circuit. The plasma jet ignition circuit was used to fire a spark that bridged the switch gap in the breakdown ignition circuit. A normal contact type switch would not switch fast enough and would suffer from severe arcing and wear problems.

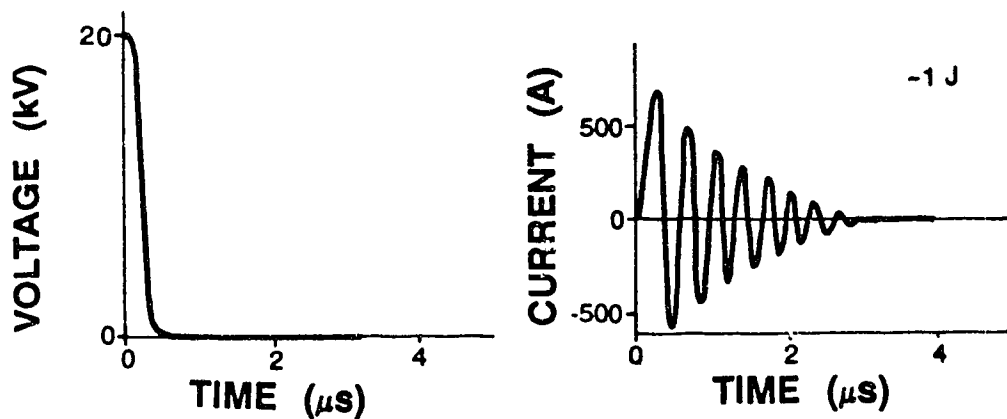
The spark characteristics for each of the above ignition systems must also be examined. Voltage and current traces were measured using a Tektronix P6015, 1000X, $100\ \text{M}\Omega$, voltage probe with compensating box and an Emerson Electronics model 411, wide band, current transformer. Typical spark characteristics (measured voltage and current traces) are shown in Figure 4.2. The spark durations are slightly different from those listed in Section 2.7 from Pischinger and Heywood [8] because of differences in circuit design details. It is important to notice the time scale for each ignition system. The duration over which energy is delivered to the mixtures decreases one order of magnitude from 0.35 ms with the standard circuit to $25\ \mu\text{s}$ with the plasma jet circuit and another order of magnitude to less than $1\ \mu\text{s}$ with the breakdown circuit. Current levels for the enhanced



STANDARD IGNITION SYSTEM



PLASMA JET IGNITION SYSTEM



BREAKDOWN IGNITION SYSTEM

Figure 4.2 Spark discharge characteristics for the ignition circuits used.

ignition circuits (≈ 500 A) are 10 000 times that for the standard ignition circuit (50 mA). Voltages coincide with capacitor voltage levels for the enhanced ignition circuits.

Another important factor to consider while discussing ignition system characteristics is the rate of energy delivered to the spark plug. Generally, high power levels are achieved by delivering the spark energy in a very short duration. Anderson [11] has shown that for similar delivered spark energies, the power can increase by five orders of magnitude by means of an equivalent decrease in spark durations. The relationships between the rate of energy delivery and the duration of the spark as reported by Anderson and from this study are shown in Figure 4.3. Also shown in this figure is the total energy delivered to the spark plug by each system. For the tests in the quiescent combustion cell, no effort was made to equalize the energy in the spark. Both enhanced ignition systems delivered about 1 J of energy. However, for subsequent testing in the turbulent combustion cell, the energy stored by the standard and breakdown ignition systems was the same. This is not to say that the energy in the spark was the same, since the efficiencies of the ignition systems vary. Anderson [11] has shown that higher rates of energy delivery can result in shorter burning times for the same delivered energy.

4.2.3 Description of the Spark Plugs Used in the Quiescent Cell

Two spark plugs were used in this part of the study: a standard surface gap Champion N-19V, and a plasma jet cavity spark plug fabricated from a surface gap

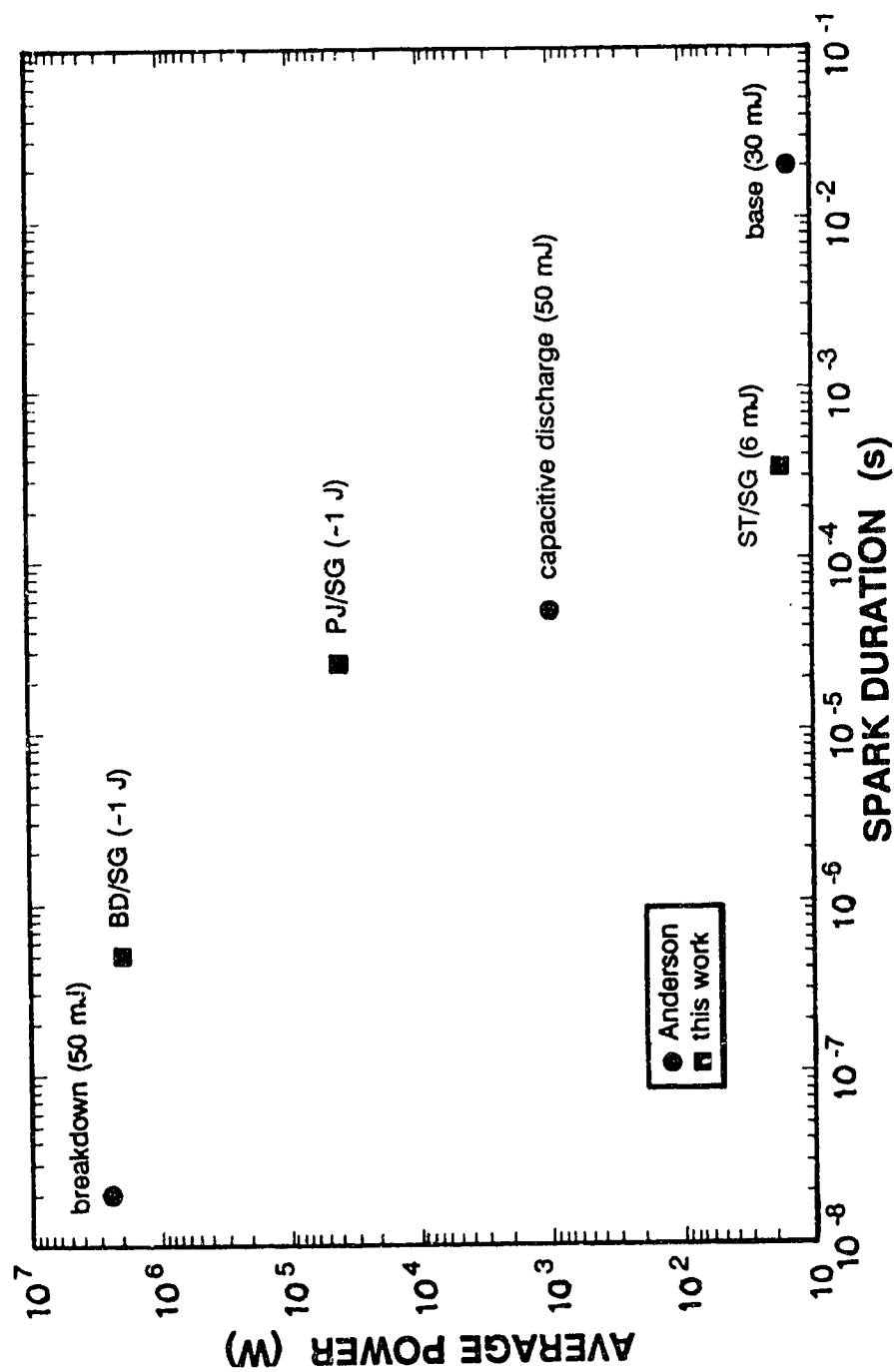
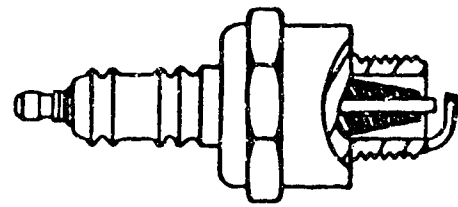


Figure 4.3 Average power and spark duration comparison of the ignition circuits used in this study and those used by Anderson [11].

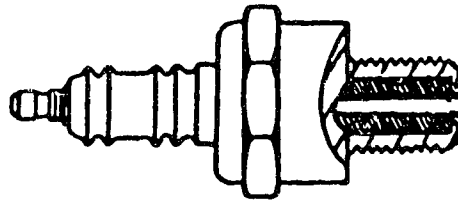
Champion N-19V. The spark plugs are shown in Figure 4.4 along with a standard electrode type spark plug for comparison purposes. With a surface gap spark plug, the spark is formed across the annulus between the centre electrode and the surrounding ground surface. With a plasma jet cavity spark plug, a spark is formed between the centre electrode, which is recessed, and the ground surface at the cavity exit. As the spark energy is deposited, the gases in the cavity heat to a very high temperature (Asik et al estimate 10 000 K to 30 000 K [35]) forming a gaseous plasma which expands and jets out of the cavity. Much research has been done recently on the geometry and construction of the plug cavities to minimise possible variations [e.g. 36, 37]. For this study, a simple, arbitrary geometry was chosen. The cavity was cylindrical with a depth of 4 mm and diameter of 1.5 mm with no restriction or orifice at the cavity opening. In addition to the above spark plugs, a standard spark plug was built with an extended reach of 40 mm for the centre ignition tests in the quiescent cell (described in Section 4.4.4). This spark plug was based on a standard type Champion 813 by extending the electrodes.

4.3 Experimental Measurements in the Quiescent Combustion Cell

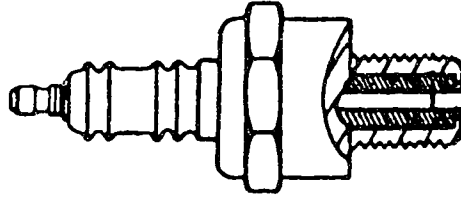
A typical experiment consisted of filling the quiescent combustion cell with a known, homogeneous fuel - air mixture, then igniting the mixture. During combustion, the output of various analog measuring devices were recorded on the FM tape recorder as described earlier in Section 3.1. For the quiescent



standard



surface gap



plasma jet

Figure 4.4 Comparison of spark plugs.

combustion cell, the four FM tape recorder channels were used as follows:

1. pressure transducer signal,
2. ionisation probe signals for flame arrival data,
3. spark timing signal,
4. signal to indicate the start of an experiment.

The pressure signal on channel one was the output from a Norwood model 111 strain gauge pressure transducer and 100X amplifier. The ionisation probe signals on channel two indicate flame arrival at the tip of each ionisation probe as described in Section 2.6. The brief current flows that occur with the passage of a flame front, produce "spikes" in the normally grounded signal to the FM tape recorder. The spark timing signal on channel three coincides with the ignition spark trigger in the quiescent combustion cell. Combustion times are all relative to the time of the ignition spark trigger. Finally, the signal on the fourth channel indicates the starting point of an experimental run and was used as a starting point for the analog to digital data conversion process. The recorded signals for an experiment were similar to those shown in Figure 4.5.

4.4 Experimental Results in the Quiescent Combustion Cell

Experiments were conducted in the quiescent combustion cell, described in Section 2.2, to measure the effects of different ignition systems on flame development and burning velocity. These results are examined in this section.

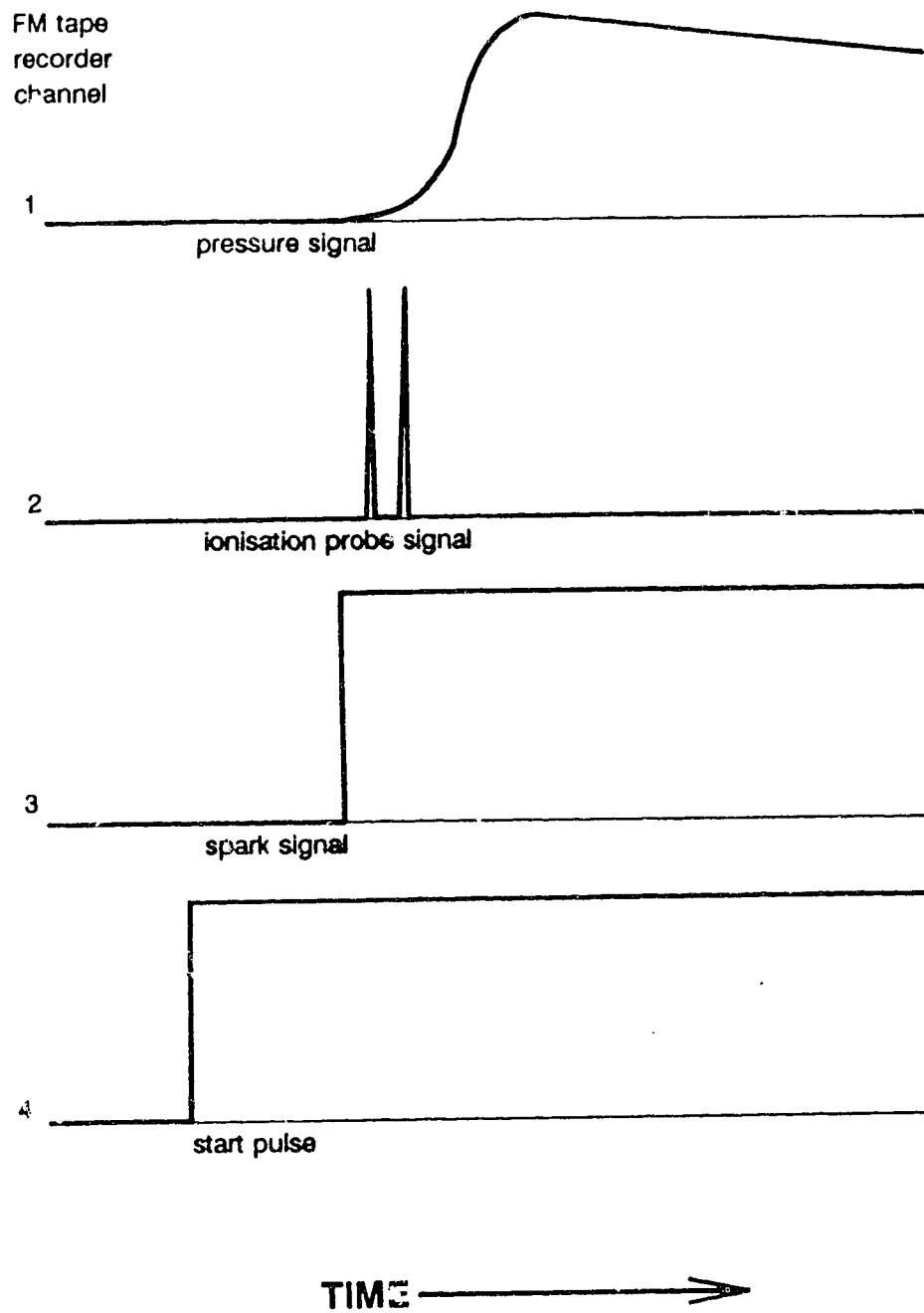


Figure 4.5 Typical analog signals recorded by the FM tape recorder during the testing of ignition system effects.

4.4.1 Burning Velocities in the Quiescent Combustion Cell

Burning velocities were calculated for all four ignition systems and two equivalence ratios (0.7 and 0.95). The Lewis and von Elbe model was used to calculate burning velocities for these preliminary tests as previously discussed in Section 3.3.4. Due to the side ignition and non-spherical flame growth, the burning velocities reported in this section will be lower by 30 to 40% than those reported by others [e.g. 2]. The average of the instantaneous burning velocities at developed pressures of 200 kPa and 350 kPa was used to represent the burning velocity of a well developed flame in each experimental run. These pressures roughly correspond to 15% of the effective cell radius. At least five experimental runs were performed for each equivalence ratio and each ignition system. Figures 4.6 and 4.8 to 4.11 show the averages of all five experimental runs.

Burning velocity comparisons for the various ignition systems are shown in Figure 4.6. Each of the enhanced ignition system - spark plug combinations produces a higher apparent burning velocity than the standard ignition system. The PJ/PJ system produced the highest burning velocity improvement of 57% at $\phi = 0.7$ and 40% at $\phi = 0.95$. With lower improvements, the BD/SG and PJ/SG systems offered approximately equal burning velocity gains of 17% at $\phi = 0.7$ and 18% at $\phi = 0.95$.

It is questionable that these burning velocity results can be attributed solely to changes in the ignition spark, especially since they are so late in flame growth period ($r_b/r_{cell} = 0.75$). Other explanations were sought, particularly flame growth

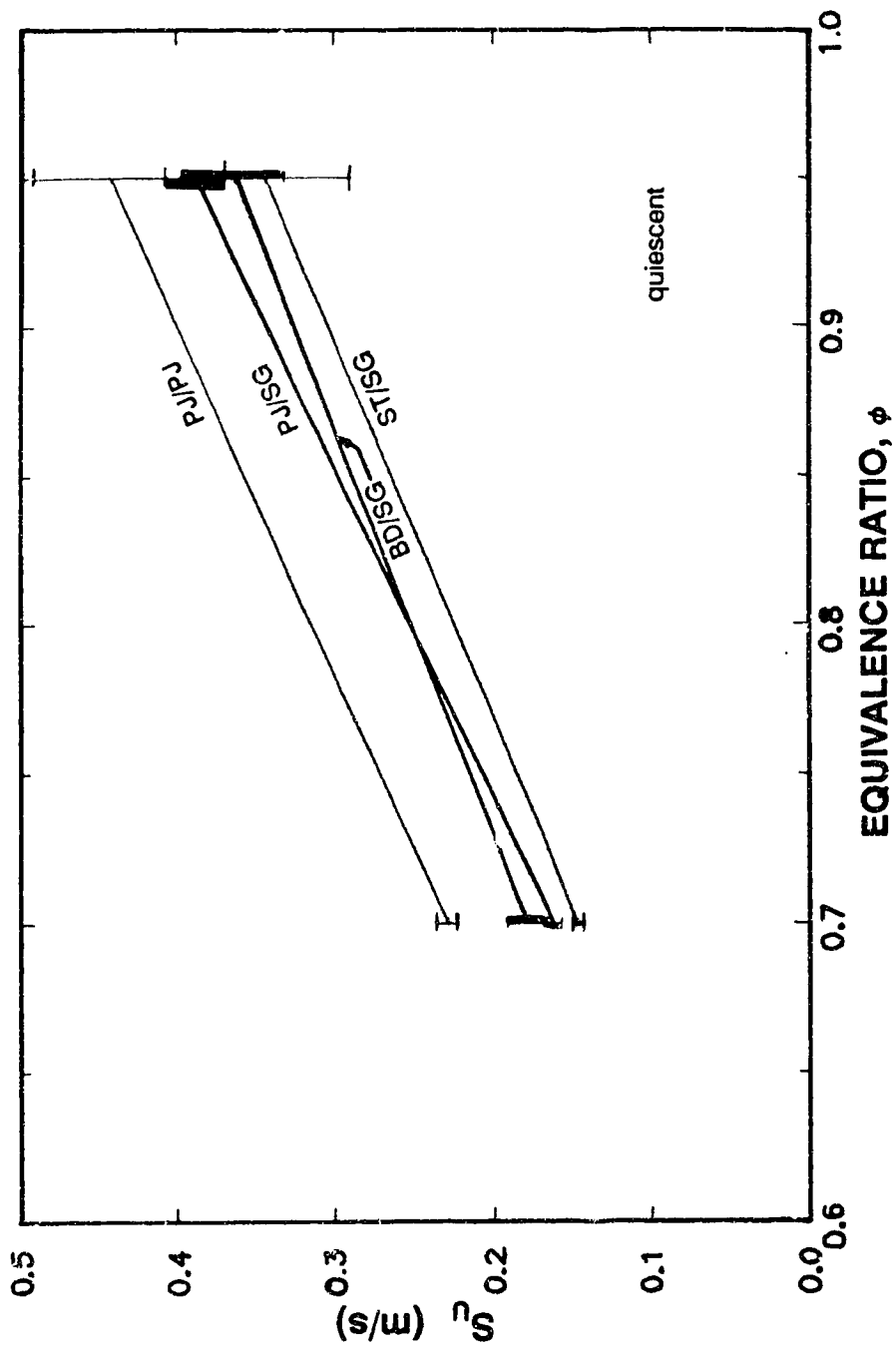


Figure 4.6 Calculated burning velocities of lean quiescent mixtures for various ignition systems.

geometry which was discussed in Section 3.3.4. Burning velocity improvements using the surface gap spark plug are thought to be due to the increased energy delivered by the ignition systems which tends to project the spark from the spark plug [38]. The projection force is the result of $\mathbf{J} \times \mathbf{B}$ where \mathbf{J} is the current density vector and \mathbf{B} is the magnetic induction vector. The PJ/PJ system produces an even higher burning velocity because of the jetting action of the plasma jet cavity spark plug. This jetting action creates some turbulence and projects the flame kernel away from the wall, resulting in a favourable flame geometry.

The measurement uncertainty of ± 2 standard deviations for each series of tests exhibits some overlap, particularly at $\phi = 0.95$. This uncertainty is shown in Figure 4.6 as error bars. An in-depth examination of enhanced ignition system performance requires stable measurement parameters without the variability of burning velocity measurements. Combustion duration has been found to be quite sensitive to the burning velocity of a mixture and is a stable indicator of the integrated effects of burning velocity. That is, a small change in burning velocity yields a measurable change in burning time. Burning times are measured from the pressure - time trace as described in the next section.

4.4.2 Pressure - Time Based Results in the Quiescent Combustion Cell

Pressure rise measurements provide information about the development and progress of combustion that the burning velocity of a well developed flame

may not reveal. Flame development period and burn duration are both important parameters which are based on pressure measurement.

The flame development period is defined in this study as the time required after ignition for the pressure to increase to five percent of the maximum pressure rise achieved during combustion. Burn duration can be defined in a similar manner as the time required for pressure to rise from 5% to 95% of the total rise. The 5% and 95% times are chosen arbitrarily by many researchers; in fact, 10% and 90% times are sometimes used when diagnostic methods are not sufficiently accurate to provide 5% and 95% times. It is more accurate to use the 95% burn time as a relative measure of the end of burning, since there is less uncertainty in time measurement at the 95% point than at the 100% point. This uncertainty is shown in Figure 4.7 by error bars based on ± 2.5 kPa on a typical pressure trace at the maximum, 5%, and 95% pressure rise points. Using the 5% and 95% percent of pressure rise times, results from all the combustion experiments in a single combustion cell can be compared in a quantitative manner.

The flame development period is important as it is considered part of the overall burning time. The flame development period and burn duration sum is of practical importance in engines. If flame development takes too long, the expansion stroke may begin while burning is taking place. Volume expansion would cause burning velocity to decrease due to lower temperatures. It may be possible for a mixture to have a high burning velocity but have an excessively long flame development period resulting in a long overall burning time.

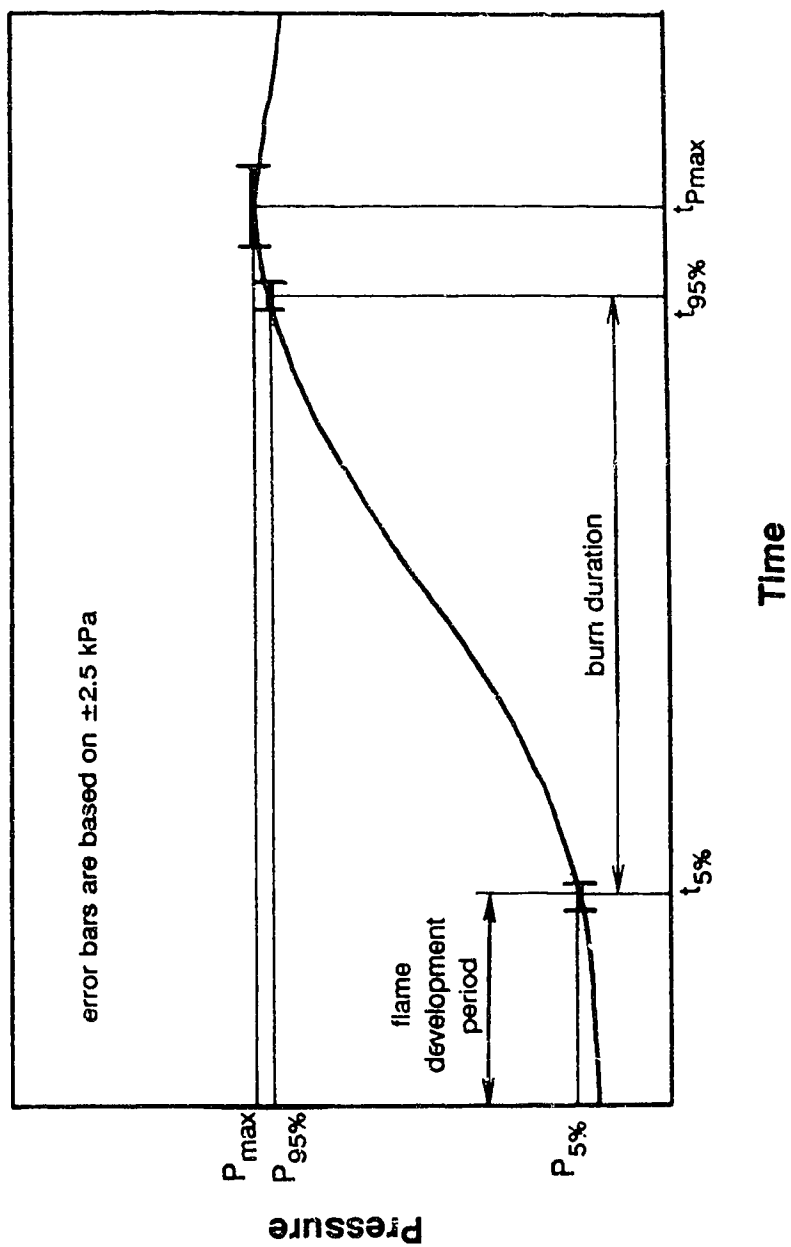


Figure 4.7 Flame development period and burn duration shown on a typical pressure trace. 2.5 kPa pressure error is shown in terms of time for 5%, 95%, and maximum pressure rise.

In tests from this study, the PJ/PJ system had a flame development period only 62% of that of the ST/SG system at $\phi = 0.7$ and 57% at $\phi = 0.95$. The BD/SG and PJ/SG systems had equivalent flame development times, roughly half way between the ST/SG and PJ/PJ systems. The significant reduction of the flame development period using enhanced ignition systems is shown in Figure 4.8. The flame development period is reduced or a larger flame kernel is developed as more spark energy is delivered and as a higher energy delivery rate is used. The jetting action of the plug resulted in a large flame kernel placed well away from the wall with the PJ/PJ system. This shows the benefit available from improved spark kernel location. Uncertainty is shown for all tests in Figure 4.8 as error bars. Unlike the burning velocity measurements, there is no overlap of the error bars in the burn duration measurements.

The same trends indicated by the burning velocity diagnostics and flame development period appear again when burn duration is considered. The burn duration times represent the integrated effects of burning velocity and flame shape. A good correlation with the burning velocities in Figure 4.6 is expected. Burn duration for the various ignition systems are shown in Figure 4.9. When compared with the ST/SG ignition system, there is only a slight reduction in burn duration using the BD/SG and PJ/SG ignition systems. A moderate reduction is found with the PJ/PJ ignition system. The greatest benefits are seen at an equivalence ratio of 0.7 where the burn durations are about twice as long as they are for a mixture with an equivalence ratio of 0.95. The effect of ignition system on burn duration

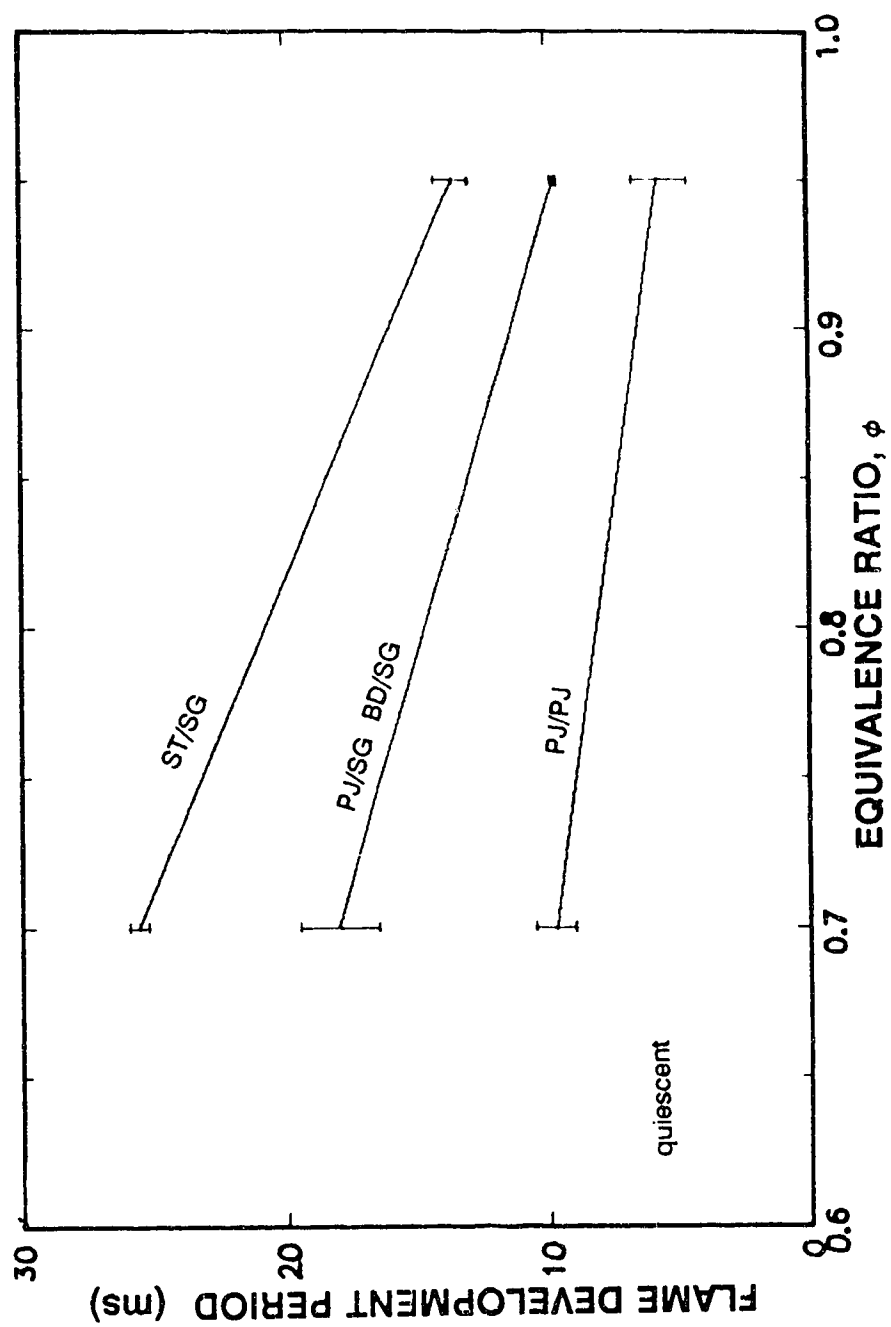


Figure 4.8 Flame development period of lean quiescent mixtures for various ignition systems.

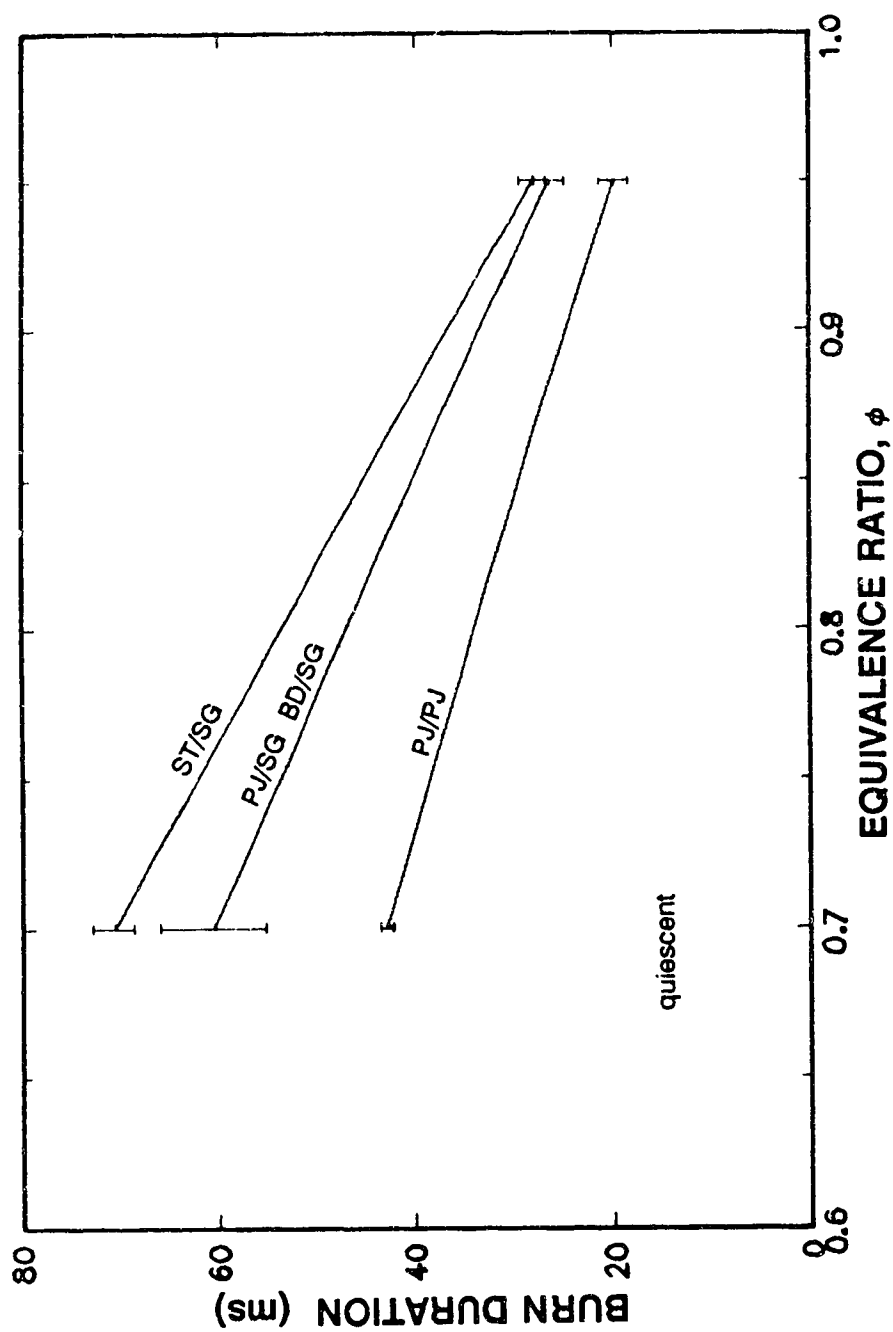


Figure 4.9 Burn duration of lean quiescent mixtures for various ignition systems.

is not nearly as great as its effect on flame development periods.

One explanation for the burn duration reductions when using the BD/SG and PJ/SG ignition systems is that the higher spark current tends to project the spark kernel away from the spark plug [38]. This results in a favourable burning geometry. That is, the flame kernel would be able to grow more spherically since it would be away from the wall. The plasma jet cavity spark plug used with the PJ/PJ ignition system projected the spark kernel even further from the spark plug.

4.4.3 Effect of Stored Voltage in the Breakdown Ignition System

A reliable ignition system - spark plug combination, suited to automotive use, was chosen for further testing in the turbulent combustion cell. The PJ/PJ system was ruled out, despite its excellent performance, due to erosion and longevity problems expected with this type of spark plug [36, 37]. Erosion is a result of the high temperature of the spark plug combined with the plasma gas rushing out of the cavity. By shortening the duration of the spark to that used by the breakdown ignition system, the spark plug surfaces would remain cooler. Cooler surfaces would result in longer spark plug life at high energy levels. As well, Anderson [11] has reported better performance with higher power ignition systems (i.e. the same energy in a shorter time). The breakdown circuit was chosen over the plasma jet circuit because of its short duration which occurs in the 94% efficient [8] breakdown mode.

A study was done to determine the effects of the stored voltage in the BD/SG system on combustion times. This was done as preliminary work to learn more about the breakdown ignition system and to determine how much stored voltage to use for optimum results. The methane-air mixture strength was varied between equivalence ratios of 0.65 and 0.95. The stored voltage was varied from the minimum required to ensure complete firing of the mixture to the maximum acceptable before spontaneous sparking occurred. The surface gap spark plug was used for all of these tests.

It was found that a stored voltage of 5 kV was insufficient to ensure complete firing at all equivalence ratios. Some misfiring with lean mixtures ($\phi = 0.65$) occurred using a stored voltage of 7.5 kV. All mixtures ignited properly at 10, 15, and 20 kV. Above 20 kV, the ignition system triggering device began sparking spontaneously, making the testing of higher stored voltages impractical with this circuit.

The flame development period is shown in Figure 4.10 for all of the stored voltages, along with the ST/SG system for comparison purposes. As could be expected, the flame development period and the burn duration were shortest with the greatest amount of stored energy. The flame development periods show a strong and systematic dependence on the stored voltages. This is expected because more energy is delivered to the mixture by the spark. This allows for the formation of a larger flame kernel. By examining the burn duration for the range of stored voltages using the BD/SG system as shown in Figure 4.11, it becomes

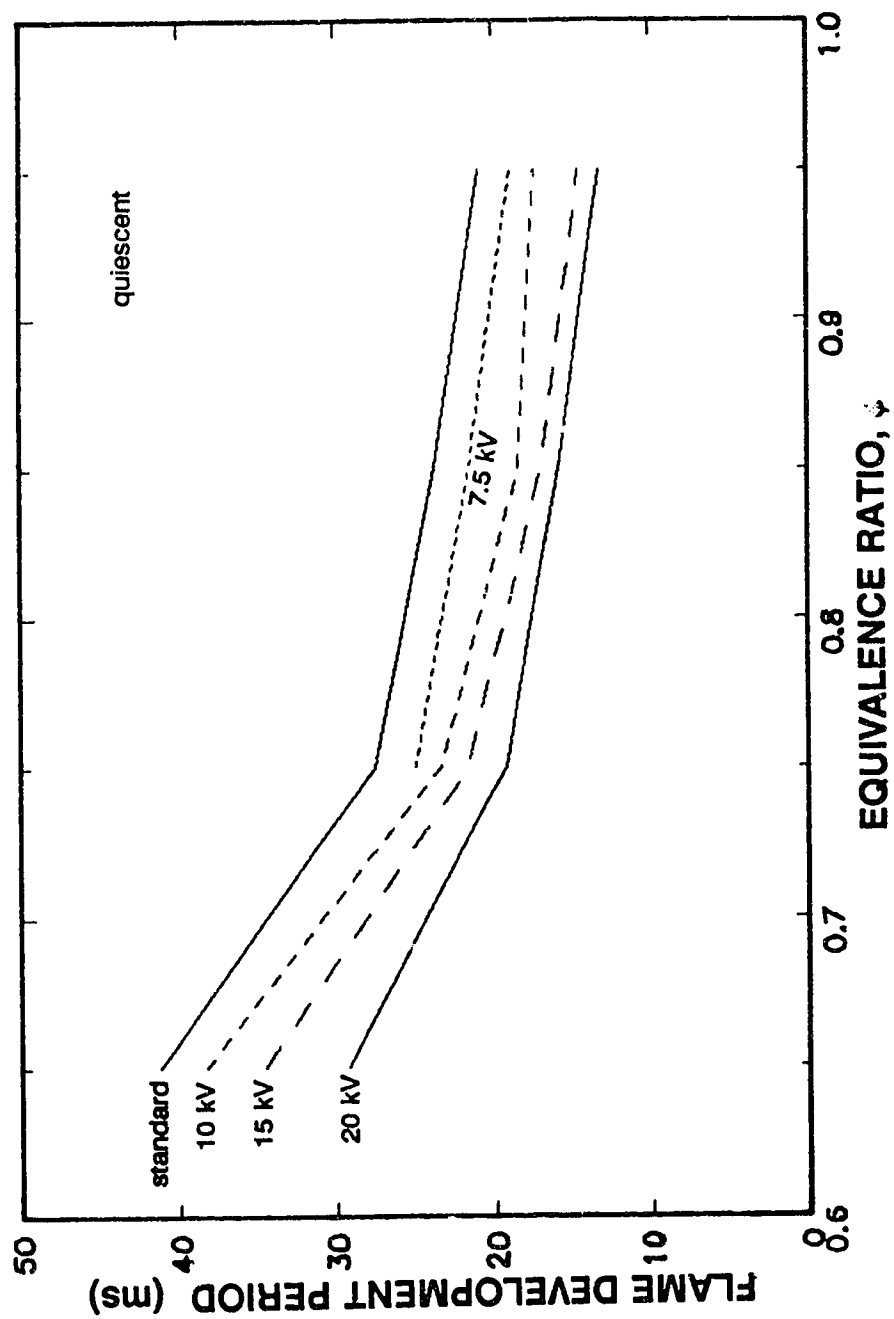


Figure 4.10 Flame development period of lean quiescent mixtures for the breakdown ignition system with various stored voltage levels.

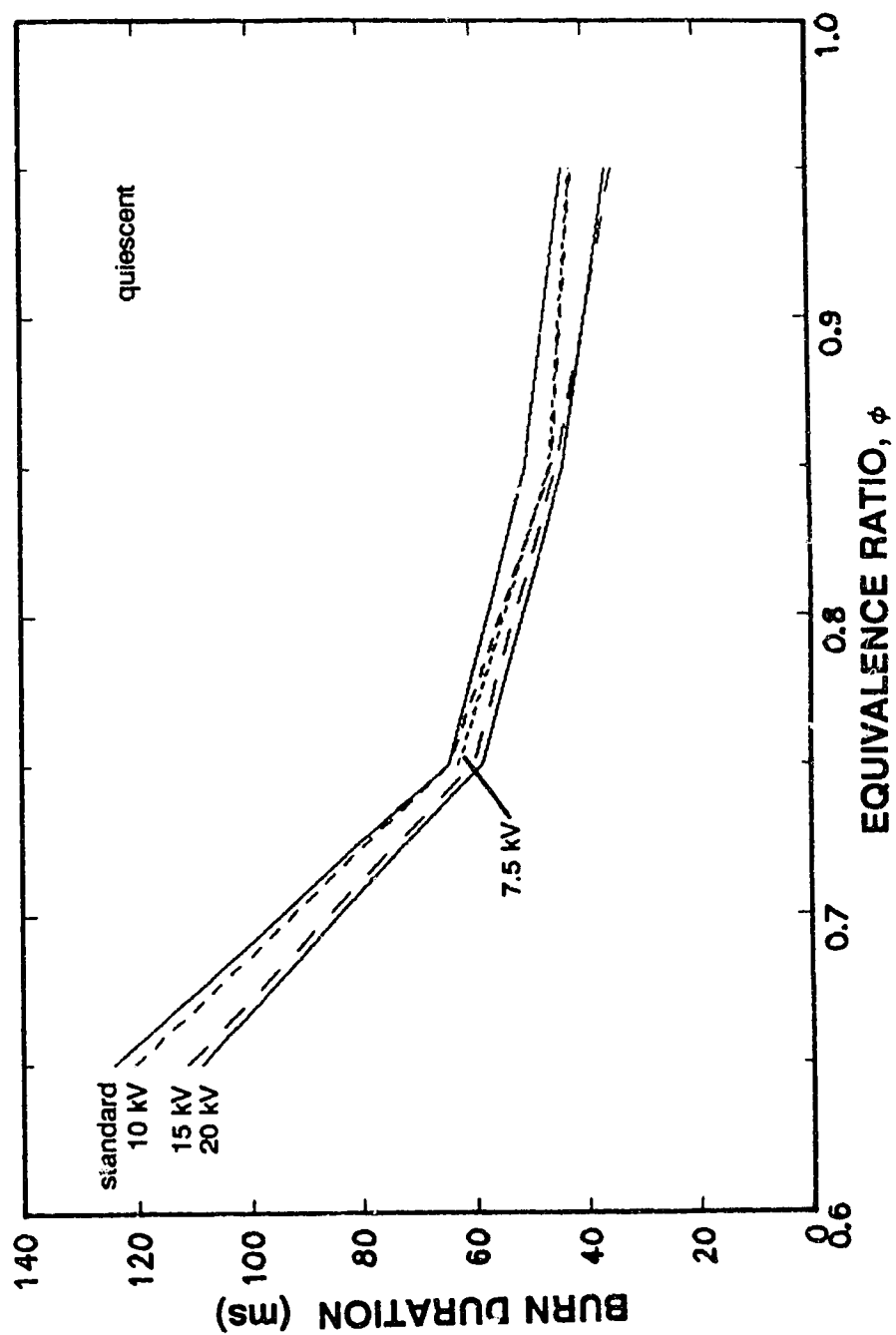


Figure 4.11 Burn duration of lean quiescent mixtures for the breakdown ignition system with various stored voltage levels.

apparent that the dependence of burn duration on stored energy is weaker than that of the flame development period. However, some dependence does exist, presumably due to the spark projection effect with higher energy. These effects might also be attributed to some ignition system effects prevailing beyond the 5% pressure rise period. Since 5% of total pressure rise corresponds to a flame that is about 60% of the effective cell radius, ignition system effects seem unlikely. After the ignition kernel has developed, the flame growth rate should depend purely on properties of the mixture (i.e. equivalence ratio) than on the ignition system. The fact that there is some ignition system dependence indicates there must be significant flame shape effects.

4.4.4 Central and Side Ignition Differences in the Quiescent Combustion Cell

A set of tests was performed to establish how great the apparent burning velocity differences were between a mixture ignited at the centre of the combustion cell and one ignited at the side of a cell. The ignition system study in the quiescent combustion cell used wall-mounted spark plugs to provide a realistic test of the benefits that could be achieved with the various ignition systems. To validate the model calculations, centrally ignited mixtures had to be used. Centrally ignited mixtures would result in a probable upper limit of the effects of flame kernel shape and location. The side-ignited mixture was expected to indicate a lower burning velocity because part of the flame would grow against the

combustion cell wall. A cool wall would quench the flame, resulting in reduced flame area for a given burned volume.

A set of tests were conducted for an equivalence ratio of 0.95 using a wall mounted spark plug and a spark plug with its reach extended to the centre of the cell. The burning velocities of developed flames as calculated by the thermodynamic equilibrium model, which assumes spherical growth, were 0.21 m/s for the side wall ignition case and 0.33 m/s for the centrally ignited case. The 36% lower apparent burning velocity for the side-ignition case is mostly due to its flame geometry as discussed in Section 3.3.4. The central ignition burning velocity corresponds well with the reported value of 0.325 m/s [2].

To confirm the burning velocity calculations for centrally ignited mixtures, high speed schlieren photography was used to directly measure the flame radii. Burned volumes were then calculated and checked against those calculated by the equilibrium. It was impossible to provide a direct calibration of the model using the schlieren data. The pressure data was only accurate after 120 kPa while the flame passes beyond the window limits just before 120 kPa. This initial inaccuracy at pressures below 120 kPa is due to spark noise with its resulting low signal-to-noise ratio and subsequent filtering as discussed previously in Section 3.3.4. Confirmation of the model results was done by extrapolating burned volumes from photographic measurements and model volume calculations. The assumption of spherical flame growth for all centrally ignited flames was confirmed as schlieren photographic data exhibited circular flames in the plane of the film as displayed

earlier in Figure 3.7. Extrapolation of flame volume results from the photographic measurements and those calculated using the thermodynamic equilibrium model coincide as illustrated by Figure 4.12. The photographic results support the spherical flame growth assumptions and confirm calculated flame sizes.

4.4.5 Ignition System Testing in the Turbulent Combustion Cell

Ignition system tests were performed with a quiescent mixture in a larger, centrally ignited, cubical cell since subsequent testing of turbulent mixtures was to take place in that cell. These tests used a pair of pointed electrodes meeting at the centre of the cell to form a spark gap as seen in Figure 2.3. The object of these tests was to ensure that results consistent with those obtained in the quiescent combustion cell could be achieved in the cubical combustion cell using quiescent mixtures. The relative flame radius growth over the initial combustion period from both photographic and pressure-based results were analyzed using the equilibrium model. As in the quiescent cell, the early portion of the pressure record was inaccurate due to electrical noise from the spark.

The breakdown ignition system provided an initial advantage in flame kernel size over the standard ignition system. The average flame development period using the standard ignition system was 27.6 ms. This was 13% higher than for the breakdown ignition system which averaged 24.6 ms. The average burn durations were practically the same for each system -- 43.9 ms for the standard system and 44.2 ms for the breakdown system. Once the effects of the ignition spark had

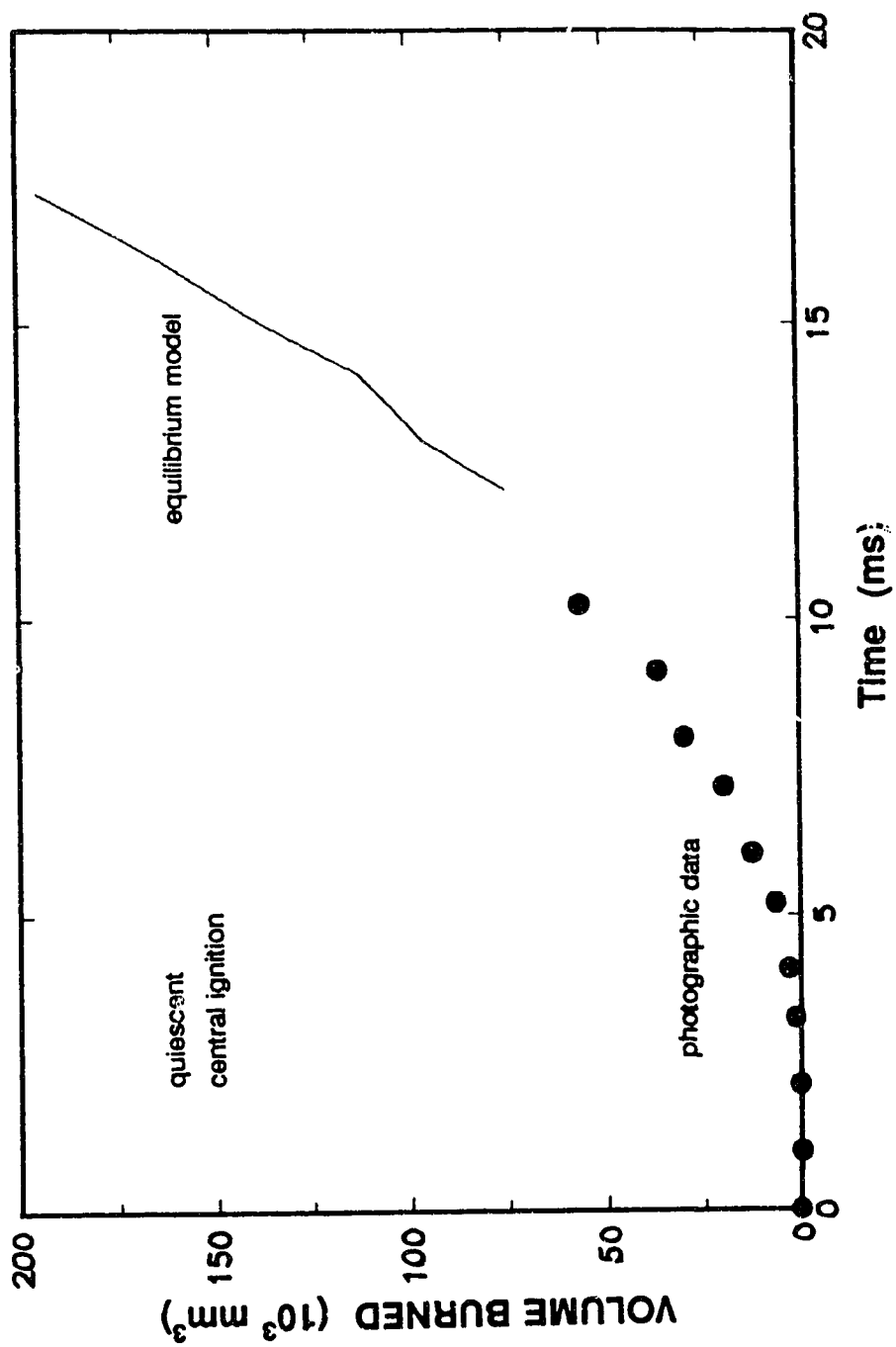


Figure 4.12 Comparison of photographically measured volume burned with that calculated by the equilibrium model for a lean ($\phi = 0.95$) quiescent mixture.

been overcome by the mixture growth, the flame growth rates were similar for each of the ignition systems as shown in Figure 4.13.

As evident from the nearly identical burn duration for each ignition system, no secondary spark energy effects were seen. This can be explained by the opposed spark electrode configuration used. This configuration was shown in a previous study not to project the spark away [38]. The theory that high ignition energy with a wall-mounted igniter reduces burn duration due to spark kernel projection and flame shape advantages is supported. This test also showed that similar ignition system benefits were realized using a breakdown ignition system with quiescent mixtures in both quiescent and turbulent combustion cells.

4.5 Summary of Enhanced Ignition System Testing

From the results of the enhanced ignition system testing, several key points should be emphasized. The PJ/PJ system consistently provided the highest burning velocity with the shortest flame development and burn duration times. This was due to three reasons: 1) higher energy delivered, creating a larger spark kernel, 2) extreme spark kernel projection, resulting in a favourable flame geometry, and 3) turbulence induced by the jetting action, resulting in a faster burning velocity. However, the system was not considered further because the operating life of a plasma jet cavity spark plug has been reported to be very short due to erosion.

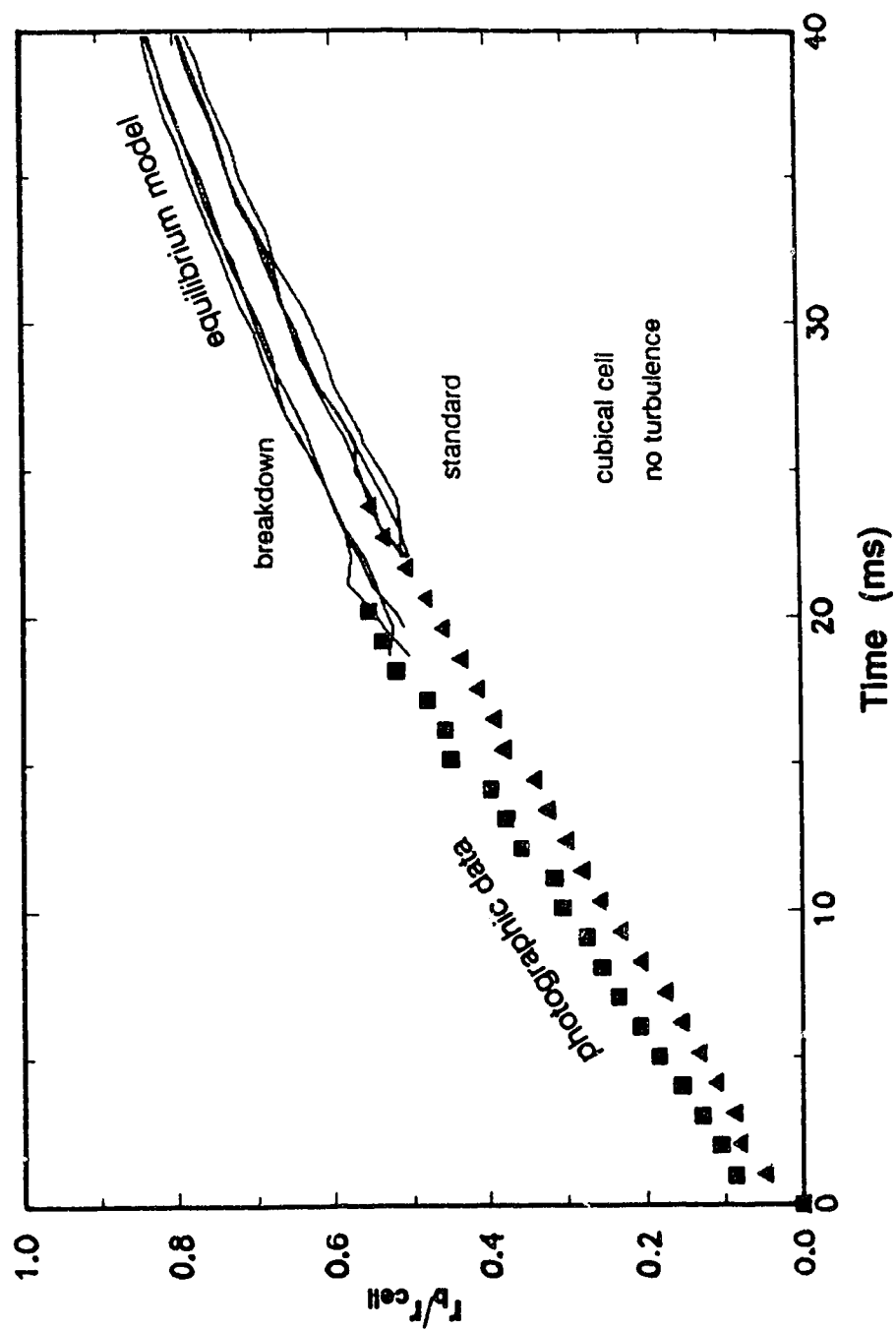


Figure 4.13 Flame growth of lean ($\phi = 0.85$) quiescent mixtures based on photographic data and equilibrium model calculations for standard and breakdown ignition systems.

The BD/SG and PJ/SG systems were similar in performance using surface gap spark plugs, lying midway between that of the ST/SG system and the PJ/PJ system. The effects of the BD/SG and PJ/SG systems were due to two effects: 1) higher energy delivered, creating a larger spark kernel, and 2) moderate spark kernel projection, resulting in a favourable flame geometry. Due to its energy release during the breakdown mode of the spark and its higher output, the breakdown circuit should prove to be more efficient than the plasma jet circuit when using the same type of spark plug.

In considering the energy stored by the BD/SG system, it was evident that the flame development time was directly related to the stored energy and by extension to the energy deposited in the spark. Furthermore, the relationship between burn duration and spark energy is not as strong as that between flame development period and spark energy. This supports the theory that the primary benefits of ignition systems are seen in the initial flame kernel development stage.

It has been reasoned that by shortened burn durations for enhanced ignition systems, secondary benefits of enhanced ignition systems can be achieved due to a favourable flame geometry. The spark kernel of a high energy ignition system is thought to be projected away from the surface, resulting in a spherical flame. This was supported by the fact that no burn duration reductions were seen when comparing the breakdown and standard ignition systems in a centrally ignited mixture which had no spark projection.

Comparative testing of the standard and breakdown ignition systems with a quiescent mixture was done in the centrally ignited turbulent combustion cell. These tests showed flame development period reductions when using the breakdown ignition system -- a result similar to that from the quiescent combustion cell. Photographic data confirmed that flame kernel development was more rapid when using the enhanced ignition system. Similar flame growth rates for developed flames were shown by the thermodynamic equilibrium model, schlieren photography, and burn duration measurements.

Through the use of high speed schlieren photography, flame radius calculations were verified. The verification was through extrapolation of the early photographic data which coincided with later thermodynamic model calculations. Extrapolation of results was required because the model was inaccurate below 120 kPa and photographic measurements were limited by window size.

These findings have all been based on a quiescent mixture. In Chapter 6, the applications of a breakdown ignition system with pointed air-gap spark electrodes for igniting turbulent mixtures will be examined.

5 EFFECTS OF MIXTURE TURBULENCE

5.1 Overview of Turbulent Combustion Studies

The effects of turbulence on combustion were studied in addition to the effects of enhanced ignition systems on combustion. This chapter will examine the effects of turbulence intensity and length scale on combustion using a standard coil ignition system. Chapter 6 will examine the combined effects of turbulence and ignition system on combustion. All of the experiments were performed in the cubical turbulent combustion cell using a lean methane - air mixture with $\phi = 0.85$. All experiments in this chapter use a standard ignition circuit.

5.1.1 Benefits of Mixture Turbulence

Until the past few decades, relatively little research had been done on the effects of turbulence on the operation of spark ignition engines [39, 40]. The effects of turbulence were known, but experimental equipment was ill-suited for making turbulence measurements. With advances in laser doppler accelerometry and velocimetry, it has become less difficult to make in-cylinder turbulence measurements in an operating or motored engine. Much of the recent work has shown that an increase in mixture turbulence will generally cause the mixture to burn faster than without turbulence [e.g. 15-20]. This increase in the burning velocity has some practical results such as an increase in power output, a

decrease in cyclic variability, and a decrease in the potential for misfire, or knock. Also, gains in power, efficiency, and emissions control are currently important.

Researchers have noted the effects of turbulence intensity (u') and turbulence integral length scale (Λ) [18, 20]. The turbulence intensity represents the speed of the average turbulent eddy. The turbulence integral length scale represents the size of the average eddy which contains the turbulent energy of the mixture. A mixture with all its eddies at intensity u' and length scale Λ would contain the same turbulent energy as the actual turbulent mixture it represents. Other turbulence length scales have also been investigated. The Taylor microscale (λ) is the average scale for the dissipation of turbulence energy through shear and the Kolmogorov scale (η) represents the smallest existing eddy size and is a function only of viscosity and dissipation rate [17, 41].

5.1.2 Turbulent Mechanisms

To understand why a turbulent mixture burns faster than a quiescent mixture, the turbulent mechanisms must be examined. If the underlying mechanisms of both turbulent flow and turbulent combustion were fully known and understood, accurate predictions of turbulent flame growth (i.e. full combustion modelling) could be carried out. Normally, this is not attainable. An empirical equation or set of equations is used to estimate the burning velocity in a turbulent mixture as a part of practical engine combustion models. To apply and develop

empirical models, it is of vital importance to understand the effects of both turbulence scale and turbulence RMS intensity on the burning velocity of a mixture.

Many of the current models use empirical relationships based on laminar burning velocity and turbulent flow field parameters [42, 43]. A testing program to determine the effects of turbulence RMS intensity and turbulence integral length scale on turbulent burning velocity was implemented.

5.1.3 Overview of the Turbulent Combustion Program

Past research has shown that the greatest effects on combustion are by turbulence RMS intensity (u') and turbulence integral length scale (Λ) [e.g. 18, 20]. Two types of test sequences were conducted. One sequence held the turbulence integral length scale at some fixed value while the turbulence RMS intensity was varied. The other sequence held the turbulence RMS intensity at some fixed value while the turbulence integral length scale was varied. A range of test values was chosen to correspond to typical internal combustion engines operating at low to moderate speeds ($u' = 0.5$ m/s to 2.0 m/s and $\Lambda = 1.5$ mm to 9.5 mm) as summarized by Collings et al [44]. The testing program and test sequences used were:

- 1) tests at constant turbulence RMS intensities of 0.5 m/s and 1.0 m/s while varying the integral length scale over full range and
- 2) tests at constant integral length scales of 3.8 mm and 7.6 mm while varying the turbulence RMS intensities over full range.

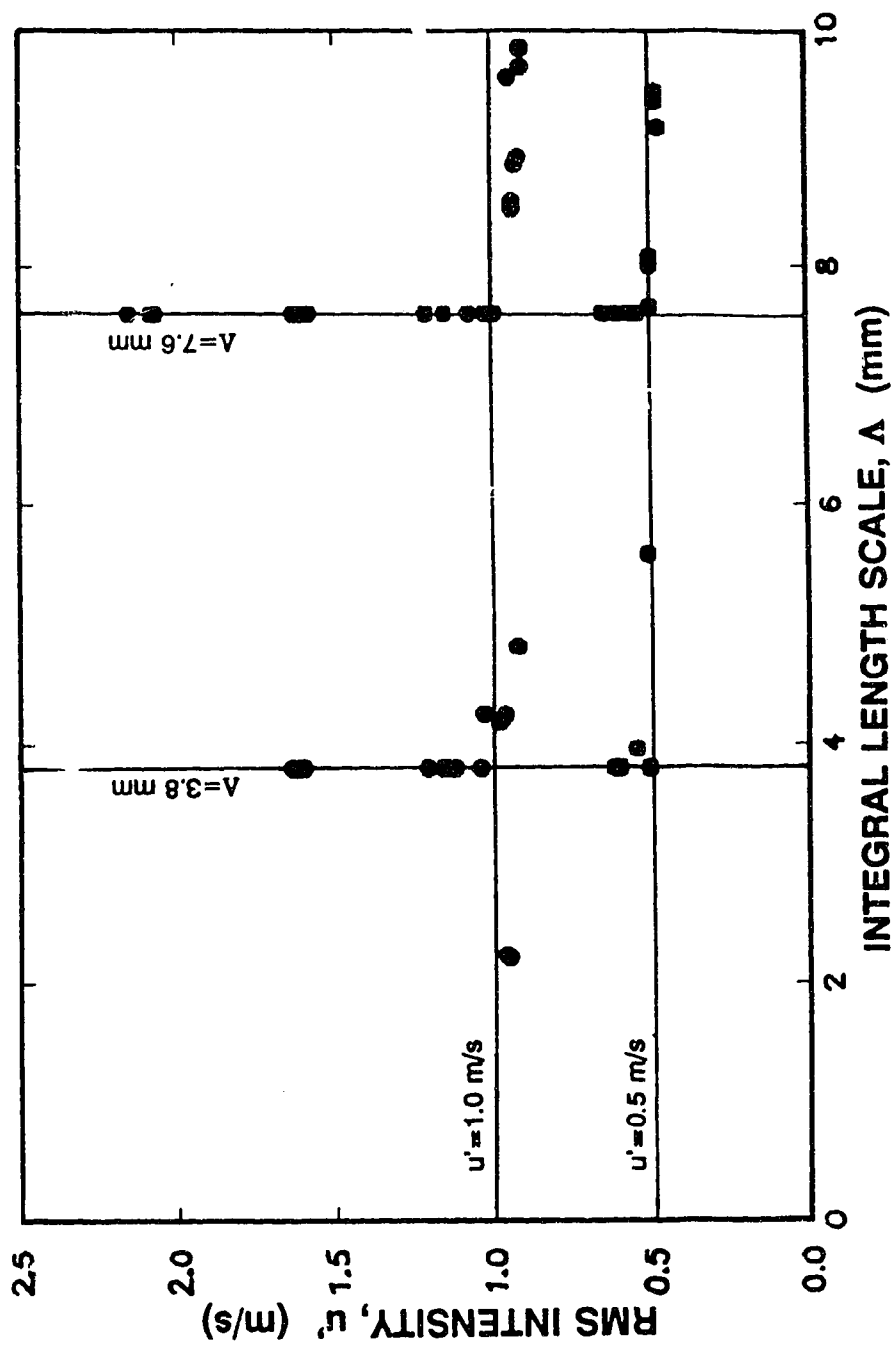


Figure 5.1 Graphical representation of turbulent combustion experimental program.

An overview of the testing program can be seen in Figure 5.1.

5.2 Experimental Details of Mixture Turbulence Testing

The experimental work for this and subsequent sections was conducted in the turbulent combustion cell which was described in Section 2.3. In general, the operating procedures of the turbulent combustion cell and the quiescent combustion cell were identical except for the generation of turbulence. The differences due to turbulence generation are outlined in the next section.

5.2.1 Measurement Differences from the Quiescent Combustion Cell

The perforated plate motion for generating turbulence required that two additional parameters be monitored. First, the average plate velocity across the combustion cell was measured. The perforated plate moved at a nearly constant velocity across the cell, except for the first 10 mm and the last 10 mm of travel where acceleration and deceleration took place. These two 10 mm lengths were not used in determining the average plate velocity. The second parameter measured to determine the turbulence characteristics within the combustion cell was the delay time. This is the period between the plate crossing the spark gap at the centre of the cell and the spark time. This delay time was set using a California Avionics Laboratories, Inc., digital delay generator, model 201AR, electronic delay. The plate crossing the spark gap at the centre of the cell caused

a pulse be sent to the electronic delay generator. After the preset delay time, a pulse was sent to trigger the ignition circuit.

The actual perforated plate velocity and spark delay time leading to combustion in a given experiment were determined by analyzing the tape recorded data after digitisation. If either the plate velocity or the delay time were not as expected, adjustments to the apparatus were made and the experiment was repeated. This trial and error method often required several attempts before the plate velocity and the spark delay time coincided with their desired values. Once plate velocity and delay period were exactly as planned, it was possible to use the turbulence decay calibration equations to calculate the turbulence intensity and length scale at the time of ignition. It should be noted that the deviations from lines of constant RMS intensity in Figure 5.1 are due to refinements of the turbulence decay model made after the experiments had been completed. The new turbulence calibration equations caused a slight shift in the apparent RMS intensity values.

Light emission measurements were also made for some of the experiments in the turbulent combustion cell. The photomultiplier apparatus used for measuring light emissions was described in Section 2.6. No formal study was done using light emission results due to the low repeatability and high variability of the photomultiplier output as discussed earlier.

5.2.2 Experimental Measurements

Analog data were recorded on the FM tape recorder in much the same manner as when operating the quiescent combustion cell. The four channels were as follows:

1. pressure transducer signal,
2. plate motion sensor,
3. photomultiplier,
4. pulse channel (start timing and ionisation sensors).

The pressure signal on channel one was from a flush-mounted, Norwood model 111, strain gauge, pressure transducer and 100X amplifier. The plate motion sensor signals on channel two were from a photo-diode emitter/sensor pair focused on an 11 cm white and black scale attached to the perforated plate mechanism. Channel three was the light emission sensor output. The fourth channel recorded a timing signal with several purposes. The start of an experimental run and the arrival of flames at the ionisation sensors were both indicated on this channel as in Figure 5.2 which shows all the analog signals for a typical experiment.

5.3 Experimental Results

The experimental results will be examined in the following sections on flame growth and burning velocity, turbulence decay, rapid distortion of turbulence, and turbulence regimes. It should be noted that when turbulence parameters are

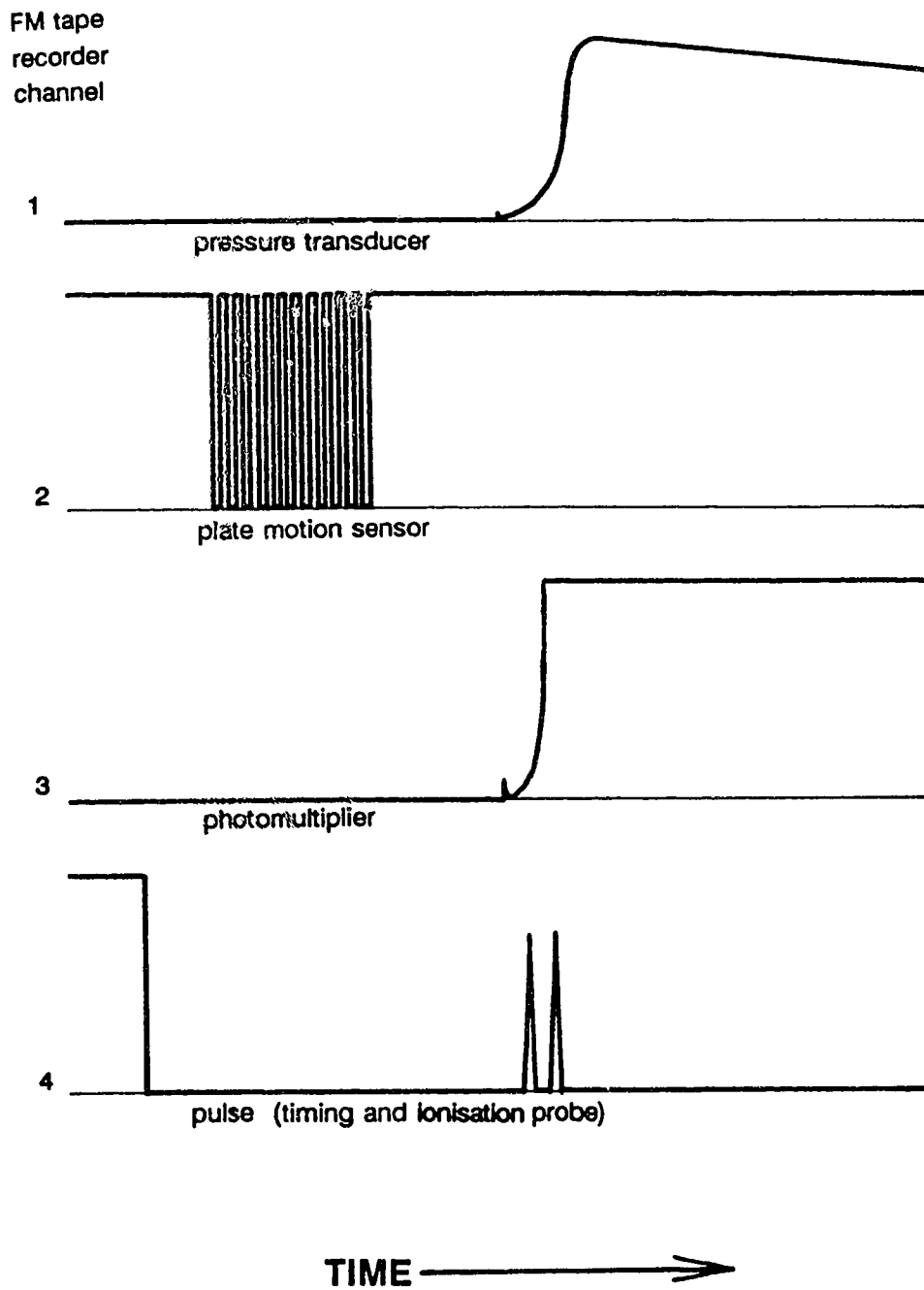


Figure 5.2 Typical analog signals recorded by the FM tape recorder during the testing of turbulence effects.

discussed in Section 5.3.1, they are the parameters at the time of ignition. The decay of turbulence and its enhancement through rapid distortion are discussed in Sections 5.3.2 and 5.3.3.

5.3.1 Flame Growth and Burning Velocity

All of the burning velocity and flame growth calculations made from turbulent combustion cell data were based on the multi-zone thermodynamic equilibrium model. The accuracy of the equilibrium model was previously shown in Chapter 3 for quiescent flames. In a similar manner, the early photographic data and the later model results must be extrapolated to show agreement for turbulent flames. Photographic data were used for comparison with the equilibrium model. Digitally enhanced images of the photographic data are shown in Figure 5.3 where growth rates and flame structure can be compared. Data for a quiescent mixture are shown in this figure for comparative purposes. It should be noted that the flame kernel grows at the same rate for all turbulence levels up to a time of 2 ms. Afterwards, the growth rate is a function of the mixture turbulence.

To check the equilibrium model accuracy, flame growth calculations for the photographed experiments were compared with photographic data as shown in Figure 5.4. When extrapolated, it was seen that the photographic data points corresponded with the equilibrium model. Since the photographic data were roughly continuous with the equilibrium data, burning velocities calculated using

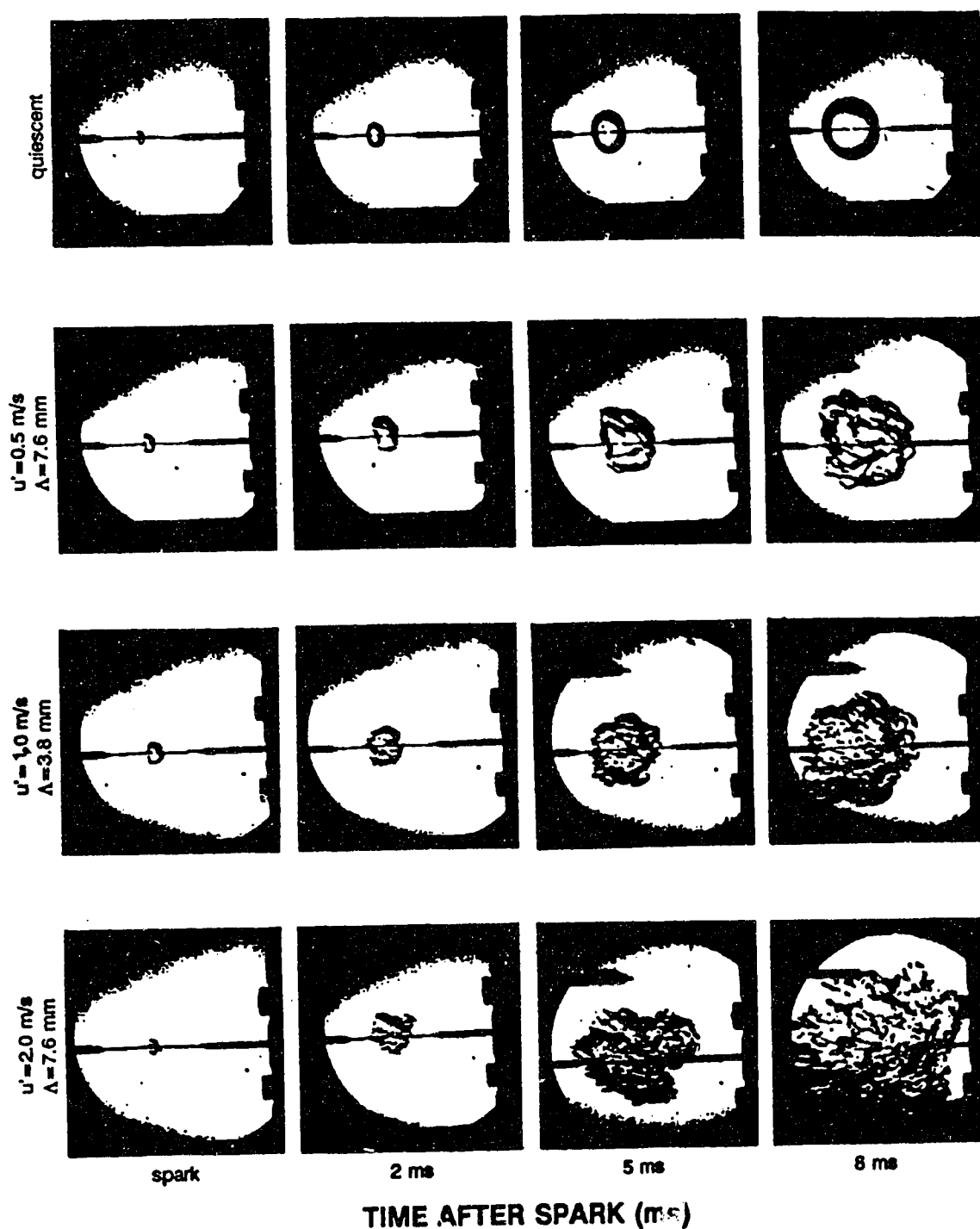


Figure 5.3

Digitally enhanced, high-contrast images of schlieren photographs of lean ($\phi = 0.85$) mixtures with various levels of turbulence.

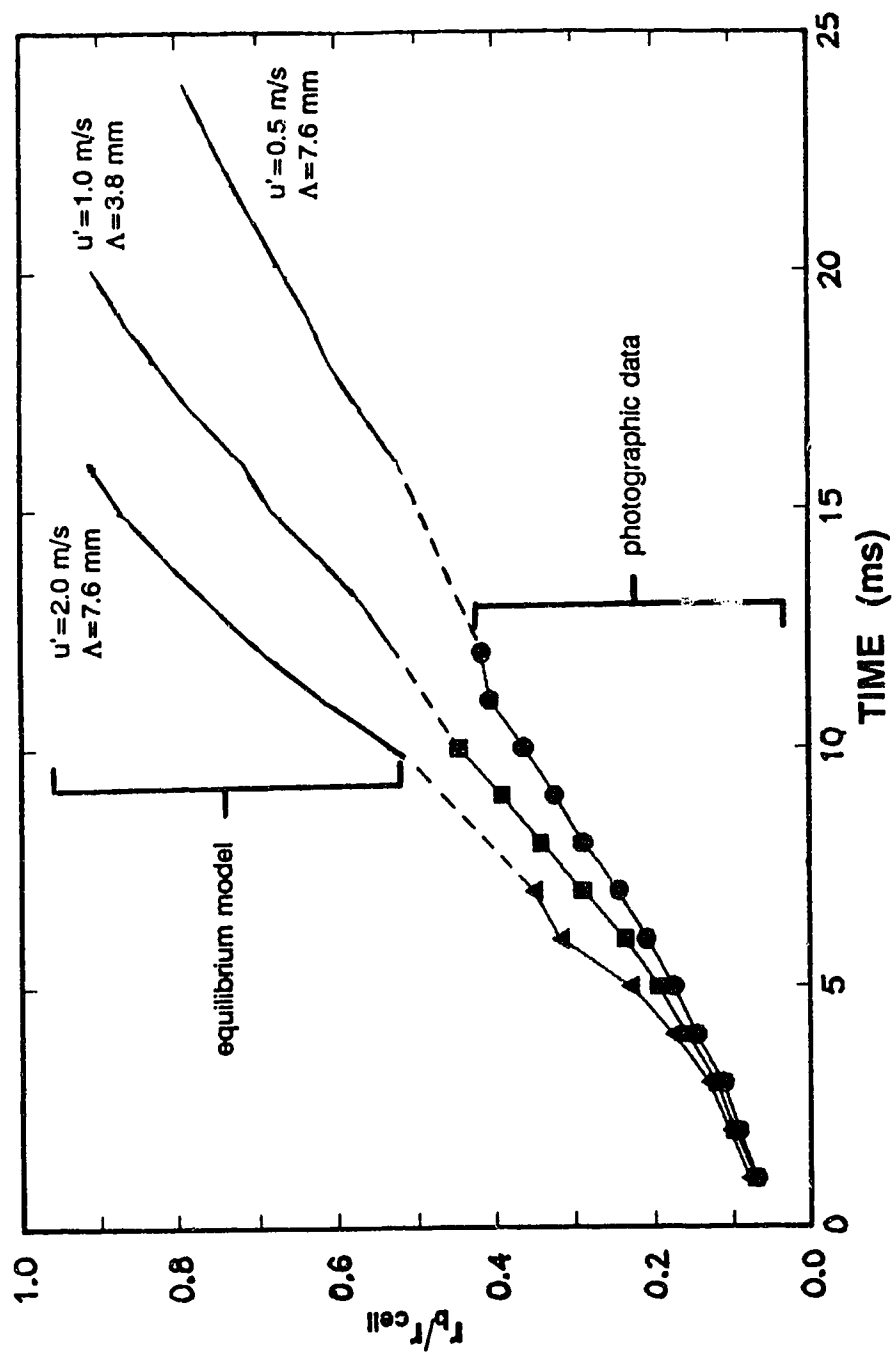


Figure 5.4 Flame growth measured photographically and calculated using the equilibrium model for lean ($\phi = 0.85$) turbulent mixtures.

either method are similar. Similar growth rates are seen for all mixtures over the first few milliseconds. This implies that flame kernel development is ignition-dominated in the early stages. It should be emphasized that the listed scales and intensities are those at the time of the spark unless otherwise stated.

5.3.1.1 Effects of Turbulence Intensity

Past research has generally shown that turbulence intensity has the greatest effect on the burning velocity of a particular mixture [e.g. 18, 20]. To quantify the effects of turbulence RMS intensity, u' , experiments were done with the integral length scale held constant while the intensity at the time of ignition was varied. Two series of experiments were performed using fixed integral length scales of 7.6 mm and 3.8 mm.

The effect of turbulence intensity on burning velocity was investigated for both sets of constant integral length scale data. The turbulence effects are shown in Figure 5.5 where each point represents the average of a group of experiments. Measurement uncertainty of ± 2 standard deviations is shown in terms of both variables as error bars. For comparative purposes, the burning velocities for quiescent runs (i.e. without turbulence) are also shown. All burning velocities are an average of the instantaneous values taken at 200 kPa and 250 kPa. It was seen that 0.5 to 2.0 m/s turbulence intensity in a mixture produced a burning velocity at least twice that of a mixture without turbulence. The relative benefits of increased turbulence intensity became lower as the intensity of turbulence became

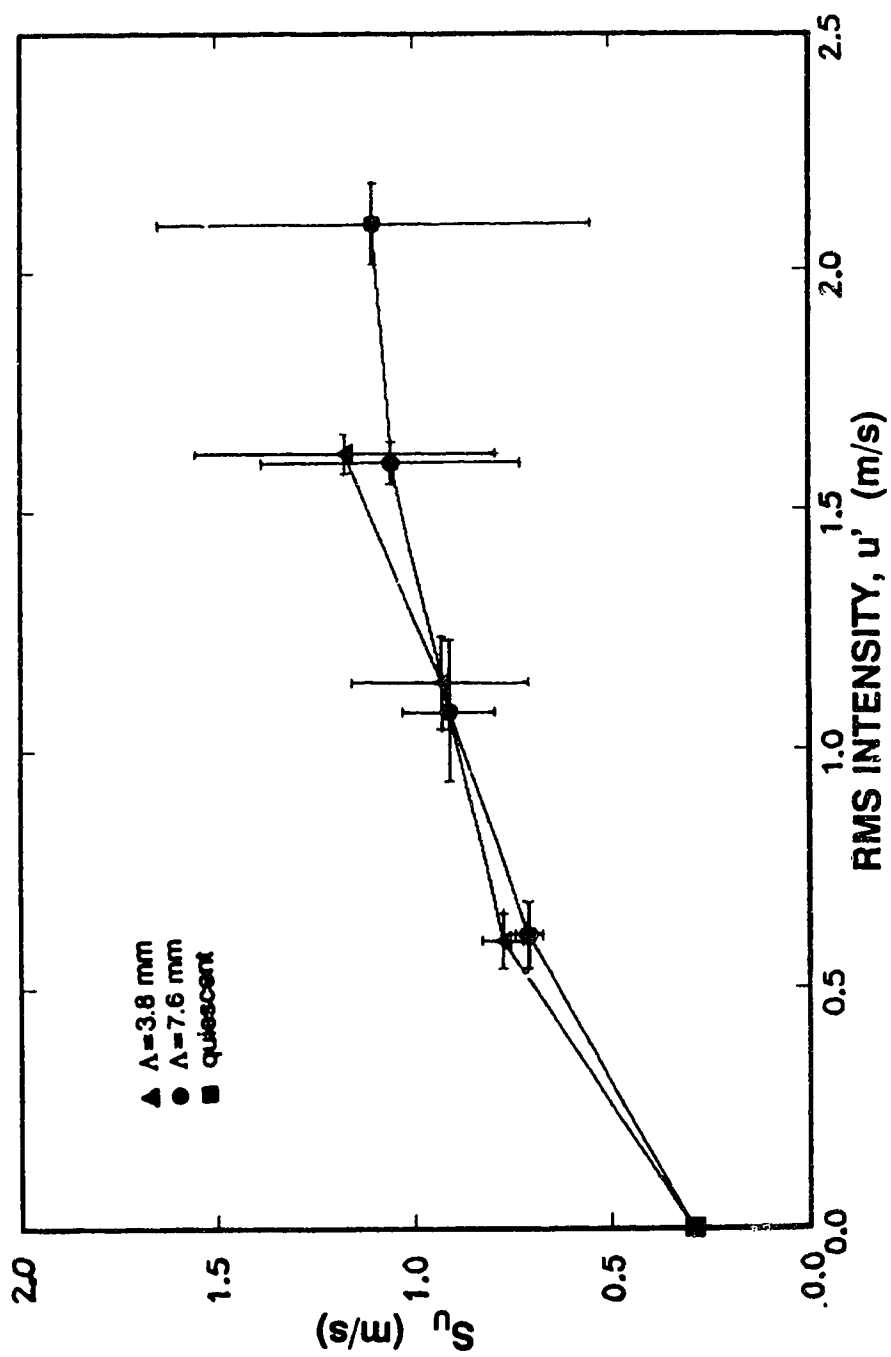


Figure 5.5 Calculated burning velocities for various turbulence RMS intensity with $\Lambda = 3.3$ mm and $\Lambda = 7.6$ mm at the time of ignition for lean ($\phi = 0.85$) turbulent mixtures.

greater. Raising the turbulence from 0 m/s (quiescent) to 0.5 m/s increased burning velocity by a factor of two. Doubling the intensity from 0.5 m/s to 1.0 m/s resulted in only a 25% increase in burning velocity. The measurement uncertainty shown in Figure 5.5 is quite large for burning velocity.

It has been shown by some research that there is a limit to the level of turbulence intensity in a mixture before the flame becomes quenched through strain [45]. This limit is described as:

$$\frac{u'}{S_L} \geq 3.1 \left(\frac{R_\Lambda}{Le^2} \right)^{\frac{1}{4}} \quad (5.1)$$

for $R_\Lambda > 300$ where: $R_\Lambda = u'\Lambda/\nu$ (≈ 2500 for these experiments)

$$Le = k'/(\rho C_p d) (\approx 1 \text{ for these experiments})$$

Due to physical limitations of the equipment used, the levels in this study were not high enough (i.e. $u' > 7.7$ m/s) to show any flame quenching.

5.3.1.2 Effects of Turbulence Scale

Some idea of the effects of scale can be obtained by looking at the two sets of data in Figure 5.5. The smaller scale turbulence seems to give slightly higher burning velocities. In a manner similar to that used to determine the effects of turbulence intensity, two series of experiments were used to examine the effects of turbulence integral length scale. The intensity was held constant at 0.5 m/s and 1.0 m/s for these experiments. Burning velocities from both sets of data for a

range of integral length scales were determined. Results show that any amount of turbulence is better than none; however, there is very little if any dependence on the turbulence integral length scale. The burning velocities remain at about 0.7 m/s for all length scales with a turbulence RMS intensity of 0.5 m/s and average about 0.9 m/s for an intensity of 1.0 m/s as shown in Figure 5.6.

The turbulence integral length scale is only one indicator of the dimensional structure of turbulence. Two others which are used extensively are the Taylor microscale and the Kolmogorov scale which are turbulent shear and viscous energy dissipation scales. In this study, only the turbulence integral length scale was examined as it is the most commonly used measure. The other two scales can be determined from the integral length scale, RMS intensity, and other turbulence properties.

5.3.2 Turbulence Decay and Rapid Distortion Theory

So far, the experimental work in this study has been classified according to the turbulence characteristics at the time of ignition. Classification at the time of ignition is convenient when dealing with decaying turbulence. To make comparisons with some of the published results for well developed flames, the level of turbulence must be estimated. For this reason, the following turbulence decay and rapid distortion theory must be introduced.

In the turbulent combustion cell, the turbulence decays rapidly after passage of the perforated plate. This decay of turbulence RMS intensity

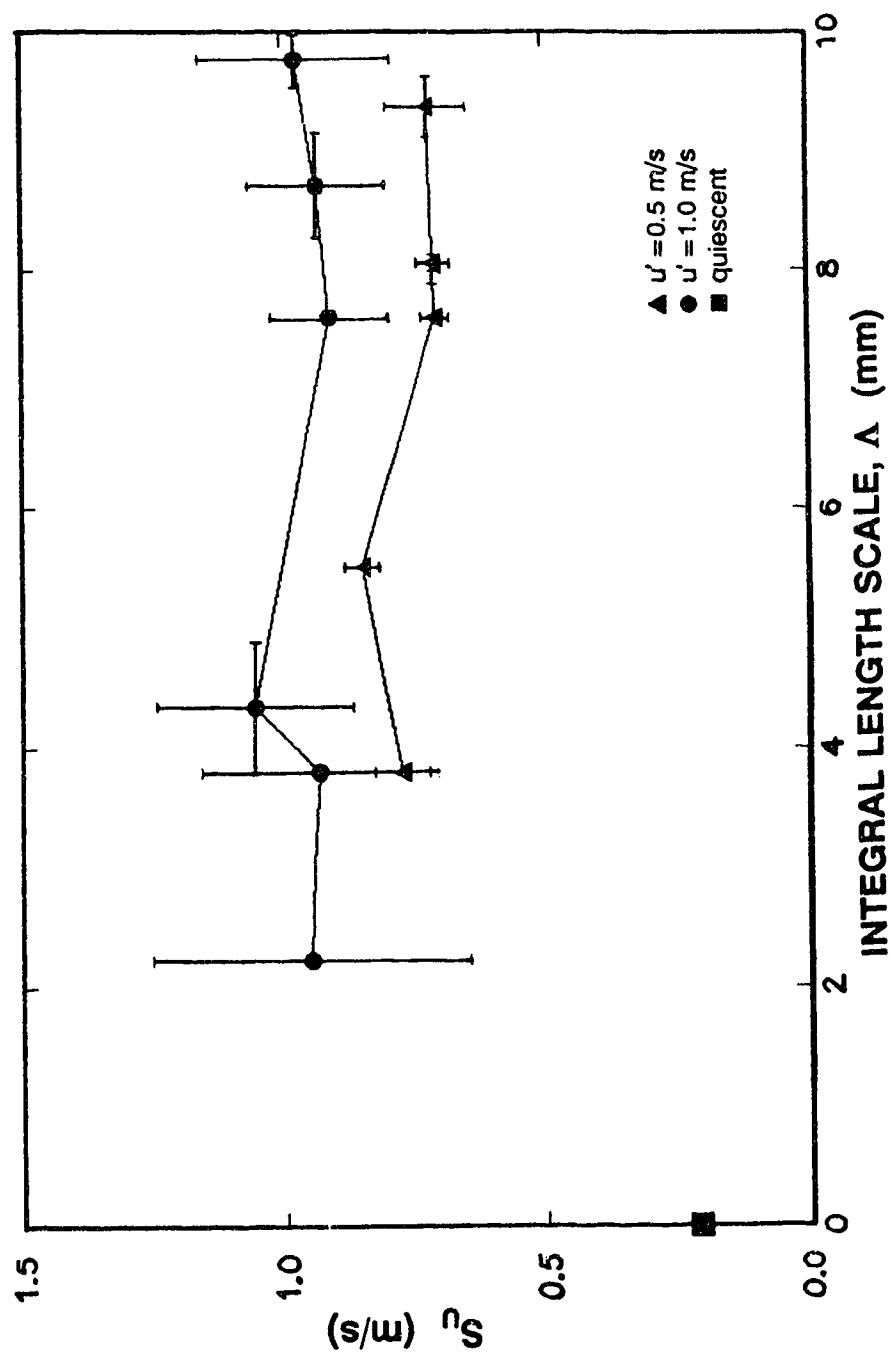


Figure 5.6 Calculated burning velocities for various integral length scales with $u' = 0.5$ m/s and $u' = 1.0$ m/s at the time of ignition for lean ($\phi = 0.85$) turbulent mixtures.

normalized by the perforated plate velocity or flow velocity, u'/v , is shown in Figure 5.7 as a function of downstream distance, x/D , which represents a temporal scale $= t \times v / D$. Since the calibration equations shown in this figure were determined for different ranges of x/D values, the curve has three distinct zones: $5 < x/D < 10$, $10 < x/D < 20$, and $20 < x/D < 40$. These calibration equations are based on the work of McDonell [22] but have been extended over a wide data range and modified to account for variable decay rate. These zones blend smoothly into one another and are based on fitted power law decay equations.

During flame growth, expansion of the flame front into the unburned gases causes turbulence intensity to increase in front of the flame front or across the flame [27, 46, 47]. This increase in intensity is due to the stretching of the vortices in the unburned gases and is modelled by rapid distortion theory (RDT). An increase in turbulence intensity due to combustion can be calculated using the equations of Chew and Britter [27] which were specifically developed for spherically growing combustion in a closed volume. Recent work by Hall and Bracco [46, 47] has shown little increase before the flame front but a large increase across the flame. It will be assumed that the equations of Chew and Britter remain applicable for either case.

In examining turbulence with regard to a spherically expanding flame, it may be separated into radial (r) and tangential (θ, α) components. The turbulent velocity components are each modified by a distortion factor as follows:

$$u'_{r, RDT} = \mu_r u'_{r,} \quad u'_{\theta, RDT} = \mu_{\theta} u'_{\theta,} \quad \text{and} \quad u'_{\alpha, RDT} = \mu_{\alpha} u'_{\alpha,}. \quad \text{These distortion factors}$$

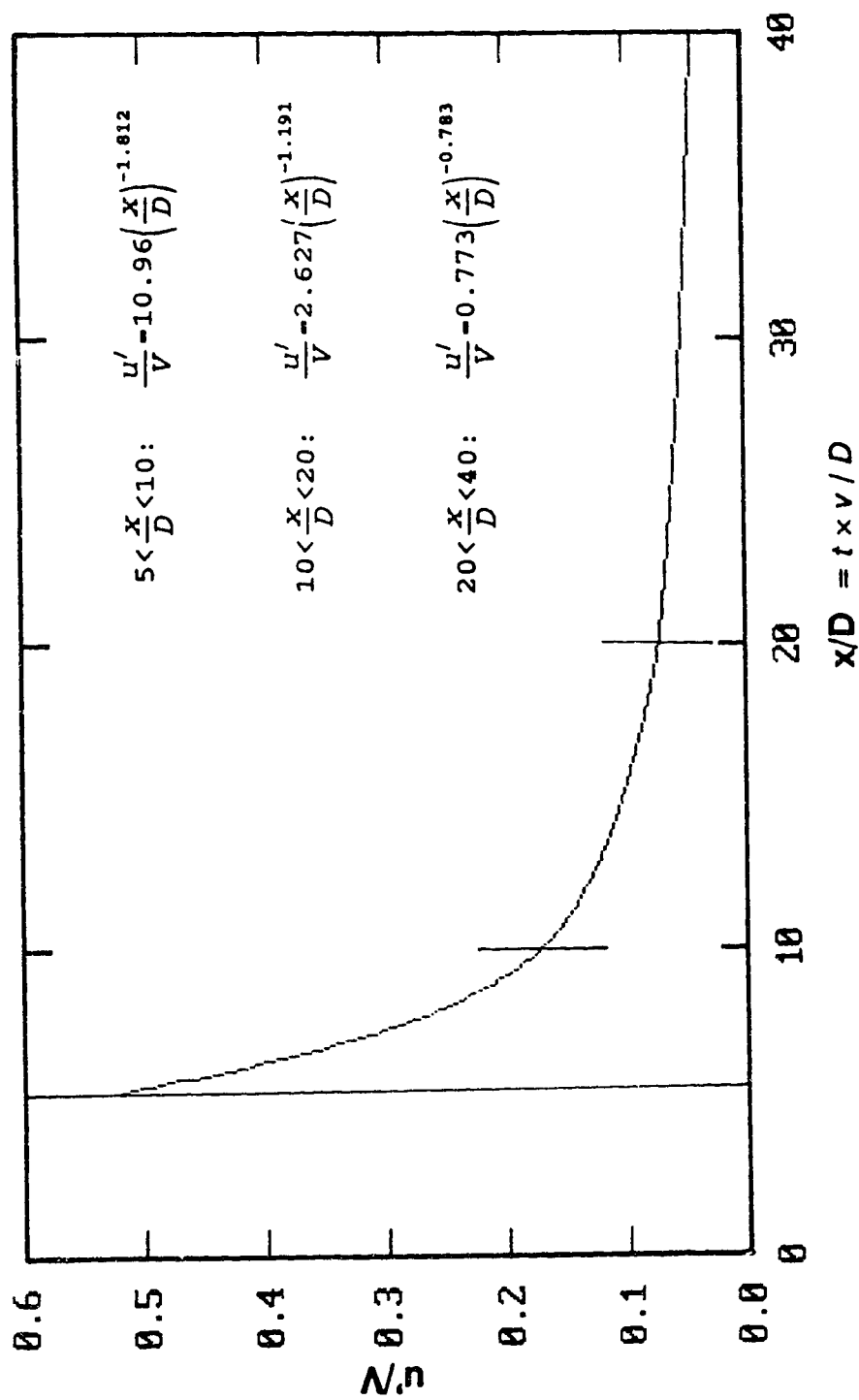


Figure 5.7 Decay of turbulence RMS intensity with downstream distance.

represent modified turbulent velocities normalized by unmodified turbulent velocities. Equations 5.2 and 5.3 show the radial and tangential turbulence distortion factors using this rapid distortion theory.

$$\mu_r = \zeta^{-3} c^{-2} \frac{3}{4} \left(\frac{\beta^2 - 1}{\beta^3} \tan^{-1} \beta + \beta^{-2} \right) \quad (5.2)$$

$$\mu_\theta = \mu_\alpha = \frac{3}{4} \frac{c}{\zeta} + \frac{3}{8} \frac{1}{\zeta^5 c^5} \left(\frac{1}{\beta^3} \tan^{-1} \beta - \frac{1}{\beta^2 (\beta^2 - 1)} \right) \quad (5.3)$$

where:

$$\beta^2 = \frac{1}{\zeta^2 c^3} - 1 \quad (5.4a)$$

$$\zeta = \left(\frac{\rho}{\rho_I} \right)^{-1} \quad (5.4b)$$

$$c = \left(\frac{r_I}{r_b} \right)^2 \quad (5.4c)$$

μ = turbulence distortion factor

ζ = compression factor ($\zeta \leq 1$)

c = normal strain due to geometrical straining ($c \leq 1$)

The radial component has the greatest effect on flame front growth while the tangential components have smaller effects. To equally account for all distortion

factors, a root-mean-square distortion factor was used. Thus the rapid distortion enhancement is:

$$\frac{U'_{RDT}}{U'} = \sqrt{\frac{\mu_r^2 + \mu_\theta^2 + \mu_a^2}{3}} \quad (5.5)$$

In terms of r_b/r_{cell} and in terms of pressure, the actual RDT enhancement as a multiplier was the same for all of the experiments tested ($u' = 1.0$ m/s) as shown in Figure 5.8. Due to the fact that the multiplier is greater than unity at all times, the turbulence intensity will always be greater than that due to its normal decay. The effect of the rapid distortion amplification due to a growing flame on the normal decay of turbulence was investigated. Initially, turbulence levels decayed because early flame growth was slow and flame kernel radii were small. After some time, the intensity levels increased because distortion had become a greater factor than decay as illustrated in Figure 5.9. Due to the viscous dissipation of turbulence at small scales, small turbulence scales decay faster than large ones. The larger scales obtain greater enhancement from the rapid distortion of turbulence.

Now that rapid distortion enhancements to intensity have been determined, the burning velocity relationship in Figure 5.5 can be modified to use turbulence parameters corresponding to the conditions in which the flame is developing. Turbulence conditions at the time when burning velocity calculations were made

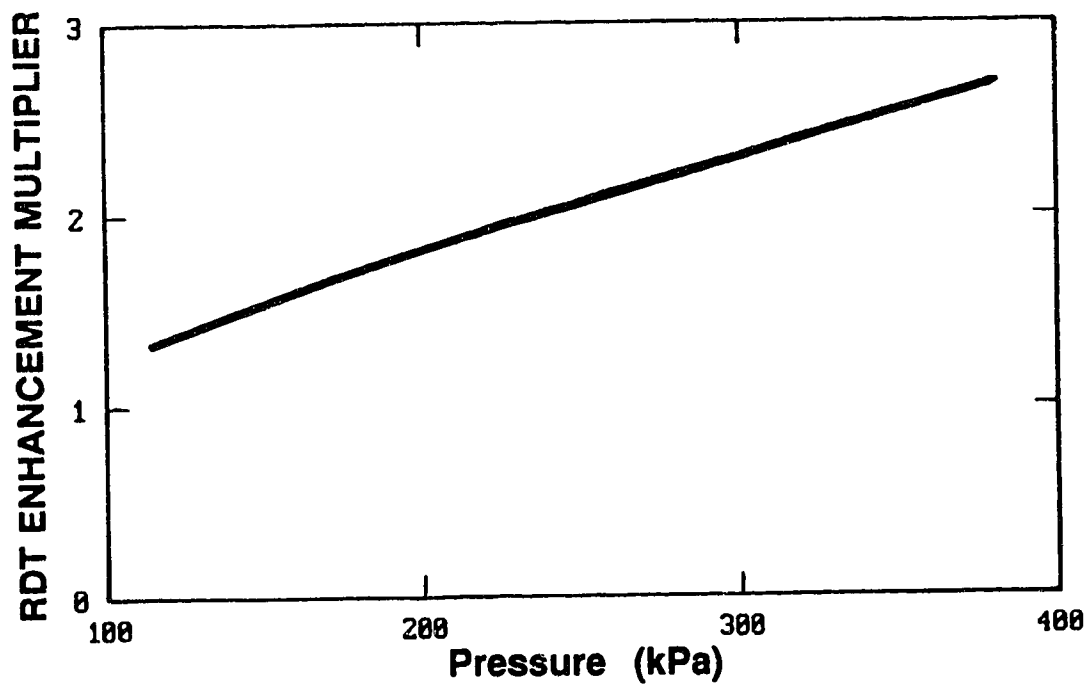
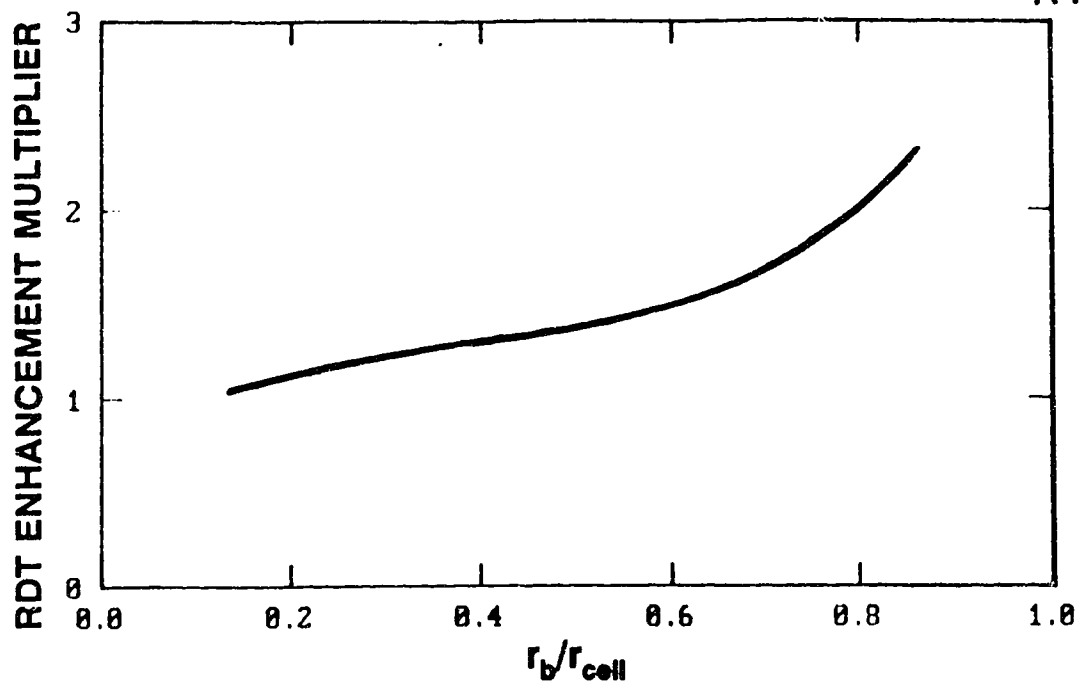
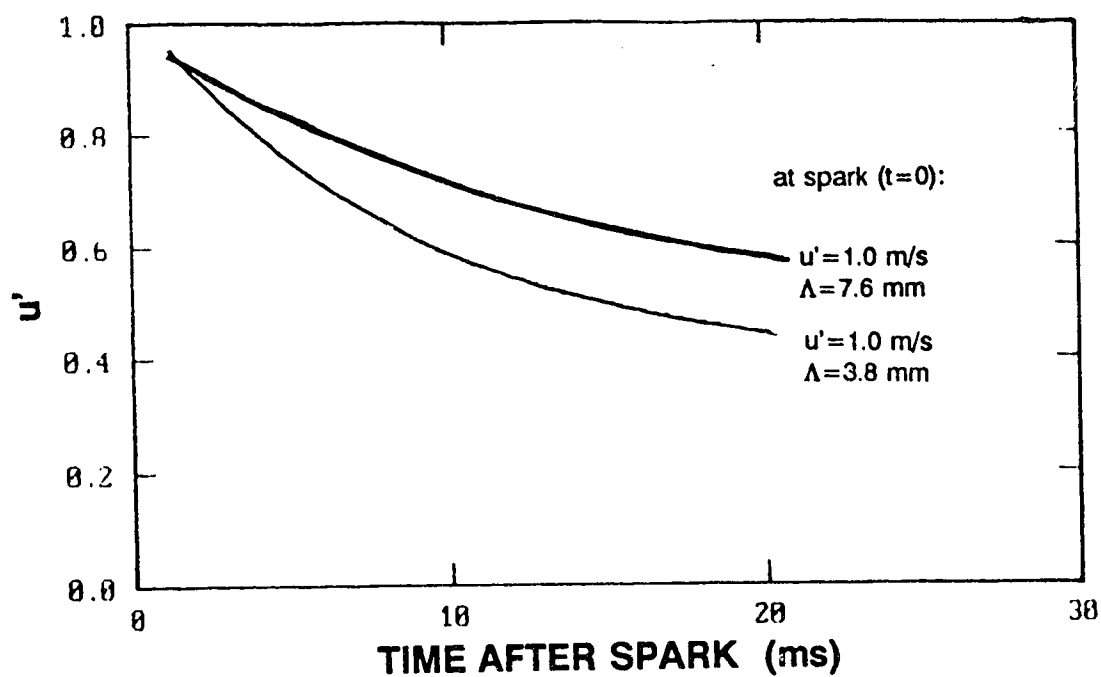
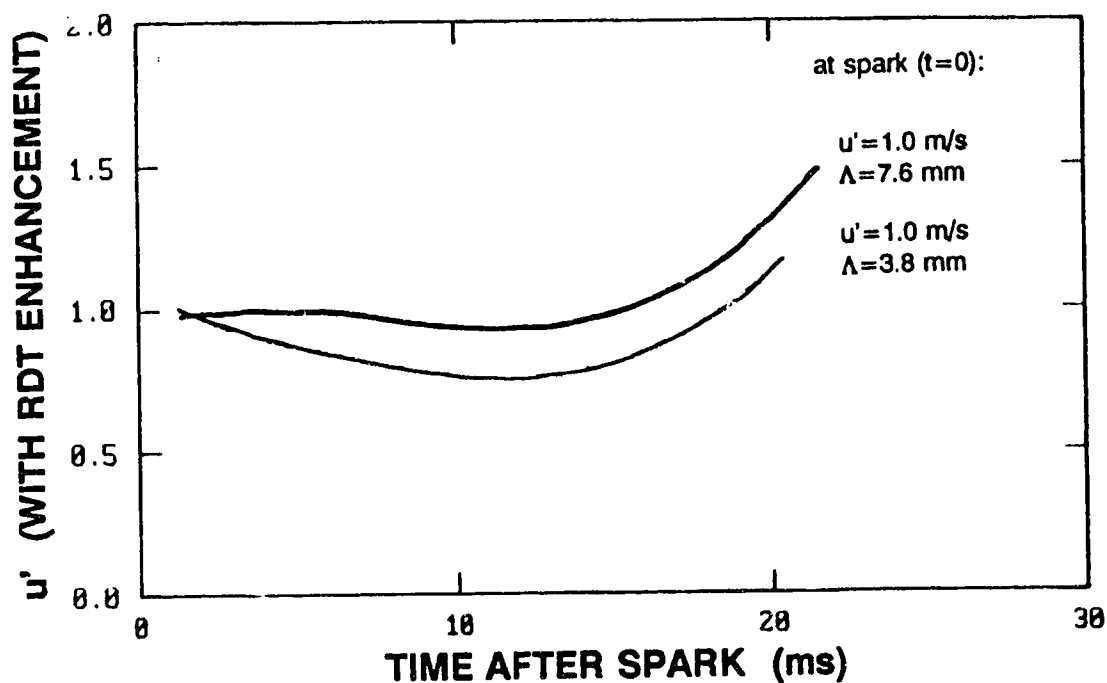


Figure 5.8 Rapid distortion theory turbulence intensity enhancement multiplier in terms of (a) relative radius and (b) pressure for all experiments.



(a) normal temporal decay



(b) normal temporal decay with rapid distortion enhancements

Figure 5.9 Turbulence RMS intensity with (a) normal temporal decay and (b) normal temporal decay with rapid distortion enhancements accounted for.

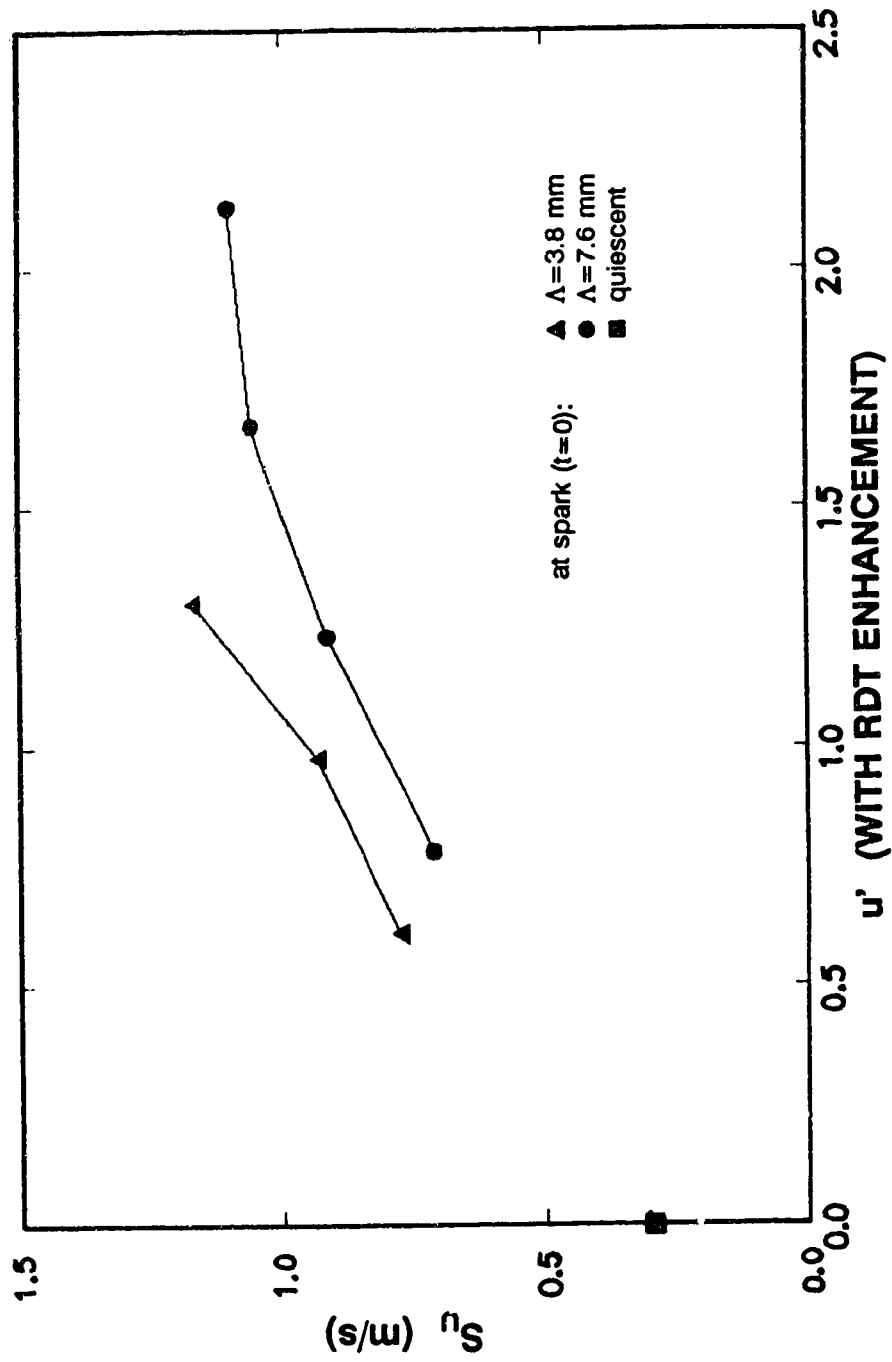


Figure 5.10 Calculated burning velocities for various turbulence intensity with rapid distortion enhancements. Average burning velocities and turbulence intensities are averages at pressures of 200 kPa and 250 kPa (about a 40 mm flame radius).

can be used instead of comparing in terms of ignition-time turbulence. Figure 5.10 shows calculated burning velocities as a function of intensity with rapid distortion enhancements included. The two curves are still classed in terms of their length scales at the time of ignition for ease of comparison. It can be seen that effects of smaller scales tend to increase the burning velocity for a given turbulence intensity. This scale effect is seen since turbulence intensity tends to decrease more rapidly for smaller scale turbulence as shown in Figure 5.9.

5.3.3 Turbulence Regimes

Relationships have been discussed by several researchers [48-50] where turbulent burning velocity has been given in terms of laminar burning velocity and turbulence intensity. To compare the results of this study to the results of others, the relationship between burning velocity and turbulence intensity was examined. The turbulent burning velocity and the turbulence intensity were both normalized by the laminar burning velocity. The relationship that is developed depends upon the regime that the turbulence is in. From previous research, reviewed by Zur Loye and Bracco [49], the following relationships for turbulent flame regimes have been developed.

a) A single-sheet subregime is where the flame burns in a continuous sheet. For this regime which applies to experiments in this study (u' not $> S_L$),

$$S_T = S_L \sqrt{\frac{1}{2} \left(1 + \sqrt{1 + 8C_1 \left(\frac{u'}{S_L} \right)^2} \right)} \quad (5.6)$$

where C_1 is a constant between 1 and 10.

b) Moderate turbulence, where $u' \approx S_L$, does not account for all the experiments in this study. S_L is not necessarily on the same order of magnitude as u' . For moderate turbulence,

$$S_T = S_L + C_2 u' \quad (5.7)$$

where C_2 has been determined empirically to be 1, 2.2, and 4 depending upon the experimental engine set-up.

c) For strong turbulence ($u' > S_L$),

$$S_T = 3.5 S_L \left(\frac{u'}{S_L} \right)^{0.7} \quad (5.8)$$

d) For engines,

$$S_T = S_L + 4.5 S_L \left(\frac{u'}{S_L} \right)^{0.7} \quad (5.9)$$

These regimes are illustrated in Figure 5.11 which shows the various relationships between relative turbulence intensity and relative turbulent burning velocity. The shaded portion on this graph shows where the experimental results from this investigation lie.

To closely examine the relationship of the results in this study, individual points representing groups of data were used to determine the value of C_1 . As stated in the references, the constant, C_1 , should be between 1 and 10. All the

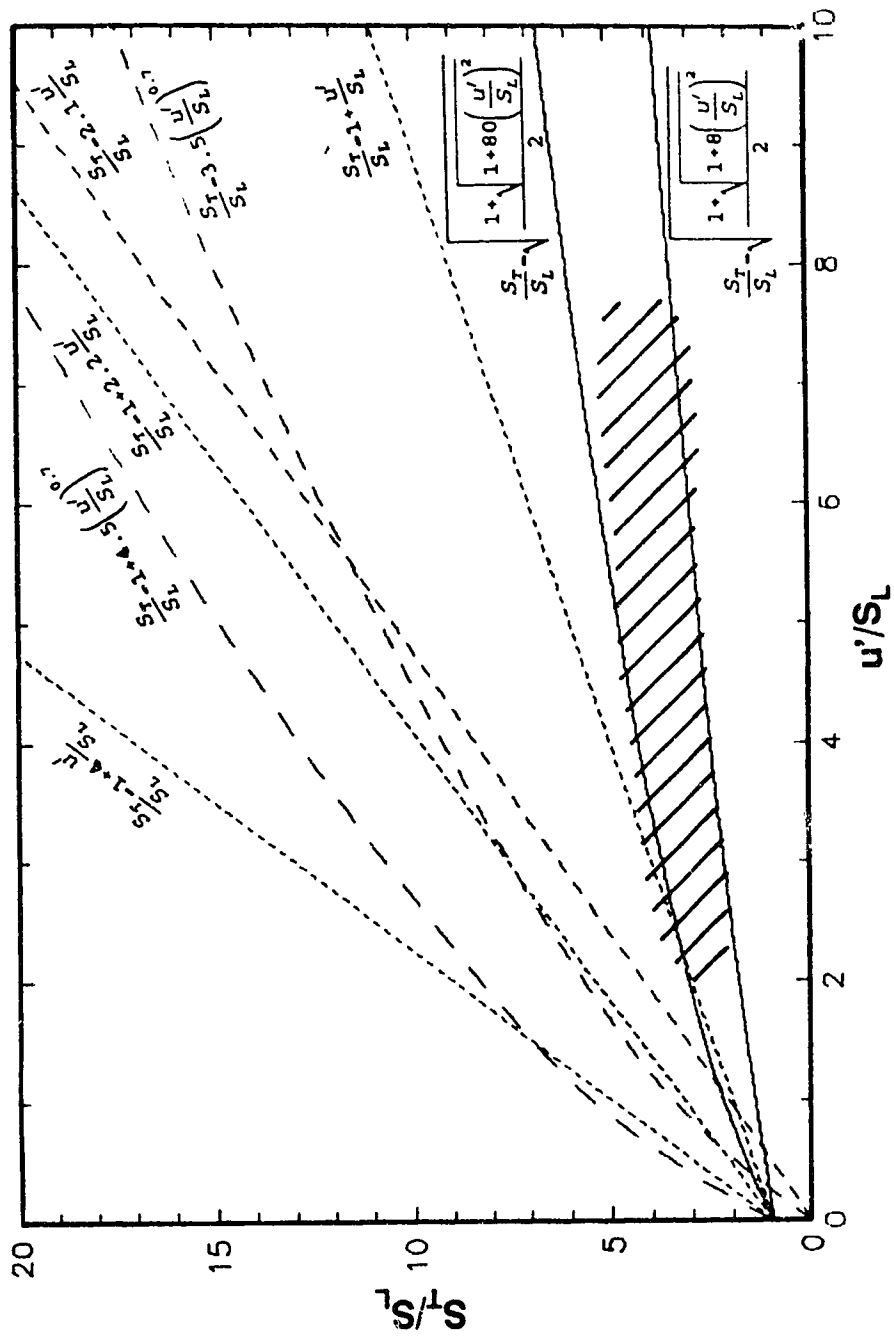


Figure 5.11 Various turbulence regimes as reviewed by Zur Loye and Bracco [49].

points fall within the limits defined by $C_T = 1$ and $C_T = 10$ for the relationship, as shown in Figure 5.12. Also shown in this figure are the effects of turbulence length scale. Experiments with length scales of 7.6 mm or greater tended to lie along a line where $C_T = 3$ while those with length scales less than 7.6 mm tended to lie along a line where $C_T = 6$. The experimental results of this study are clearly in the single-sheet subregime of turbulence as shown by the values of the constant C_T . As well, schlieren photographs similar to those in Figure 5.3 confirm that the flame is a single-sheet. In this study, the largest values of turbulence RMS intensity are about eight times the laminar burning velocity, which match the condition of a single-sheet subregime.

5.4 Summary of Turbulent Testing

Several of the findings are summarized below. The multi-zone thermodynamic equilibrium model accurately modelled flame growth over a range of turbulence conditions in the single-sheet flame regime. An increase in turbulence RMS intensities from 0 to 0.5 m/s resulted in a doubling of burning velocities, from about 0.35 m/s to about 0.7 m/s, for a mixture with a constant equivalence ratio ($\phi = 0.85$). Doubling turbulence RMS intensity from 0.5 m/s to 1.0 m/s resulted in only a 25% increase in burning velocity. Very little dependence upon the turbulence integral length scale was seen by the burning velocity results when compared on the basis of ignition-time turbulence.

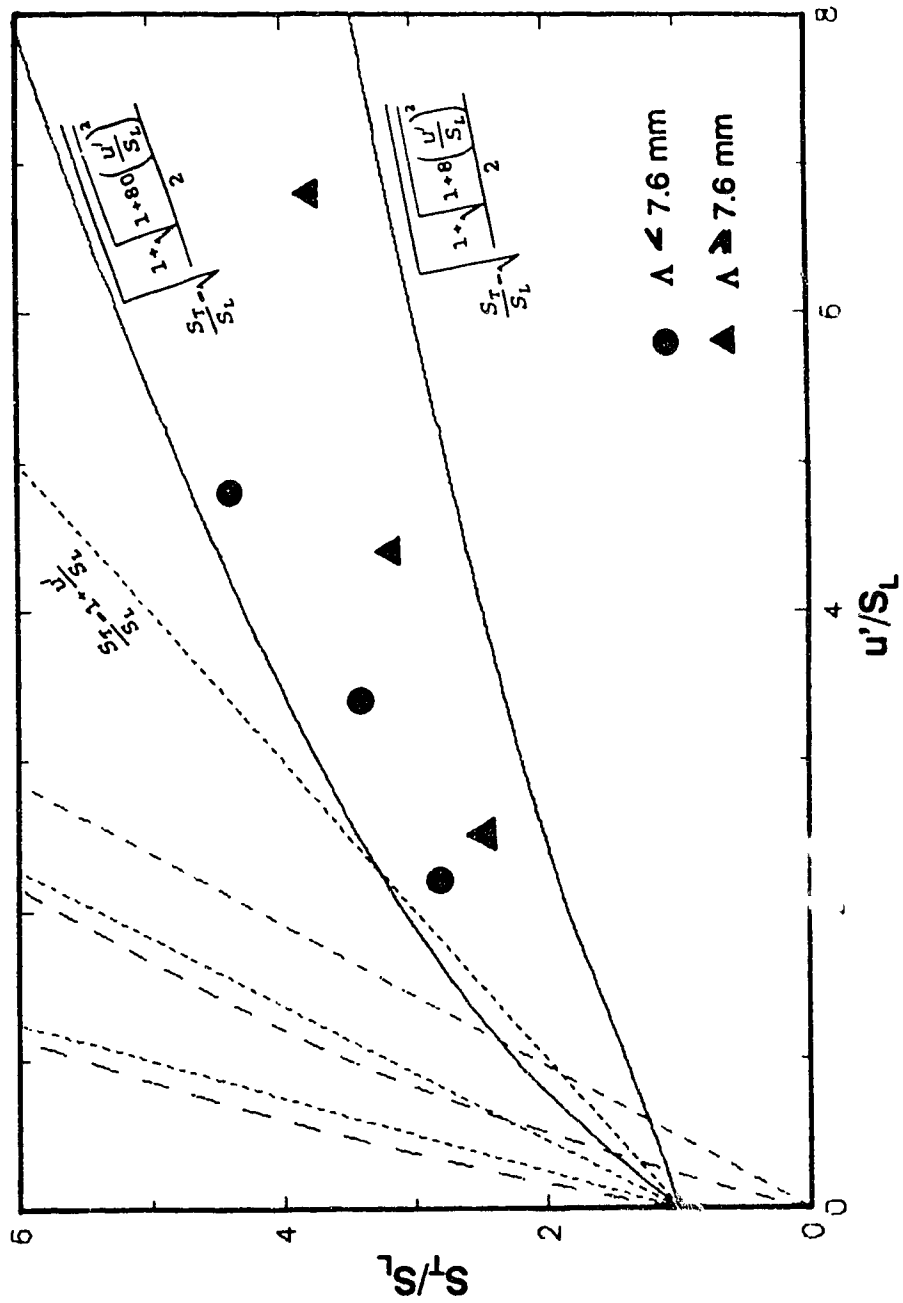


Figure 5.12 Comparisons of turbulence regimes from this study using lean ($\phi = 0.85$) mixtures and those reported.

Rapid distortion of turbulence theory was used to determine turbulence modification factors in a mixture with decaying turbulence. The turbulence RMS intensity ahead of the flame front was seen to increase beyond its level at the time of ignition. Using this rapid distortion theory to account for enhancements to turbulence intensity, comparisons to published results for well developed flames were possible. The turbulence levels in this study were seen to be in the single-sheet subregime (i.e. u' not $> S_L$) as expected, and were described by Equation 5.6:

$$\frac{S_T}{S_L} = \sqrt{\frac{1}{2} \left(1 + \sqrt{1 + 8C_1 \left(\frac{u'}{S_L} \right)^2} \right)}$$

The constant C_1 was determined to be 3 for integral length scales greater than 7.6 mm and 6 for those less than 7.6 mm.

6 COMBINED EFFECTS OF TURBULENCE AND ENHANCED IGNITION

6.1 Overview of Testing Program

Testing was done to determine the effects of the breakdown ignition circuit in lean, $\phi = 0.85$, turbulent mixtures. Flame growth was compared using both the standard and the breakdown, with 20 kV stored voltage, ignition systems in a turbulent mixture with $u' = 0.55$ m/s and $\Lambda = 7.6$ mm. The multi-zone thermodynamic equilibrium model was used to evaluate flame growth based on measured pressure data.

6.2 Experimental Results

Ignition system effects were determined by examining the flame growth in turbulent mixtures when ignited using both the standard and the breakdown ignition systems. No photographic data were available for the early portion of the flame growth for these turbulent tests. By comparing the pressure-based results, similar growth rates (i.e. similar slopes) were seen for the later stages of flame growth as shown in Figure 6.1. Only the later stages can be compared because the low signal-to-noise ratio caused inaccurate model results below pressures of 120 kPa as previously discussed. Measurements revealed that the breakdown ignition circuit had a flame development period of 16.0 ms while that for the standard ignition circuit was 18.4 ms (15% higher). Measurements also indicate that the burn durations for each ignition circuit are within 1 ms. This is within

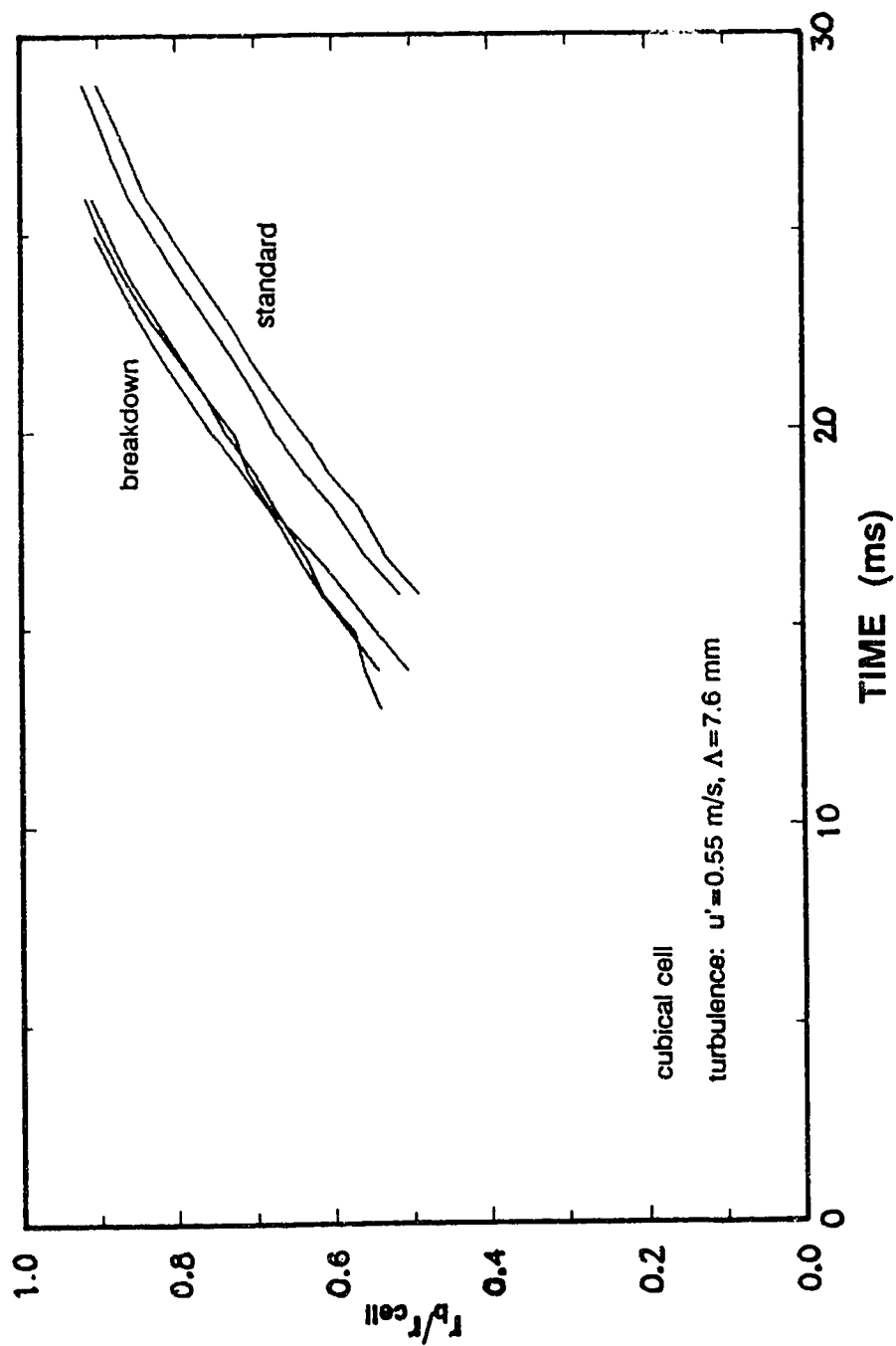


Figure 6.1 Flame growth of lean ($\phi = 0.85$) turbulent mixtures based on equilibrium model calculations for standard and breakdown ignition systems.

experimental uncertainty for these turbulence tests which inherently show high variability. Since their growth rates are similar and a flame from the breakdown ignition system reached a particular flame radius before a flame from the standard system did, it can be concluded that the breakdown ignition system accelerated flame growth during the early flame development period.

Comparison of the effects of ignition system and the effects of turbulence must be made on a relative basis. The averaged and smoothed data of Figure 4.13 for quiescent mixtures were compared to the averaged and smoothed data of Figure 6.1 for turbulent mixtures. Both set of experiments were performed in mixtures with an equivalence ratio of 0.85. In both quiescent and turbulent mixtures, the advantage of the breakdown ignition system was to shift flame development forward due to its rapid flame kernel development. These relative flame radii are shown in Figure 6.2. A time advantage of about 2.5 ms when using the breakdown system is similar for both quiescent and turbulent mixtures.

It can be seen that regardless of the ignition system used, a turbulent mixture is advantageous, resulting in a 70% higher rate of flame growth or higher burning velocity. With the shorter total burning time of about 37 ms, from spark to 95% of developed pressure rise, for the turbulent mixtures, the relative benefits are greater than for the quiescent mixtures with a total burning time of about 71.5 ms. A 2.5 ms decrease in flame development period would result in a 7% decrease in total burn time for a turbulent mixture and only a 3.5% decrease for a quiescent mixture. The greatest benefits are seen while using a combination of

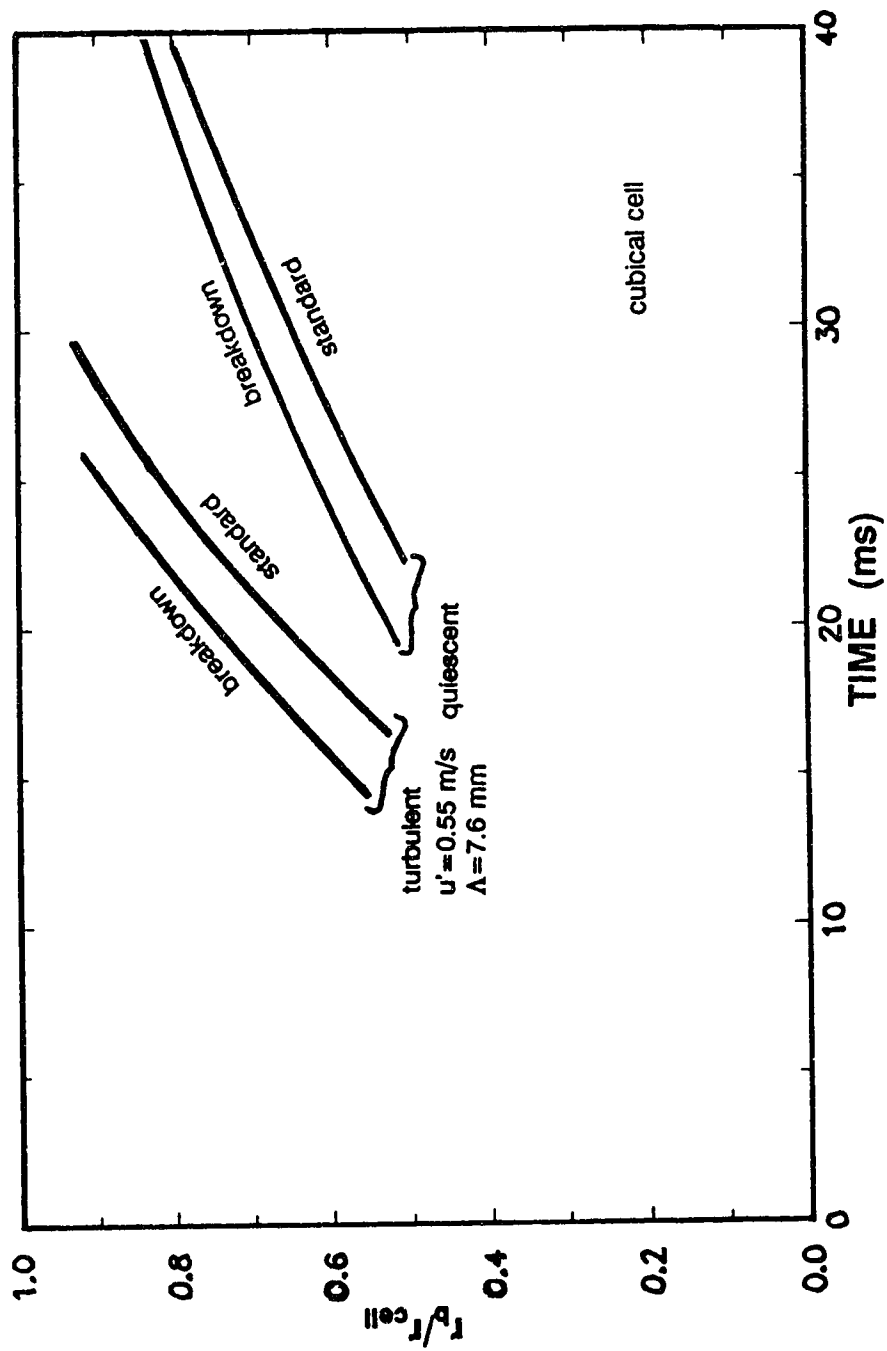


Figure 6.2 Average flame growth of lean ($\phi = 0.85$) quiescent and turbulent mixtures using standard and breakdown ignition systems.

an enhanced ignition system and mixture turbulence.

6.3 Flame Kernel Growth Regimes

In the previous section, it was determined that the flame kernel growth in the early stages was accelerated with the use of an enhanced ignition system. This coincides with the work of others revealing that the very early flame kernel growth is dominated by the ignition system [8, 11, 51]. These same studies showed that the later stages of flame development were dominated by the effects of combustion chamber geometry, flow field, and mixture properties. The data reported here concur with these results as shown by the nearly identical flame growth rates after ignition in both quiescent and turbulent conditions.

6.4 Summary of Combined Effects

In testing the combined effects of enhanced ignition systems and turbulence enhancement, it was shown that flame kernel development was affected by the ignition system and that flame growth rate was affected by the mixture turbulence. It was also shown that the reduction in total burn time was constant at about 2.5 ms using a breakdown ignition system. This decrease in total burn time was realised through a decrease in the flame development period of 2.5 ms. As total burn time reduced with an increase of mixture turbulence, the relative benefit increased -- 7% decrease in total burn time for a turbulent mixture and 3.5% for a quiescent mixture.

7 SUMMARY OF RESULTS AND CONCLUSIONS

7.1 Overview of This Investigation

This investigation of the effects of enhanced ignition systems, the effects of turbulence, and their combined effects was undertaken to gain a better understanding of the combustion of lean mixtures. Combustion of lean mixtures may be desirable due to the potentially higher thermal efficiency and the ability to use higher compression ratios in engines. The investigation was to study methods of improving slow burning which may result in power reduction, misfire, cyclic variations, and knock.

Both enhanced ignition systems and increased turbulence have been seen to decrease the combustion period of lean mixtures and to extend the lean operating limit of an engine. In the past, some research has given inconsistent explanations for the causes of reductions in combustion period. This may have been due to the analysis of results and the diagnostic methods used.

This study has tested two enhanced ignition circuits against a standard circuit. Ignition energy, energy delivery rate, and spark geometry were each investigated in this study. This study has isolated the effects of turbulence RMS intensity and turbulence integral length scale in controlled, homogeneous, decaying, turbulence. To restate the objectives of this work, they were to determine the effects of ignition system and turbulence, both individually and together, on burning velocity for lean methane - air mixtures.

7.2 Trends of Results and Conclusions

When comparing enhanced ignition systems, it was found that a plasma jet circuit using a plasma jet cavity spark plug consistently resulted in the shortest flame development period, shortest burn duration, and highest burning velocity. When using a surface gap spark plug, the plasma jet circuit provided performance similar to the breakdown ignition circuit with the same energy level. Their performance was midway between the plasma jet circuit with a plasma jet cavity spark plug and the standard, low energy spark. Since the breakdown system releases most of its energy during the efficient (up to 94%) breakdown mode of a spark, it was chosen for further investigation.

Using the breakdown system, it was seen that the flame kernel development period was closely related to the stored voltage levels of the system. Burn duration was affected by the stored voltage levels, but the effects were thought to be due a projection of the spark kernel from the igniter, resulting in a favourable spark position and geometry. This supports previous findings showing that direct ignition system benefits are seen in the early flame kernel development period. Secondary benefits were seen due to the projection of the spark. Schlieren photographic results confirmed these findings.

While examining the effects of turbulence, it was found that the turbulence integral length scale at the time of ignition had little effect on subsequent burning velocity but the turbulence RMS intensity at the time of ignition had a strong effect. Increasing from a quiescent mixture to an intensity of 0.5 m/s resulted in a

doubling of burning velocity from 0.35 m/s to 0.7 m/s. Doubling the turbulence RMS intensity from 0.5 m/s to 1.0 m/s resulted in 25% higher burning velocities.

By accounting for rapid distortion enhancements in decaying turbulence, the turbulence RMS intensity ahead of the flame front could increase to beyond its level at the time of ignition. In comparing the flames of this study with others, it was found that they were in the single-sheet subregime, as seen in photographic measurements, and corresponded very well with the existing relationship.

In combining enhanced ignition systems with turbulence enhanced mixtures, it was found that their effects were additive. Similar ignition system benefits were seen in both quiescent and turbulent mixtures and turbulence benefits were seen when using standard or enhanced ignition systems. Due to the shorter total burning time for turbulent mixtures, a reduced flame development period gave greater relative benefits than for a quiescent mixture.

7.3 Suggested Improvements and Further Research

One of the major problems in using the thermodynamic equilibrium model as described in this study or any pressure based model was the low signal-to-noise ratio during the early stages of combustion. It is suggested that a highly sensitive pressure transducer be used in conjunction with a reduction in ignition system noise, achieved through isolation and shielding, to increase the signal-to-noise ratio to a higher level. It is also suggested that a higher rate of pressure data acquisition be used and that none of the data be eliminated through

"compression" averaging methods. Alternative pressure measurement methods might also be tested such as laser interferometry as discussed by Haley and Smy [52].

Increasing the number of direct measurements in the early flame development period would be very informative. Increasing the filming rate of the schlieren photography system to 10 000 frames per second would require a higher speed camera or modification to the existing unit. A much brighter light source or faster film would also be required.

To account for flame shape, flame kernel images could be computer digitized and then flame areas and nominal radii objectively calculated. Simultaneous, multiple views of the flame would provide a more accurate definition of the flame shape perhaps replacing the spherical flame assumption.

To reduce the trial and error time required to pinpoint the desired turbulence parameters, it would be beneficial to develop the electronics to immediately provide average plate speed and spark delay time measurements. This would eliminate the need to digitize each experimental run as it is conducted, resulting in more efficient use of time.

As far as the directions to be taken for further research, it is suggested that the time constants or capacitance of the breakdown ignition system be altered so that spark durations may range from about 1 ns to 1 μ s to determine the effect of spark duration. The effects of the smaller length scales of turbulence, such as Taylor microscale and Kolmogorov scale, should be investigated, as there is some

research [17, 53] that suggests that these smaller scales may affect the flame development period and cyclic variations.

REFERENCES

- 1 G.J. van Wylen and R.E. Sonntag, Fundamentals of Classical Thermodynamics, SI Version 2^e, John Wiley & Sons, 1978.
- 2 G.E. Andrews and D. Bradley, "The Burning Velocities of Methane-Air Mixtures", *Combustion and Flame*, **19**: 275-288, 1972.
- 3 T. Iijima and T. Takeno, "Effects of Temperature and Pressure on Burning Velocity", *Combustion and Flame*, **65**: 35-43, 1986.
- 4 H. Schwarz, "Ignition Systems for Lean Burn Engines", I.Mech.E. C95/79, 1979.
- 5 G.F.W. Ziegler, E.P. Wagner, B. Saggau, R. Maly, and W. Herden, "Influence of a Breakdown Ignition System on Performance and Emission Characteristics", SAE 840992, 1984.
- 6 J.A. Harrington, R.C. Shishu, and J.R. Asik, "A Study of Ignition System Effects on Power, Emissions, Lean Misfire Limit, and EGR Tolerance of a Single-Cylinder Engine -- Multiple Spark versus Conventional Single Spark Ignition", SAE 740188, 1974.
- 7 R.W. Anderson and J.R. Asik, "Lean Air-Fuel Ignition System Comparison in a Fast-Burn Engine", SAE 850076, 1985.
- 8 S. Pischinger, and J.B. Heywood, "A Study of Flame Development and Engine Performance with Breakdown Ignition Systems in a Visualization Engine", SAE 880518, 1988.
- 9 J.D. Dale and A.K. Oppenheim, "Enhanced Ignition for I. C. Engines with Premixed Gases", SAE 810146, 1981.
- 10 R. Maly, B. Saggau, E. Wagner, and G. Ziegler, "Prospects of Ignition Enhancement", SAE 830478, 1983.
- 11 R.W. Anderson, "The Effect of Ignition System Power on Fast Burn Engine Combustion", SAE 870549, 1987.
- 12 L.E. Gettel and K.C. Tsai, "The Effect of Enhanced Ignition on the Burning Characteristics of Methane-Air Mixtures", *Combustion and Flame*, **54**: 183-193, 1983.

- 13 G.F.W. Ziegler, R. Maly, and E.P. Wagner, "Effect of Ignition System Design on Flammability Requirements in Ultra-Lean Turbulent Mixtures", I.Mech.E. C47/83, 1983.
- 14 R.F. Haley, "A Schlieren Study of Flame Initiation", M.Sc. Thesis, University of Alberta, 1986.
- 15 J.A. Gatowski and J.B. Heywood, "Flame Photographs in a Spark-Ignition Engine", *Combustion and Flame*, **56**: 71-81, 1984.
- 16 A.F. Ghoniem, "Effect of Large Scale Structures on Turbulent Flame Propagation", *Combustion and Flame*, **64**: 321-336, 1986.
- 17 P.G. Hill, "Cyclic Variations and Turbulence Structure in Spark-Ignition Engines", *Combustion and Flame*, **72**: 73-89, 1988.
- 18 D. Bradley, J. Hynes, M. Lawes, and C.G.W. Sheppard, "Limitations to Turbulence-Enhanced Burning Rates in Lean Burn Engines", I.Mech.E. C46/88, 1988.
- 19 D.R. Lancaster, R.B. Kriger, S.C. Sorenson, and W.L. Hull, "Effects of Turbulence on Spark Ignition Engine Combustion", SAE 760160, 1976.
- 20 S. Ohigashi, Y. Hamamoto, and A. Kizima, "Effects of Turbulence on Flame Propagation in Closed Vessel", *Bulletin of the JSME*, **14**: 849-858, No. 74, 1971.
- 21 T. Wakisaka and Y. Hamamoto, "Effects of Mixture Turbulence on the Limits of Flame Propagation", *Bulletin of the JSME*, **22**: 382-389, No. 165, 1979.
- 22 B.J. McDonell, "Burning Rates of Propane-Air Mixtures in Homogeneous Decaying Turbulence", M.Sc. Thesis, University of Alberta, 1988.
- 23 J.D. Wilson, J.D. Dale, and A. Bobey, "Design and Testing a Cell for Ignition Studies", Presented at the Spring Technical Meeting of the Combustion Institute / Canadian Section, Waterloo, May, 1983.
- 24 M.D. Checkel and A. Thomas, "Turbulent Explosions in Closed Vessels", I.Mech.E. C57/83, 1983.
- 25 M.D. Checkel, "Turbulence Enhanced Combustion of Lean Mixtures", Ph.D. Thesis, Cambridge University, 1981.

- 26 M.D. Checkel, "Measurements of Turbulence Generated by 60% Solid Perforated Plates", *ASME Transactions, Journal of Fluids Engineering*, p55, March, 1985.
- 27 T.C. Chew and R.E. Britter, "Effect of Geometrical Straining on Turbulence Levels in Explosions and Common Burner Configurations", Cambridge University Engineering Department report.
- 28 M.S. Hancock, M.R. Belmont, and D.J. Buckingham, "The Correlation Between Early Light Emission and Peak Pressure in a Spark Ignition Engine", *I.Mech.E. C56/88*, 1988.
- 29 B. Lewis and G. von Elbe, Combustion, Flame, and Explosions of Gases, Academic Press, 1951.
- 30 R.R. Burgett, J.M. Leptich, and K.V.S. Sangwan, "Measuring the Effect of Spark Plug and Ignition System Design on Engine Performance", *SAE 720007*, 1972.
- 31 R.Maly and Vogel, "Initiation and Propagation of Flame Fronts in Lean CH₄-Air Mixtures by the Three Modes of the Ignition Spark", Seventeenth Symposium (International) on Combustion, Combustion Institute, p821, 1979.
- 32 E.K. Dabora, "Ignition by a Laser Generated Plasma Jet", Presented at The Combustion Institute/Central States Section spring meeting, March, 1981.
- 33 R.S. Benson, Advanced Engineering Thermodynamics, 2nd Ed., Pergammon Press, 1977.
- 34 W.C. Reynolds, "STANJAN, An Interactive Program for Equilibrium Analysis by the Method of Element Potentials", v3.81, Mechanical Engineering Department, Stanford University, 1987.
- 35 J.R. Asik, P. Piatkowski, M.J. Foucher, and W.G. Rado, "Design of a Plasma Jet Ignition System for Automotive Application", *SAE 770355*, 1977.
- 36 P.R. Smy, R.M. Clements, and D.R. Topham, "Efficiency and Erosion of Plasma Jet Igniters -- Variation with Voltage", *Combustion Science and Technology*, **42**: 317-324, 1985.
- 37 P.R. Smy, R.M. Clements, J.D. Dale, D. Simeoni, and D.R. Topham, "Efficiency and Erosion Characteristics of Plasma Jet Igniters", *J. Phys. D.: Appl. Phys.*, **16**: 783-791, 1983.

- 38 D. Bradley and I.L. Critchley, "Electromagnetically Induced Motion of Spark Ignition Kernels", *Combustion and Flame*, **22**: 143-152, 1974.
- 39 C.L. Bouchard, C.F. Taylor, and E.S. Taylor, "Variables Affecting Flame Speed in the Otto-Cycle Engine", *SAE Journal*, **41**: 514-520, No. 5, 1937.
- 40 G.M. Rassweiler and L. Withrow, "Motion Pictures of Engine Flames Correlated with Pressure Cards", *SAE Journal*, **42**: 185-204, No. 5, 1938.
- 41 R.J. Tabaczynski, "Turbulence Measurements and Modelling in Reciprocating Engines -- An Overview", *I.Mech.E. C51/83*, 1983.
- 42 P.O. Witze, J.K. Martin, and C. Borgnakke, "Measurements and Predictions of the Precombustion Fluid Motion and Combustion Rates in a Spark Ignition Engine", SAE 831697, 1983.
- 43 N.C. Blizard and J.C. K  ck, "Experimental and Theoretical Investigation of Turbulent Burning Model for Internal Combustion Engines", SAE 740191, 1974.
- 44 N. Collings, A.W. Roughton, and T. Ma, "Turbulence Length Scale Measurements in a Motored Internal Combustion Engine", SAE 871692, 1987.
- 45 R.G. Abdel-Gayed and D. Bradley, "Criteria for Turbulent Propagation Limits of Premixed Flames", *Combustion and Flame*, **62**: 61-68, 1985.
- 46 M.J. Hall and F.V. Bracco, "Cycle-Resolved Velocity and Turbulence Measurements Near the Cylinder Wall of a Firing S.I. Engine", SAE 861530, 1986.
- 47 M.J. Hall and F.V. Bracco, "A Study of Velocities and Turbulence Intensities Measured in Firing and Motored Engines", SAE 870453, 1987.
- 48 J. Abraham, F.A. Williams, and F.V. Bracco, "A Discussion of Turbulent Flame Structure in Premixed Charges", SAE 850345, 1985.
- 49 A.O. zur Loye and F.V. Bracco, "Two-Dimensional Visualization of Premixed-Charge Flame Structure in an IC Engine", SAE 870454, SP-715, 1987.
- 50 P.O. Witze and J.M.C. Mendez-Lopes, "Direct Measurement of the Turbulent Burning Velocity in a Homogeneous-Charge Engine" SAE 861531, 1986.

- 51 D. Bradley and F.K. Lung, "Spark Ignition and Early Stages of Turbulent Flame Propagation", *Combustion and Flame*, **69**: 71-93, 1987.
- 52 R. Haley and P.R. Smy, "Combustion Chamber Pressure Measurement at Very Early Times: Comparison of Plasma Jet Ignition with Conventional Ignition", *Combustion Science and Technology*, **63**: 131-137, 1989.
- 53 J.A. Gatowski, J.B. Heywood, and C. Deleplace, "Flame Photographs in a Spark-Ignition Engine", *Combustion and Flame*, **56**: 71-81, 1984.
- 54 D.J. Patterson, "Cylinder Pressure Variations, A Fundamental Combustion Problem", SAE 660129, 1966.
- 55 F.A. Matekunas, "Modes and Measures of Cyclic Combustion Variability", SAE 830337, 1983.
- 56 J.W. Daily, "Cycle-To-Cycle Variations: A Chaotic Process?", SAE 870165, 1987.
- 57 H. Yamamoto and M. Misumi, "Analysis of Cyclic Combustion Variation in a Lean Operating S.I. Engine", SAE 870547, 1987.
- 58 D.M. Heaton and J.R. Thomas, "A Novel Combustion Chamber Enabling Open Chamber Lean Burn Natural Gas S.I. Engines to Meet Exhaust Emission Regulations -- The Ricardo Nebula System", Ricardo Consulting Engineers report DP 88/0515, 1988.
- 59 R.H. Thring and M.T. Overington, "Gasoline Engine Combustion -- The High Ratio Compact Chamber", SAE 820166, 1982.

APPENDIX

The details of the multi-zone thermodynamic equilibrium model are given in this appendix. It contains five parts:

- 1) the thermodynamic equilibrium modelling program -- NEWBOMB -- which creates a data base for a given set of initial conditions (i.e. P , T , ϕ ,...),
- 2) the data base file which was created by NEWBOMB,
- 3) a standard experimental data file containing 256 information integers, 512 pressure integers, and 512 light emission integers,
- 4) the interpolating program, NEWBPR2, which correlates the NEWBOMB data base information with an experimentally measured pressure trace to arrive at burned volume or mass burned as a function of time, and
- 5) an output file, containing all the thermodynamic data required for future calculations.

PART 1

NEWBOMB -- the thermodynamic equilibrium modelling program.

```

DECLARE SUB PROPCOEFF ()
DECLARE SUB EQCONST ()
DECLARE SUB REACTPROP (EQUIV!, FCA!, FHA!, FMW!, MF!, MOXY#, MN2#, MWR!)
DECLARE SUB FLAME (INDV!, HEAT!, WORK!, PE!, FCA!, FHA!, FMW!, S!, TR!, T!, MWR!, MWP!,
FLAG%)

```

```

NEWBOMB
*****

```

```

25-NOV-88 M.D. CHECKEL
11-MAY-89 Cleaned up to use for *.CEL data. -- RUSS MODIEN
05-MAY-90 Combined BMBPR2 & BOMB to make NEWBOMB. -- RUSS MODIEN

```

```

NOTE: After any major alteration, update the above list and VERDAT$.

```

PROGRAM HISTORY:

```

BMBPR2 is BMBPRESS.BAS modified to include propane or methane explosions.
Converted back from BMBPR5N on 23 November, 1988.
Based on BOMB.BAS per Alun Thomas's BOMB.BAS with corrections re units, etc

```

```

This program is used in conjunction with the program NEWBPR2 which uses
measured pressure and light emission records and combines them with the
calculated quantities from this program. For most properties, a simple
interpolation is used to match measured pressures with corresponding values
from this program. (See NEWBPR2 for more information.)
By itself, this program calculates fates of elements of lean fuel-air
mixtures at specified starting conditions, burning in a constant volume
combustion cell. It has been set up for specific use with CLF and CEL
combustion experiments in mind (ie Cambridge & Alberta) but is should be
fairly adaptable for other purposes. The subroutines that are called in
the CMBSUB subroutine file are fairly well tested and proven. Please do
NOT change them since they are called by many different programs. If any
modifications have to be made, create a new version of the CMBSUB file and
then alter it. (The same common sense should be used for all the standard
combustion lab / Checkel programs or subprograms!) Read CMBSUB.DOC for
in understanding the program and subroutines.

```

```

Thermodynamic properties and methods are used as described in:

```

```

Rowland S. Benson,
"Advanced Engineering Thermodynamics"
Pergammon Press, 1977, 2nd Edition
(eg pg 153, Appendix A)

```

' Include common statements and routines, then dimension some variables.

```

REM $INCLUDE: 'C:\QB\COMB\CMBCOM.BAS'
REM $INCLUDE: 'C:\QB\LIB\PLOTCOM.BAS'
REM $INCLUDE: 'C:\QB\LIB\COLORCHC.BAS'
REM $INCLUDE: 'C:\QB\COMB\CMBFN-RP.BAS'
REM $DYNAMIC

```

```

VERDAT$ = '05-MAY-90'

```

```

REDIM IC(8, 7), IS(8), CC(6), CW(6), R(7), P(7), M#(6), W(8)
REDIM N%(10), FUEL$(2)
DIM STORE(600, 11), STORE2(600, 12)

```

' These are the INSCRN variables.

```

X% = 5
REDIM DS(X%), T%(X%), P$(X%), LG%(X%), L%(X%), C%(X%)
REDIM IP$(X%), IP%(X%), IP!(X%), IP#(X%)

```

' Set up some constants.

```

RMOL = 8314.3      'ideal gas constant in J/kmol.K

```

' The subroutine PROPCOEFF fills an array with coefficients used in
' calculating enthalpy and Gibbs function for CO, CO2, H2, H2O, N2, O2,
' and fuel. (See CMBSUB for details.)

' IS() is the alphanumeric name.

' W() is the molecular weight.

' IC() is the coefficient array.

```

CALL PROPCOEFF

```

' The subroutine EQCONST calculates chemical equilibrium constants used
' for CO2 and CO2-H2O dissociation reactions. The IC() array is used for
' this. (See CMBSUB for details.)

```

CALL EQCONST

```

' Get run type and set the cell volume and fuel type. This assumes that the
' standard Cambridge CLF or Alberta CEL runs will be modelled.

' V# is the bomb volume in m³. It remains constant.

' FUEL% is an integer constant to indicate which fuel is present.

' FUEL\$() contains the alphanumeric fuel names.

```
CLS
AST$ = STRING$(79, "**")
LOCATE 1, 1: PRINT AST$: PRINT AST$: PRINT AST$
LOCATE 2, 30: PRINT " NEWBOMB " + VERDAT$ + " "
LOCATE 4, 1: PRINT
```

RUNTYPE:

```
PRINT "Enter 1 = PROPANE CLF run,"
PRINT " 2 = METHANE CEL run,"
INPUT " 3 = QUIESCENT METHANE CEL run. > "; IN%
IF IN% = 1 THEN V# = .001684#: FUEL% = 1
IF IN% = 2 THEN V# = .001882#: FUEL% = 2
IF IN% = 3 THEN V# = .0005094#: FUEL% = 2
```

```
FUEL$(1) = "C3H8"
FUEL$(2) = "CH4"
```

' Enter initial conditions and number of volume elements to work on.

```
TINIT = 293.15      ' pre-combustion temperature in K
PINIT = 101325      ' pre-combustion pressure in Pa
EQUIV = .85         ' equivalence ratio
```

' Print a bit of a header and verify some parameters with user.

INPUTSECTION:

```
COLOR NFC%, NBC%
PRINT
PRINT "BOMB COMBUSTION EFFECTS CALCULATION PROGRAM"
PRINT
PRINT "MODIEN version of "; VERDAT$; ", run at "; TIME$; " on "; DATE$
```

```
D$(1) = STR$(V#): T%(1) = 3: LG%(1) = 9: L%(1) = 12: C%(1) = 10
P$(1) = "Enter volume of bomb in m3 (0=" + D$(1) + ") >"
D$(2) = STR$(TINIT): T%(2) = 1: LG%(2) = 7: L%(2) = 14: C%(2) = 10
P$(2) = "Enter initial temperature (0=" + D$(2) + ") >"
D$(3) = STR$(PINIT): T%(3) = 2: LG%(3) = 15: L%(3) = 16: C%(3) = 10
P$(3) = "Enter initial pressure in Pa (0=" + D$(3) + ") >"
D$(4) = STR$(EQUIV): T%(4) = 1: LG%(4) = 7: L%(4) = 18: C%(4) = 10
P$(4) = "Enter equivalence ratio (0<E<0.9999), (0=" + D$(4) + ") >"
D$(5) = STR$(FUEL%): T%(5) = 0: LG%(5) = 3: L%(5) = 20: C%(5) = 10
P$(5) = "Enter FUEL code (1=propane, 2=methane; default="
P$(5) = P$(5) + D$(5) + ") >"
```

```

CALL INSCRN(5, 1, T%, P$, LG%, D$, L%, C%, IP$, IP%, IP!, IP#, FX$)

-----

' Echo back some of the initial parameters for the user.
'
CLS
PRINT 'Press <Ctrl><PrtSc> to get a hard copy. (Probably not) ';
INPUT 'Then press <Return>.'; JUNK$
CLS
AST$ = STRING$(79, "**")
LOCATE 1, 1: PRINT AST$: PRINT AST$: PRINT AST$
LOCATE 2, 30: PRINT ' NEWBOMB  ' + VERDAT$ + ' '
LOCATE 4, 1: PRINT
PRINT 'INPUT VALUES:'
PRINT
IF IP#(1) > 0 THEN V# = IP#(1)
PRINT 'Bomb Volume is '; V#; ' m^3'
RBOMB = (.75 * V# / 3.141592654#) ^ (1! / 3!)
IF IP!(2) > 0 THEN TINIT = IP!(2)
PRINT 'Initial Temperature is '; TINIT; ' K'
IF IP#(3) > 0 THEN PINIT = IP#(3)
PRINT 'Initial Pressure is '; PINIT; ' Pa'
IF IP!(4) > 0 AND IP!(4) < .99991 THEN EQUIV = IP!(4)
IF FUEL% = 1 THEN AFRSTOIC = 15.5797 ELSE AFRSTOIC = 17.12
AFR = AFRSTOIC / EQUIV
PRINT USING 'Equivalence ratio is #.### (A/F=##.##)'; EQUIV; AFR

'
GETN:
PRINT
PRINT 'NOTE: Burn 600 of 1500 elements for < 1kPa increments to 400kPa.'
INPUT 'Enter total number of elements to consider. >'; N
INPUT 'Enter number of elements to burn. >'; NB
IF NB > 600 THEN PRINT 'Must be 600 or less (for array DIM)!'; CHR$(7): GOTO GETN
IF NB > N THEN PRINT 'Cannot exceed total number of elements!'; CHR$(7): GOTO GETN

'
-----

' Get some of the fuel properties from the FUELSORT subroutine.
' This routine is attached to the bottom of this program.
' (Returns FCA, FHA, and FMW.)
'
GOSUB FUELSORT

'
-----

' MAIN LOOP:
'
' SELECT ELEMENT FOR PROCESSING - will burn NB elements
'

```

```

' Time the number crunching and output section of the program.
'
'  TSTART = TIMER
'
' REACTPROP determines the reactant properties (See CMBSUB).
'
'  CALL REACTPROP(EQUIV, FCA, FHA, FMW, MF, MOXY#, MN2#, MWR)
'  GMR = FNGAMR(TINIT)
'  MASS = MWR * PINIT * V# / RMOL / TINIT
'  PRINT 'Initial mass is: "; MASS; " (MWR="; MWR; ")
'
' Everything from here until the end of the loop is repeated NB times.
'
'  FOR I% = 1 TO NB
'
'  Pressure before burning element I% is set to PINIT if I%=1 or to PE,
'  the pressure after burning the last element, if I% is greater than 1.
'  PI is the initial pressure of the element (not to be confused with PINIT).
'
'    IF I% = 1 THEN
'      PI = PINIT
'    ELSE
'      PI = PE
'    END IF
'
'  Estimate P after next element burns.
'  PE is the end pressure for the element which is just a guess now.
'
'    PE = PI + EQUIV * 9 / N * PINIT
'
'  Flag is set to 0 to indicate that P is only a guess.
'
'    IFLP = 0
'
'  Treactants and GAMMAreactants are evaluated for this PI.
'
'    TR = TINIT * (PI / PINIT) ^ ((GMR - 1) / GMR)
'    GMR = FNGAMR(TR)
'
' CALCVOLUMES:
'
'  This section now calculates the volume of the remaining unburnts before and
'  after combustion of this element. The work done to compress the unburnts is
'  evaluated and then a loop adds the work done to compress each previously
'  burned element. If the correct pressure has been selected, the work done on
'  all elements will equal the work done by the burning element during its
'  combustion and expansion...ie it will match the difference between internal
'  energy of that element before and after combustion. When this happens, the
'  selected pressure will be the correct pressure after this element burns.
'
'  If the correct pressure is guessed, the sum of the volumes will equal the

```

```

' total volume.
'
' VUB is the total volume of all the unburnt gases in m^3 BEFORE combustion
' of the lth element (excludes the lth element).
' VUA is the total volume of all the unburnt gases in m^3 AFTER combustion
' of the lth element.

```

$$VUB = (V\# / N) * (N - I\%) * (PINIT / PE) ^ (1 / GMR)$$

$$VUA = VUB * (PI / PE) ^ (1 / GMR)$$

```

' Calculate the work of compression (VUB -> VUA) on unburnt elements in J.
'

```

$$WU = (PE * VUA - PI * VUB) / (1 - GMR)$$

```

' Volume sum and work sum are set equal to the volume of unburned gas and
' work done to compress the unburned gas in m^3 and joules respectively.
'

```

$$SUMW = WU$$

```

' If there are previously burned elements, calculate the volume of each before
' and after compression to new pressure, PE. Then calculate the work done to
' compress each one and add it to the work sum done by the burning element.
'

```

```

' VB is the volume of the Jth element before compression.
' VA is the volume of the Jth element after compression.
' WB is the compression work of the Jth element in Joules.
' SUMVBA is the volume of the burnt gases after combustion of element I.
'

```

```

' STORE(J,8) is the volume of the Jth element after combustion.
' STORE(J,9) is the pressure of the Jth element after combustion.
' STORE2(J,6) is the specific heat ratio of products in element J. (=FNGAMP(T))
'

```

```

IF I% > 1 THEN
  SUMVBA = 0!
  FOR J = 1 TO I% - 1
    VB = STORE(J, 8) * (STORE(J, 9) / PI) ^ (1 / STORE2(J, 6))
    VA = STORE(J, 8) * (STORE(J, 9) / PE) ^ (1 / STORE2(J, 6))
    WB = (PE * VA - PI * VB) / (1 - STORE2(J, 6))
    SUMVBA = SUMVBA + VA
    SUMW = SUMW + WB
  NEXT J
END IF
SUMV = VUA + SUMVBA
SUMW2 = SUMW

```

```

' Use subroutine FLAME to find the temperature of combustion of the burning
' element knowing its starting conditions and work output, SUMW.
'

```

```

  CALL FLAME(0, 0, SUMW, PE, FCA, FHA, FMW, EQUIV, TR, T, MWR, MWP, FLAG%)

```

```

' Calculate the volume this element would have if it burned to temperature T

```

' at pressure PE. (MOLP is number of moles of products per mole of fuel, MOLR
' is moles of reactants per mole of fuel. Hence VE is in m³ like V).

$$VE = V\# / N * PINIT / PE * 1 / TINIT * MOLP / MOLR$$

' Compare this with volume left over from unburned gas and all previous burned
' elements at this pressure, PE.

$$ERV = VE - (V\# - SUMV)$$

' If the error is greater than .001%, then make a new estimate of pressure
' and go back to try again.

$$ERRLIM = (PE - PINIT) * .00001$$

$$IF ABS(ERV) > V\# / N * ERRLIM THEN$$

' IFLP is a flag which determines whether a previous estimate has been made.
' If it has, extrapolate/interpolate to get a new estimate.
' Otherwise, simply make a small step in pressure.

```

IF IFLP > 0 THEN
    PE3 = (PE * ERV1 - PE1 * ERV) / (ERV1 - ERV)
    PE1 = PE
    PE = PE3
ELSE
    PE1 = PE
    IFLP = 1
    IF ERV > 0 THEN
        PE = PE + 1.2 * (PE - PI)
    ELSE
        PE = PE + (PE - PI) / 1.2
    END IF
END IF

```

' Having established this estimate for pressure after combustion,
' record the current volume error and go back to re-calculate the
' volumes and compression work with the new pressure value.

```

ERV1 = ERV
GOTO CALCVOLUMES
END IF

```

' Calculation of volumes having converged, enter values for the I%th element
' into the storage arrays, STORE and STORE2. Since this program has been
' through many changes, some of the items below are now meaningless but are
' kept in place rather than risking total confusion by reordering the
' storage arrays.

```

STORE(I%, 1) = MH2 ' MH2 is number of moles of H2 at equilibrium
STORE(I%, 2) = MCO ' MCO is number of moles of CO at equilibrium
STORE(I%, 3) = MN2 ' MN2 is number of moles of N2 at equilibrium

```

```

STORE(I%, 4) = MCO2 ' MCO2 is number of moles of CO2 at equilibrium
STORE(I%, 5) = MO2 ' MO2 is number of moles of O2 at equilibrium
STORE(I%, 6) = MH2O ' MH2O is number of moles of H2O at equilibrium
STORE(I%, 7) = MOLP ' MP is number of moles of products at equilibrium
STORE(I%, 8) = VE ' VE is volume of element after combustion
STORE(I%, 9) = PE ' PE is pressure of element after combustion
STORE(I%, 10) = T ' T is temperature of element after combustion
IF N <> I% THEN
    STORE(I%, 11) = VUA / (N - I%) 'Unburnt element size.
ELSE
    STORE(I%, 11) = 0! 'Nothing left to burn.
END IF
STORE2(I%, 1) = P1 ' P1 -\
STORE2(I%, 2) = P2 ' P2 | - constants for evaluating properties of
STORE2(I%, 3) = P3 ' P3 | products of element i% after combustion
STORE2(I%, 4) = P4 ' P4 -/
STORE2(I%, 6) = FNGAMP(T) ' specific heat ratio of products in element I%
STORE2(I%, 7) = VUA ' VUA = volume of unburned after element has burned
STORE2(I%, 10) = VUB ' VUB = volume of unburned before element has burned
STORE2(I%, 11) = TR ' TR = temperature of the reactants
STORE2(I%, 12) = MWP ' Molecular weight of products

IF I% = 1 THEN TB0 = T: PB0 = PE
GAMMAP = FNGAMP(T)
TB1 = TB0 * (PE / PB0) ^ ((GAMMAP - 1) / GAMMAP) 'T of 1st element
TUNB = TINIT * (P0 / PINIT) ^ ((GMR - 1) / GMR) 'unburned gas T

' RR = relative radius of flame after element i% burns (assuming a spherical
' flame and bomb). R0R = radius of this element at spark time

RR = ((V# - VUA) / V#) ^ (1 / 3)
STORE2(I%, 8) = RR
R0R = (I% / N) ^ (1 / 3)

' Print out a running listing to let the user know the progress of the
' calculations that are going on.

PRINT USING '###/####: P=#####Pa, Tb=####k, "; I%; N; PE; T;
PRINT USING 'Tb1=####k, Tu=####k, r/R=#####, "; TB1; TUNB; RR;
PRINT USING 'r0/R=#####; R0R

' The total work done is summed in order to compare this program with
' STANJAN. (ie internal energy change = work done)

TOTWRK = TOTWRK + SUMW2
PRINT 'TOTAL WORK DONE IS "; TOTWRK

NEXT I%

' This is the end of the main loop.

```

```

'
'-----
'
' Calculate the final temperature of each element after NB elements have
' burned and the pressure has risen to STORE(NB,9).
' THIS IS ONLY VALID IF NB=N! (ie Complete combustion occurs.)
'
'   FOR I% = 1 TO NB
'       STORE2(I%, 9) = STORE(I%, 10) * (STORE(NB, 9) / STORE(I%, 9)) ^ ((STORE2(I%, 6)
- 1) / STORE2(I%, 6))
'       NEXT I%
'
'-----
'
' Print out the elapsed time.
'
'   TIMEND = TIMER
'   TDIFF = TIMEND - TSTART
'   MINS = INT((TIMEND - TSTART) / 60)
'   PRINT
'   PRINT "Elapsed time is"; MINS; " min,"; TDIFF - 60 * MINS; " sec"
'   PRINT
'
' Make a warbling sound to notify user that the calculations are done.
'
'   FOR NSOUND = 1 TO 10
'       FREQ = 200 + 100 * NSOUND
'       SOUND FREQ, 1
'   NEXT NSOUND
'
'-----
'
' Pause to look at screen data before going on.
'
'   PRINT
'   PRINT "Hit any key to continue >";
'   WHILE INKEY$ = "": WEND
'   PRINT CHR$(12);           ' New page
'
'-----
'
' List out the calculated values.
'
'   CLS
'   AST$ = STRING$(79, "**")
'   LOCATE 1, 1: PRINT AST$: PRINT AST$: PRINT AST$
'   LOCATE 2, 30: PRINT " NEWBOMB  " + VERDAT$ + " "
'   LOCATE 4, 1: PRINT
'   PRINT
'   PRINT USING "EQUIV=#.##, #### total elements in bomb"; EQUIV; N;
'   PRINT USING " , #### burned"; NB

```

```

PRINT 'ELE- INITIAL ENSUING PRESS COMB TEMP FLAME FINAL TEMP'
PRINT 'MENT RADIUS AFTER COMB degrees RADIUS degrees'
PRINT ' # ro/R kPa kelvin r/R kelvin'
PRINT

```

```

FOR I% = 1 TO NB
  PRINT USING '### '; I%;
  PRINT USING ' ###'; (I% / N) ^ (1 / 3);
  PRINT USING ' #####'; STORE(I%, 9) / 1000;
  PRINT USING ' #####'; STORE(I%, 10);
  PRINT USING ' ###'; STORE2(I%, 8);
  PRINT USING ' #####'; STORE2(I%, 9)
NEXT I%

```

```

' Print a reminder to make sure printer is off.

```

```

PRINT
PRINT 'Is printer on? Hit <Ctrl><PrtSc> to shut off, (then hit enter).'
INPUT JUNK$

```

```

' Prepare all data for writing to data file.

```

```

NR% = NB + 1
NC% = 2
NP% = 5
ND% = 9
REDIM DD(NR%, ND%), COM$(NC%), PAR(NP%), PAR$(NP%), C1$(ND%), C2$(ND%)

```

```

COM$(1) = 'NEWBOMB output: MODIEN version of ' + VERDAT$ + ', run on' + DATE$ +
' at ' + TIME$
COM$(2) = 'Burning ' + STR$(NB) + ' elements of ' + STR$(N)

```

```

RBOMB = (.75 * V# / 3.141593) ^ (1 / 3!)
PAR(1) = EQUIV: PAR$(1) = 'Equivalence Ratio,'
PAR(2) = PINIT: PAR$(2) = 'Pa Initial Pressure'
PAR(3) = TINIT: PAR$(3) = 'K Initial Temperature'
PAR(4) = RBOMB: PAR$(4) = 'm bomb radius'
PAR(5) = MASS: PAR$(5) = 'kg mixture mass'
C1$(1) = 'Element': C2$(1) = ''
C1$(2) = 'Pressure': C2$(2) = 'Pa'
C1$(3) = 'FI Radius': C2$(3) = 'Rb/R'
C1$(4) = 'Mass Brnt': C2$(4) = 'Mb/M'
C1$(5) = 'dVOLunb': C2$(5) = 'm ^ 3'
C1$(6) = 'dVOLbrn': C2$(6) = 'm ^ 3'
C1$(7) = 'Tb after': C2$(7) = 'K'
C1$(8) = 'Tu before': C2$(8) = 'K'
C1$(9) = 'GAMMA react': C2$(9) = ''

```

```

      DD(1, 1) = 0
      DD(1, 2) = PINIT
      DD(1, 3) = 0
      DD(1, 4) = 0
      DD(1, 5) = V# / N
      DD(1, 6) = 0
      DD(1, 7) = TINIT
      DD(1, 8) = TINIT
      DD(1, 9) = FNGAMR(TINIT)

      FOR I = 2 TO NR%
        DD(I, 1) = I - 1
        DD(I, 2) = STORE(I - 1, 9)
        DD(I, 3) = STORE2(I - 1, 8)
        DD(I, 4) = 1! * (I - 1) / N
        DD(I, 5) = STORE(I - 1, 11)
        DD(I, 6) = STORE(I - 1, 8)
        DD(I, 7) = STORE(I - 1, 10)
        DD(I, 8) = STORE2(I - 1, 11)
        DD(I, 9) = STORE2(I - 1, 6)
        'LOCATE 23, 1
        'PRINT USING "### P=#####.# Rb/Ro=##### X=#####"; DD(I, 1); DD(I, 2);
DD(I, 3); DD(I, 4)
      NEXT I

      F$ = ""
      CALL DWRITE(NR%, ND%, NC%, NP%, F$, COM$, DD(), PAR(), PAR$, C1$, C2$())
      PRINT "Write to "; F$; " finished."

      -----
      ' End of the program.

      END

      =====
      =====

      ' FUELSORT
      ' *****

      '
      '
      ' Fuelsort is a subroutine which switches the correct fuel into the
      ' property array and sets up correct fuel molecule variables.

      FUELSORT:
      IF IP%(5) > 0 AND IP%(5) < 3 THEN FUEL% = IP%(5)

      -----

```

```

' If fuel = propane.
,
  IF FUEL% = 1 THEN
    FCA = 3          'fuel has FCA carbon atoms per atom
    FHA = 8          'fuel has FHA hydrogens per atom
    FMW = 44.09      'fuel molar mass in kg/kgmol
  ,
  -----
  ,
' If fuel = methane.
,
  ELSE
    FCA = 1
    FHA = 4
    FMW = 16.043
  END IF
,
  -----
,
' If we don't have the current fuel in I$(7), then swap with I$(8).
,
  IF FUEL$(FUEL%) <> I$(7) THEN
    FOR I = 1 TO 6
      TEMP = IC(7, I)
      IC(7, I) = IC(8, I)
      IC(8, I) = TEMP
    NEXT I
    TEMP$ = I$(7)
    I$(7) = I$(8)
    I$(8) = TEMP$
  END IF
  PRINT "Fuel is " + I$(7) + " and coefficients are:"
  FOR I = 1 TO 7
    PRINT SPACE$(10); IC(7, I)
  NEXT I
RETURN

```

PART 2

The data base file created by NEWBOMB.

c:\qb\ch4-85.stp

601 9 2 5

NEWBOMB output: MODIEN version of 05-MAY-90, run on 05-31-1990
at 16:01:22

Burning 600 elements of 1500

.85 101325 293.15 7.659087E-02 2.175224E-03

Equivalence Ratio,

Pa Initial Pressure

K Initial Temperature

m bomb radius

kg mixture mass

Element

Pressure

Fl Radius

Mass Brnt

dVOLunb

dVOLbrn

Tb after

Tu before

GAMMA react

Pa

Rb/R

Mb/M

m³

m³

K

K

0	101325	0	0	1.254E-06	0	293.1	293.1	1.382
1	101879	.16638	6.666E-04	1.249E-06	8.668E-06	2035.1	293.1	1.258
2	102434	.20929	1.333E-03	1.244E-06	8.622E-06	2035.4	293.5	1.258
3	102987	.23919	0.002	1.239E-06	8.577E-06	2035.8	294.0	1.258
4	103541	.26285	2.666E-03	1.235E-06	8.533E-06	2036.1	294.4	1.258
5	104094	.28271	3.333E-03	1.230E-06	8.489E-06	2036.4	294.9	1.258
6	104647	.29995	0.004	1.225E-06	8.445E-06	2036.7	295.3	1.258
7	105200	.31528	4.666E-03	1.221E-06	8.402E-06	2037.1	295.7	1.258
8	105752	.32912	5.333E-03	1.216E-06	8.359E-06	2037.4	296.2	1.258
9	106304	.34178	0.006	1.211E-06	8.317E-06	2037.7	296.6	1.258
10	106856	.35345	6.666E03	1.207E-06	8.276E-06	2038.0	297.0	1.258

PART 3

A standard experimental data file.

PART 4

NEWBPR2 -- the interpolating program.

```

DECLARE SUB CELREAD (ID%, PR!, LIGHT%, F$, IRUN%, TF)
DECLARE SUB CLFRUN (F$, ID%, P!, L!, I%, DIR%, RNUM%, IRUN%, TF)
DECLARE SUB CLFDIR (F$, DIR%, RNUM%)
DECLARE SUB READRUN (F$, ID%, PR!, L!, I%, DIR%, RNUM%, IRUN%, TF)
'
'
' NEWBPR2
' *****
'
'
' 25-NOV-88    M.D. CHECKEL
' 11-MAY-89    Cleaned up to use for *.CEL data. -- RUSS MODIEN
' 07-MAY-90    Created NEWBPR2 to read bomb data from a NEWBOMB output
'              file. This allows pressure to drop, etc. -- RUSS MODIEN
'
'
' BMBPR2 is BMBPRESS.BAS modified to include propane or methane explosions.
' Converted back from BMBPR5N on 23 November, 1988.
' Based on BOMB.BAS per Alun Thomas's BOMB.BAS with corrections re units, etc
' Uses thermodynamic properties and methods as described in
' Rowland S. Benson, "Advanced Engineering Thermodynamics"
' Pergamon Press, 1977, 2nd Edition (eg pg 153, Appendix A)
'
' This program calculates fates of elements of lean fuel-air mixtures
' at specified starting conditions, burning in a constant volume bomb,
' based on the recorded pressure trace from the bomb. It reads results
' from NEWBOMB and then interpolates them to mesh with the measured pressure
' results (along with light emission measurements).
'
'-----
'
' Include and dimension the files.
'
' REM $INCLUDE: 'C:\QB\COMB\CMBCOM.BAS'
' REM $INCLUDE: 'C:\QB\LIB\PLOTCOM.BAS'
' REM $INCLUDE: 'C:\QB\LIB\COLORCHC.BAS'
' REM $INCLUDE: 'C:\QB\COMB\CMBFN-RP.BAS'
' REM $DYNAMIC
'
' REDIM IC(8, 7), IS(8), CC(6), CW(6), R(7), P(7), M#(6), W(8)
' REDIM N%(10), DIR%(760), RNUM%(230)
' REDIM ID%(30), PR!(512), LIGHT%(512), TIME!(512), FUEL$(2)
'
' NPAR% = 18
' NCOM% = 4
' NC% = 11
' REDIM RES(600, NC%), TOTVOL#(600)
' REDIM COM$(NCOM%), PAR!(NPAR%), PAR$(NPAR%), C1$(NC%), C2$(NC%)
'
' These are the INSCRN variables.
'

```

```

X% = 6
REDIM D$(X%), T%(X%), P$(X%), LG%(X%), L%(X%), C%(X%)
REDIM IP$(X%), IP%(X%), IP!(X%), IP#(X%)
,
-----
,
' Set up some constants.
,
VERDAT$ = "07-MAY-90"
RMOL = 8314.3      'ideal gas constant in J/mol.K
PN = 101325        'standard atmosphere in Pa (for Go and So)
,
-----
,
' Set up arrays and open a file to read from.
,
AST$ = STRING$(79, "**")
CLS
LOCATE 5, 1: PRINT AST$: PRINT AST$: PRINT AST$
LOCATE 6, 30: PRINT " NEWBPR2  01-JUN-90 "
,
-----
,
' Read the data base information file.
,
GETFILE2:
DF$ = "C:\QB\CH4-85.STP"
LOCATE 8, 1
PRINT "Enter the name of the data base file. (Enter="; DF$; ") >";
INPUT ; DF2$
IF DF2$ <> "" THEN DF$ = DF2$
ON ERROR GOTO NOFIL
LOCATE 8, 1: PRINT SPACE$(80): PRINT SPACE$(80): LOCATE 8, 1
FILES DF$
ON ERROR GOTO 0
,
-----
,
' File reading routine.
,
YESFILE:
REDIM DD!(20, 20), DPAR!(20), DPAR$(20), DCOM$(20), DCOL1$(20), DCOL2$(20)
,
LOCATE 8, 1: PRINT SPACE$(80): PRINT SPACE$(80): PRINT SPACE$(80)
LOCATE 8, 1: PRINT "Reading "; DF$; " . . ."
CALL DDIM(DNR%, DNC%, DNCOM%, DNPARG%, DF$, TITLE$)
,
REDIM DCOM$(DNCOM%), DPAR$(DNPARG%), DPAR!(DNPARG%), DD(DNR%, DNC%)
REDIM DCOL1$(DNC%), DCOL2$(DNC%)
,
CALL DREAD(DNR%, DNC%, DNCOM%, DNPARG%, DF$, DCOM$(), DD(), DPAR!(), DPAR$(),

```

```

DCOL1$, DCOL2$())
,
-----
,
' If there was an error in reading the file print message, otherwise skip.
,
    GOTO SETNR
,
NOFIL:
    LOCATE 8, 1: PRINT SPACES$(80): PRINT SPACES$(80): LOCATE 8, 1
    PRINT "Enter a suitable file name, "; DF$; " is not found."; CHR$(7)
    RESUME GETFILE2
,
SETNR:
    NROW% = DNR%
    NCOL% = DNC%
    LOCATE 8, 1: PRINT SPACES$(80): PRINT SPACES$(80): LOCATE 8, 1
,
,
GETRUN:
    PRINT "Enter 0 = binary CLF file read,"
    PRINT "    1 = TURBULENT CEL file read,"
    INPUT "    2 = QUIESCENT CEL file read. > "; IN%
    IN% = 1
,
    IF IN% = 0 THEN
        CALL CLFDIR(F$, DIR%(), RNUM%())
        IF F$ = "" THEN GOTO GETRUN
        CALL CLFRUN(F$, ID%(), PR!(), TIME!(), -1, DIR%(), RNUM%(), IRUN%, TFACT)
        V# = .001684#           ' Bomb volume in m^3
        FUEL% = 1
    END IF
    IF IN% = 1 THEN
        CALL CELREAD(ID%(), PR!(), LIGHT%(), F$, IRUN%, TFACT)
        V# = .001882#           ' Bomb volume in m^3
        FUEL% = 2
    END IF
    IF IN% = 2 THEN
        CALL CELREAD(ID%(), PR!(), LIGHT%(), F$, IRUN%, TFACT)
        V# = .0005094#          ' Bomb volume in m^3
        FUEL% = 2
    END IF
,
-----
,
' Calculate info to store from ID% array.
,
    VPLATE = ID%(13) / 6000! + ID%(14) / 6000! + ID%(15) / 6000! + ID%(16) / 6000! + ID%(17)
/ 6000! + ID%(18) / 6000!
    IF VPLATE > 8 THEN
        VPLATE = ID%(15) / 5000! + ID%(16) / 5000! + ID%(17) / 5000! + ID%(18) / 5000! +

```

```

ID%(19) / 5000!
END IF
TSPARK = ID%(10) / 10!
IF ID%(30) > 0 THEN TIONS = ID%(30) / 1000! ELSE TIONS = -1
IF ID%(5) >= 0 THEN TPHOTO = ID%(5) / 1000! ELSE TPHOTO = -1
IF TPHOTO >= 0 THEN PPHOTO = ID%(25) * .1 ELSE PPHOTO = -1
IF TPHOTO >= 0 THEN LPHOTO = ID%(28) * .1 ELSE LPHOTO = -1
PSPK! = ID%(8) * .1
IF PSPK! < 90 THEN PSPK! = ID%(8) / 1.836
PRINT "ID%(1 to 30)"
FOR I = 1 TO 30
    PRINT USING "#####"; ID%(I);
NEXT
NP% = ID%(21)
IF NP% > 500 THEN NP% = 500
IF NP% <= 0 THEN NP% = 500
,
-----
,
' Enter initial conditions and number of volume elements to work on.
,
    TINIT = 293.15          ' pre-combustion temperature in K
    PINIT = 101325          ' pre-combustion pressure in Pa
    EQUIV = ID%(3) / 1000!  ' equivalence ratio
    IF EQUIV > .9999 THEN EQUIV = .9999
    FUEL$(1) = "C3H8"
    FUEL$(2) = "CH4"
,
-----
,
' Print a bit of a header and verify some parameters with user.
,
INPUTSECTION:
    COLOR NFC%, NBC%
    CLS
    LOCATE 5, 1: PRINT AST$: PRINT AST$: PRINT AST$
    LOCATE 6, 30: PRINT "NEWBPR2 01-JUN-90"
    LOCATE 8, 1: PRINT "BOMB COMBUSTION EFFECTS CALCULATION PROGRAM"
    PRINT
    PRINT "MODIEN version of "; VERDAT$; ", run at "; TIMES$; " on "; DATE$
,

D$(1) = STR$(V#): T%(1) = 3: LG%(1) = 9: L%(1) = 7: C%(1) = 10
P$(1) = "Enter volume of bomb in m3 (0=" + D$(1) + ") >"
D$(2) = STR$(TINIT): T%(2) = 1: LG%(2) = 7: L%(2) = 9: C%(2) = 10
P$(2) = "Enter initial temperature (0=" + D$(2) + ") >"
D$(3) = STR$(PINIT): T%(3) = 2: LG%(3) = 15: L%(3) = 11: C%(3) = 10
P$(3) = "Enter initial pressure in Pa (0=" + D$(3) + ") >"
D$(4) = STR$(EQUIV): T%(4) = 1: LG%(4) = 7: L%(4) = 13: C%(4) = 10
P$(4) = "Enter equivalence ratio (0<E<0.9999), (0=" + D$(4) + ") >"
IF PRI(1) < 150000 THEN
    MX = 300

```

```

ELSEIF PR!(1) > 250000 THEN
    MX = 900
ELSE
    MX = 600
END IF
D$(5) = "400000.0": T%(5) = 1: LG%(5) = 10: L%(5) = 18: C%(5) = 10
P$(5) = "Enter maximum pressure to analyze in Pa. (0= " + D$(5) + " Pa) >"
D$(6) = STR$(FUEL%): T%(6) = 0: LG%(6) = 3: L%(6) = 21: C%(6) = 10
P$(6) = "Enter FUEL code (1=propane, 2=methane; default=" + D$(6) + ") >"
,
CLS
CALL INSCRN(6, 1, T%(), P$(), LG%(), D$(), L%(), C%(), IP$(), IP%(), IP!(), IP#(), tx$)
,
-----
,
' Echo back some of the initial parameters for the user.
,
CLS
LOCATE 5, 1
PRINT BOMB$
PRINT
PRINT "INPUT VALUES:"
PRINT
IF IP#(1) > 0 THEN V# = IP#(1)
PRINT "Bomb Volume is "; V#; " m^3"
RBOMB = (.75 * V# / 3.141592654#) ^ (1! / 3!)
IF IP!(2) > 0 THEN TINIT = IP!(2)
PRINT "Initial Temperature is "; TINIT; " K"
IF IP#(3) > 0 THEN PINIT = IP#(3)
PRINT "Initial Pressure is "; PINIT; " Pa"
IF IP!(4) > 0 AND IP!(4) < .99991 THEN EQUIV = IP!(4)
IF FUEL% = 1 THEN AFRSTOIC = 15.5797 ELSE AFRSTOIC = 17.12
AFR = AFRSTOIC / EQUIV
PRINT USING "Equivalence Ratio is ###.### (A/F=###.###)"; EQUIV; AFR
IF IP!(5) > PSPK THEN MAXP = IP!(5)
PRINT "Maximum pressure to analyze is MAXP="; MAXP; "Pa"
N = NP%
NB = NP%
,
-----
,
' Set up TIME array and determine PMAX and TPMAX.
' Also convert from kPa to Pa.
,
PMAX = 0
FOR I% = 1 TO NP%
    TIME!(I%) = (I% - 1) * TFACT
    PR!(I%) = PR!(I%) * 1000!
    IF PR!(I%) < PINIT THEN PR!(I%) = PINIT
    IF PR!(I%) > PMAX THEN

```

```

        PMAX = PR!(I%)
        TPMAX = TIME!(I%)
    END IF
NEXT I%

FOR I% = 10 TO NP%           'Ignore  st 10 points
    IF PR!(I%) > MAXP THEN
        IMAXP% = I%
        GOTO TIMESTART
    END IF
NEXT I%

-----

' Time the number crunching and output section of the program.

TIMESTART:
    TSTART = TIMER

-----

' This is the start of the main loop where interpolation is done to
' determine various quantities from a data base file based on measured
' pressure.

RES(1, 1) = TIME!(1)      ' Time in ms.
RES(1, 2) = PINIT         ' Pressure after combustion of element.
RES(1, 3) = 0             ' relative radius of flame vs bomb radius
RES(1, 4) = 0             ' mass fraction burned
RES(1, 5) = DD(1, 5)      ' volume of element before combustion
RES(1, 6) = DD(1, 6)      ' volume of element after combustion
RES(1, 7) = DD(2, 7)      ' temperature of element after combustion
RES(1, 8) = TINIT         ' unburned gas temperature after combustion
RES(1, 9) = DD(1, 9)      ' specific heat of reactants
G = RES(1, 9)
RES(1, 10) = RES(1, 8) * (PMAX / PINIT) ^ ((G - 1) / G) ' T if burned to PMAX
RES(1, 11) = LIGHT%(1)    ' light emission

LASTVOL# = 0#
FOR I% = 2 TO IMAXP%
    LOCATE 15, 1: PRINT "Calculation countdown . . . "; IMAXP% - I%; " "
    RES(I%, 1) = TIME!(I%)
    RES(I%, 2) = PR!(I%)
    VOLUME# = 0#
    FOR J% = 2 TO DNR%
        IF DD(J%, 2) > PR!(I%) THEN
            INTERP = (PR!(I%) - DD(J% - 1, 2)) / (DD(J%, 2) - DD(J% - 1, 2))
            FOR K% = 3 TO 9
                RES(I%, K%) = DD(J% - 1, K%) + (DD(J%, K%) - DD(J% - 1, K%)) * INTERP
            NEXT K%
            TOTVOL#(I%) = VOLUME# + RES(I%, 5)
        END IF
    NEXT J%
NEXT I%

```

```

        GOTO SKIPOUT
    END IF
    VOLUME# = VOLUME# + DD(J% - 1, 5)
NEXT J%
SKIPOUT:
    G = RES(I%, 9)
    IF G = 0 THEN G = LASTG
    LASTG = G
    TEMP = RES(I%, 8) * (PMAX / PR!(I%)) ^ ((G - 1) / G)
    'G = (G + FNGAMP(TEMP)) * .5
    RES(I%, 10) = RES(I%, 8) * (PMAX / PR!(I%)) ^ ((G - 1) / G)
    RES(I%, 11) = LIGHT%(I%)
,
    LOCATE 18, 1
    PRINT USING "t=###.## P=#####.## Rb/Ro=###.### X=#####"; RES(I%, 1);
RES(I%, 2); RES(I%, 3); RES(I%, 4)
    'INPUT JUNK$
NEXT I%
,
' Convert from Pa to kPa.
,
    FOR L% = 1 TO IMAXP%
        RES(L%, 2) = RES(L%, 2) / 1000!
    NEXT L%
,
' Determine the elemental volume burned from total volume burned.
,
    TOTVOL#(1) = 0#
    RES(1, 5) = 0!
    FOR I% = 2 TO IMAXP%
        RES(I%, 5) = TOTVOL#(I%) - TOTVOL#(I% - 1)
    NEXT I%
,
,
-----
,
' Note how long it all took.
,
GETTEND:
    TIMEND = TIMER
,
-----
,
' Print out the elapsed time.
,
    TDIFF = TIMEND - TSTART
    MINS = INT((TIMEND - TSTART) / 60)
    PRINT
    PRINT "Elapsed time is"; MINS; " min,"; TDIFF - 60 * MINS; " sec"
    PRINT
,

```

' Make a warbling sound to notify user that the calculations are done.

```

FOR NSOUND = 1 TO 10
  FREQ = 200 + 100 * NSOUND
  SOUND FREQ, 1
NEXT NSOUND

```

' Store the calculated quantities in an output file.

```

IRUN$ = STR$(IRUN%)
IRUN$ = RIGHT$(IRUN$, LEN(IRUN$) - 1)
F$ = 'C:\QB\RUSS\DATA\' + IRUN$ + ".NP2"

```

NAMEFILE:

```

PRINT 'ABOUT TO WRITE TO ' + F$
INPUT 'Hit enter to go on, else enter a new file and extension. >'; JUNK$
IF JUNK$ <> "" THEN
  F$ = 'C:\QB\RUSS\DATA\' + JUNK$
  PRINT
  GOTO NAMEFILE
END IF

```

```

COM$(1) = 'OUTPUT OF BOMB PRESSURE TRACE ANALYSIS PROGRAM: NEWBPR2'
COM$(2) = 'MODIEN version of ' + VERDAT$ + ', run at ' + TIMES
COM$(2) = COM$(2) + ' on ' + DATE$
COM$(3) = 'Run #' + STR$(ID%(1)) + ' from' + STR$(800000 + ID%(2))
COM$(4) = F$

```

```

PAR!(1) = IRUN%: PAR$(1) = ' run number'
PAR!(2) = V#: PAR$(2) = ' m^3 =Vtotal'
PAR!(3) = TINIT: PAR$(3) = ' k =Ti'
PAR!(4) = PINIT / 1000!: PAR$(4) = ' kPa =Pi'
PAR!(5) = EQUIV: PAR$(5) = ' Equiv Ratio'
PAR!(6) = TPMAX: PAR$(6) = ' ms =Tpmx'
PAR!(7) = PMAX: PAR$(7) = ' kPa =Pmax'
PAR!(8) = R(1): PAR$(8) = ' R1-R4 are constants for mixture properties'
PAR!(9) = R(2): PAR$(9) = ' R2'
PAR!(10) = R(3): PAR$(10) = ' R3'
PAR!(11) = R(4): PAR$(11) = ' R4'
PAR!(12) = MWR: PAR$(12) = ' kg/kmol.react'
PAR!(13) = VPLATE: PAR$(13) = ' m/s =Vplate'
PAR!(14) = TSPARK: PAR$(14) = ' ms =Tspark'
PAR!(15) = TIONS: PAR$(15) = ' ms =Tions'
PAR!(16) = TPHOTO: PAR$(16) = ' ms =Tphoto'
PAR!(17) = PPHOTO: PAR$(17) = ' kPa =Pphoto'
PAR!(18) = LPHOTO: PAR$(18) = ' V =Lphoto'

```

```

C1$(1) = 'TIME': C2$(1) = '(ms)'
C1$(2) = 'PRESS': C2$(2) = '(kPa)'

```

```

C1$(3) = 'RADIUSb': C2$(3) = '/R'
C1$(4) = 'MASSb': C2$(4) = '/M'
C1$(5) = 'dVOLunb': C2$(5) = '(m^3)'
C1$(6) = 'dVOLbrn': C2$(6) = '(m^3)'
C1$(7) = 'T burn': C2$(7) = '(K)'
C1$(8) = 'Tunb': C2$(8) = '(K)'
C1$(9) = 'GAMMA u': C2$(9) = ''
C1$(10) = 'T final': C2$(10) = '(K)'
C1$(11) = 'Light': C2$(11) = '(counts)'
NR% = IMAXP%
CALL DWRITE(NR%, NC%, NCOM%, NPAR%, F$, COM$, RES(), PAR!(), PAR$, C1$,
C2$())
'-----
'
' Finish off program.

      STOP
      END

      *Enter 0 to read another run, 1 to quit >: IND
      IF IND = 0 THEN GOTO GETRUN
END
'-----
=====
=====
'
' FUELSORT
' *****
'
' Fuelsort is a subroutine which switches the correct fuel into the
' property array and sets up correct fuel molecule variables.
'
FUELSORT:
  IF IP%(6) > 0 AND IP%(6) < 3 THEN FUEL% = IP%(6)
  '-----
  '
  ' If fuel = propane.
  '
  IF FUEL% = 1 THEN
    FCA = 3      'fuel has FCA carbon atoms per atom
    FHA = 8      'fuel has FHA hydrogens per atom
    FMW = 44.09  'fuel molar mass in kg/kgmol
  '-----
  '
  ' If fuel = methane.
  '
  ELSE
    FCA = 1

```

```

        FHA = 4
        FMW = 16.043
    END IF
,
-----
,
' If we don't have the current fuel in I$(7) then swap with i$(8).
,
    IF FUEL$(FUEL%) <> I$(7) THEN
        FOR I = 1 TO 6
            TEMP = IC(7, I)
            IC(7, I) = IC(8, I)
            IC(8, I) = TEMP
        NEXT I
        TEMP$ = I$(7)
        I$(7) = I$(8)
        I$(8) = TEMP$
    END IF
    PRINT 'Fuel is ' + I$(7) + ' and coefficients are:'
    FOR I = 1 TO 7
        PRINT SPACE$(10); IC(7, I)
    NEXT I
RETURN
' =====
' =====

```

PART 5

The output file from NEWBPR2.

C:\QB\RUSS\DATA\14174.NP2

122 11 4 18

OUTPUT OF BOMB PRESSURE TRACE ANALYSIS PROGRAM: BMBPR5

MODIEN version of 07-MAY-90, run at 13:20:55 on 06-12-1990 Run

14174 from 802709

C:\QB\RUSS\DATA\14174.NP2

14174 .001882 293.15 101.325 .845 40.56 738700 0 0
0 0 0

2.925833 55.7 -1 -1 -1 -1

run number

m³ =Vtotal

k =Ti

kPa =Pi

Equiv Ratio

ms =Tpmax

kPa =Pmax

R1-R4 are constants for mixture properties

R2

R3

R4

kg/kmol.react

m/s =Vplate

ms =Tspark

ms =Tions

ms =Tphoto

kPa =Pphoto

V =Lphoto

TIME

PRESS

RADIUSb

MASSb

dVOLunb

dVOLbrn

T burn

Tunb

GAMMA u

T final

Light

(ms)

(kPa)

/R

/M

(m³)

(m³)

(K)

(K)

(K)

(counts)

.00	101.3	.00	.0	.0	.0	2035.1	293.15	1.382198	507.7539	0
.24	123.2	.5374	2.6579E-02	4.6745E-05	7.2095E-06	2046.9	308.96	1.257994	446.1033	6076
.48	103.7	.2685	2.8576E-03	-4.0522E-05	8.5204E-06	2036.2	294.59	1.258251	440.7978	9966